

TET3 impacts cardiac fibrosis partially via regulation of DNA damage response

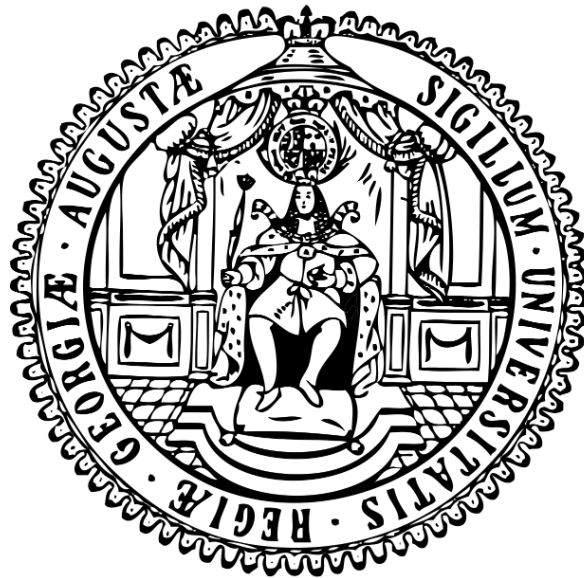
Doctoral Thesis

In partial fulfilment of the requirements for the degree

“*Doctor rerum naturalium (Dr. rer. nat.)*”

in the Molecular Medicine Study Program

at the Georg-August University Göttingen



Submitted by

Sandip Kumar Rath

Born in Jatni, India

Göttingen, November, 2019

Members of the Thesis committee

Professor Elisabeth M. Zeisberg (Supervisor)

University Medical Center Göttingen
Department of Cardiology and Pneumology
Robert-Koch-Strasse-40, Germany

Professor Doerthe Katschinski

Institute of Cardiovascular Physiology
University Medical Center, Göttingen
Humboldtalle, Germany

PD Dr. Laura Zelarayan

Institute of Pharmacology and Toxicology,
University Medical Center Göttingen
Robert-Koch-Strasse-40, Germany

Professor Steven A. Johnsen (Previous member)

Gene Regulatory Mechanisms and Molecular Epigenetics Lab
Gastroenterology Research
Mayo Clinic, Rochester, USA

Members of the extended Thesis committee

PD Dr. rer. nat. Sven Thoms

Department of Child and Adolescent Health
University Medical Center Göttingen
Robert-Koch-Strasse-40

Professor Argyris Papantonis

Institute of Pathology
University Medical Center Göttingen
Robert-Koch-Strasse-40

Professor Ralf Dressel

Institute for Cellular and Molecular Immunology
University Medical Center Göttingen
Humboldtalle, Göttingen

Date of Oral Exam-13.01.2020

I. Declaration

I hereby declare that the work presented in this thesis has not been submitted for any other degree or professional qualification, and that it is the result of my own independent work.

Sandip Kumar Rath

Date:

***“If the book is true, it will find an audience
that is meant to read it.”***

— Wally Lamb

“Dedicated to my parents, specially to my father”

II. Acknowledgements

Firstly, I would like to express my sincere gratitude to my advisor Prof. Elisabeth M. Zeisberg, for the continuous support of my Ph.D. study and related research, for her patience, motivation, and immense knowledge. I could not have imagined having a better advisor and mentor for my Ph.D. study.

Besides my advisor, I would like to thank the rest of my thesis committee: Prof. Doerthe Katschinski, Prof. Steven A. Johnson, and Dr. Laura Zelarayan, for their insightful comments and encouragement, but also for the hard questions which inspired me to widen my research from various perspectives.

My sincere thanks also go to Prof. Michael Zeisberg for providing constant motivation and experimental ideas for the project. In particular, I am grateful to Dr. Björn Tampe and Dr. Gunsmaa Nyamsuren for enlightening me with motivation and bright ideas under challenging stages of research.

I want to give my sincere thanks to Professor Steven A. Johnson, Dr. Shiba Prasad Parida, and Professor Sachidananda Das for their kind mentorship and support. I have learned a lot from them, especially from Steve and Sachi Sir. I am deeply indebted to Dr. Moonmoon Deb, Dr. Dipta Sengupta, and Professor Samir Kumar Patra for strengthening my early scientific footsteps back in India.

Special thanks to our technicians Sarah Rinkleff, Anika Erdmann, and Anika Kruger for all the scientific help and, most of all, being the most delightful friends throughout my stay in Göttingen. I would deeply cherish all those long coffee hours and of course, the weihnachtsmarkt gluwein tours. Guys, thank you a lot for being there out for me in good and challenging times.

I am thankful to Mrs. Choudhary (Head of the physiotherapy unit, Göttingen) and all my physiotherapists. Without their help in treatment, it would have been tough for me to overcome the hardship of ankylosing spondylitis.

An exceptional thanks to the IRTG-1816 program and Prof. Doerthe Katschinski again for organizing such a beautiful structured graduate training program, which has helped me to explore the scientific arena as well as develop future networks. I am also thankful to Dr. Christina Wurtz and Mrs. Fulya Oren for all their kind support in organizing courses for the IRTG-1816 cohort as well as helping in numerous academic and non-academic fields.

I am thankful to Lydia Bickford Maus, Dr. Debasis Panda and Dr. Sarah Hunt for their help in correcting English. Last but not least, I am greatly to thankful to Jagannath, Swati, Liza Swain, Manoranjan, Kirti, Shilpa, Andreas, Guntjee, Giulia, Jonas, Udhaya, Maithili, Lydia and Gregor for their friendship both in and out of the graduate school. I am also thankful to Mr. CR Mohanty and Mr. Ashok

Tripathy for their support. In the end, I can say, I am what I am because of the love and support of all those people whom I have come across in my life.

Table of Contents

MEMBERS OF THE THESIS COMMITTEE	I
MEMBERS OF THE EXTENDED THESIS COMMITTEE.....	II
I. DECLARATION	III
II. ACKNOWLEDGEMENTS.....	VI
III. LIST OF FIGURES.....	XI
IV. LIST OF TABLES	XIII
V. ABBREVIATIONS	XIV
ABSTRACT	1
1. INTRODUCTION	2
1.1 CARDIOVASCULAR DISEASES AND CARDIAC FIBROSIS.....	2
1.1.1 <i>Types of cardiac fibrosis.....</i>	3
1.1.3 <i>The role of TGF-β in fibroblast activation.....</i>	5
1.2 EPIGENETIC REGULATION OF CARDIAC FIBROSIS	5
1.2.1 <i>Epigenetics</i>	5
1.2.2 <i>TET enzymes</i>	6
1.2.3 <i>TET isoforms and mechanism of action.....</i>	7
1.2.4 <i>Role of TETs in cardiovascular diseases.....</i>	8
1.3 DNA DAMAGE	9
1.3.1 <i>DNA repair response</i>	10
1.3.2 <i>Non-Homologous-End-Joining repair response pathway</i>	10
1.3.3 <i>Homologous-Recombination repair response pathway</i>	11
1.4 ROLE OF DNA DAMAGE AND REPAIR IN CARDIOVASCULAR DISEASES	13
1.5 ROLE OF TGF-B IN DNA DAMAGE AND REPAIR RESPONSES	13
1.6 ROLE OF TETs IN DNA DAMAGE AND REPAIR RESPONSES	14
1.7 AIMS OF THESIS	15
2. MATERIALS AND METHODS	16
2.1 MATERIALS.....	16
2.1.1 <i>Cell line.....</i>	16
2.1.2 <i>Cell culture media and additives.....</i>	16
2.1.3 <i>Chemicals and reagents.....</i>	17
2.1.4 <i>Consumables</i>	19
2.1.5 <i>Recombinant proteins.....</i>	20
2.1.6 <i>Antibodies.....</i>	21
2.1.7 <i>Buffers.....</i>	22
2.1.8 <i>Primers</i>	23
2.1.9 <i>Commercial Kits.....</i>	23
2.1.10 <i>Plasmids.....</i>	24
2.1.11 <i>Equipment</i>	24
2.1.12 <i>Softwares</i>	26
2.2 METHODS	27
2.2.1 <i>Human myocardial tissue sections</i>	27
2.2.2 <i>Animal welfare and ethics statement</i>	27
2.2.3 <i>Fibrosis induction using angiotensin II osmotic minipump in mice.....</i>	27

2.2.4 Cell culture	27
2.2.5 Neocarzinostatin (NCS) and transforming growth factor beta (TGF- β) treatment	27
2.2.6 Generation of clustered regularly interspaced short palindromic repeats/CRISPR-associated protein 9 (CRISPR/Cas9) Tet methylcytosine dioxygenase 3 (TET3) knockdown constructs	28
2.2.7 Plasmid isolation using midi-prep kit.....	28
2.2.8 In vitro transfection	28
2.2.9 Histology.....	29
2.2.10 Immunohistochemistry	29
2.2.11 Single-cell, neutral gel electrophoresis.....	29
2.2.12 Amplex Red assay	29
2.2.13 Protein extraction and quantification.....	30
2.2.14 TET and glutathione/glutathione disulfide (GSH/GSSG) activity assays	30
2.2.15 Immunofluorescence.....	30
2.2.16 Confocal image analysis.....	31
2.2.17 RNA isolation	31
2.2.18 Complementary DNA synthesis	31
2.2.19 Real-time quantitative polymerase chain reaction (RT-qPCR)	32
2.2.20 Western blot.....	32
2.2.21 Flow cytometry	33
2.2.22 Proximity ligation assay	33
2.2.23 Non-homologous end joining (NHEJ) and homologous recombination (HR) reporter plasmids.....	33
2.2.24 Cell counting assay.....	34
2.2.25 MTT cell proliferation assay	34
2.2.26 Analysis of publicly available microarray datasets	34
2.2.27 BrdU DNA end resection assay.....	34
2.2.28 Statistics.....	34
3. RESULTS	35
3.1 Mouse fibrotic hearts accumulate ROS and oxidative stress	35
3.2 Mouse fibrotic hearts have increased DNA damage.....	36
3.3 Mouse fibrotic fibroblasts show increased proliferation despite DNA damage.....	37
3.4 Mouse fibrotic hearts lose TET3 expression.....	38
3.5 Mouse fibrotic fibroblasts show decreased TET3 expression	40
3.6 Ischemic human hearts show decreased TET3 expression.....	41
3.7 TET3 is positively associated with RAD51 and negatively associated with 53BP1 expression in ischemic human hearts	41
3.8 TET3 is recruited to the DNA DSBs in vitro in MCFs when challenged with H ₂ O ₂	42
3.9 TET3 is recruited to the DNA DSBs in vitro in MCFs when challenged with NCS	43

3.10 Proximity ligation assay confirms TET3 recruitment at DNA DSBs in MCFs	44
3.11 ChIP sequencing analysis shows TET3 overlaps at DNA DSBs in HEK293T cells.....	46
3.12 Loss of TET3 is associated with spontaneous DNA damage in MCFs	46
3.13 Knockdown of TET3 results in decreased HR but unchanged NHEJ efficacy in MCFs.....	49
3.14 Knockdown of TET3 results in decreased DNA end resection in MCFs	50
3.15 Knockdown of TET3 results in impaired recruitment of RAD51 to DNA DSBs in MCFs.....	52
3.16 Knockdown of TET3 results in unchanged recruitment of 53BP1 to DNA DSBs in MCFs.....	53
3.17 Knockdown of TET3 results in decreased global chromatin accessibility	55
3.18 TGF- β treatment results in decreased TET3 expression but increased proliferation in MCFs	56
3.19 TGF- β treatment results in decreased DSBs in MCFs	59
3.20 TGF- β treatment activates increased NHEJ repair	60
3.21 TGF- β treatment promotes proliferation in cardiac fibroblasts which can be rescued by TET3 overexpression	61
3.22 TGF- β treatment results in increased H3s10p in MCFs.....	63
3.23 TET3 overexpression in TGF- β treated MCFs results in an increased HR repair	65
3.24 Mouse fibrotic fibroblasts have increased NHEJ mediated repair in in vivo	67
3.25 Human fibrotic hearts lose TET3 expression	68
4. DISCUSSION	69
4.1 TET3 affects DNA damage and repair in cardiac fibroblasts	70
4.2 TET3 may affect replication stress in cardiac fibroblasts.....	72
4.3 TET3 affects chromatin relaxation during DNA damage response in cardiac fibroblasts	73
4.4 TGF- β affects DNA repair and proliferation in cardiac fibroblasts	74
4.5 TET3 affects DNA repair and proliferation in cardiac fibroblasts	75
5. CONCLUSION AND THERAPEUTIC OUTLOOK.....	76
REFERENCES.....	77

III. List of figures

Figure 1. Pie-chart showing overall mortality % (worldwide) in both men and women due to various diseases.....	2
Figure 2. Schematic representation of replacement and repairment cardiac fibrosis.....	3
Figure 3. Schematic illustration showing the source of cardiac fibroblasts.	4
Figure 4. Schematic representation showing active DNA demethylation process catalyzed by the TET enzymes in Homo sapiens.	7
Figure 5. Schematic illustration of TET enzymes in Homo sapiens.	8
Figure 6. Schematic representation of DNA damage repair response.....	9
Figure 7. Schematic representation of NHEJ-mediated DNA repair pathway.	11
Figure 8. Schematic representation of HR-mediated DNA repair pathway. ...	12
Figure 9. Mouse fibrotic hearts have increased ROS and oxidative stress.	35
Figure 10. Mouse fibrotic hearts have increased DNA damage.	36
Figure 11. Mouse fibrotic fibroblasts have increased DNA DSBs.	37
Figure 12. Mouse fibrotic fibroblasts have increased Ki67 expression.....	38
Figure 13. Mouse fibrotic hearts have decreased TET3 expression and reduced TET activity.....	39
Figure 14. Mouse fibrotic fibroblasts have decreased TET3 expression.....	40
Figure 15. Ischemic human hearts have decreased TET3 expression.....	41
Figure 16. TET3 is negatively associated with RAD51 expression and positively associated with 53BP1 expression in ischemic human hearts.	42
Figure 17. TET3 is co-localized at DNA DSBs induced by H ₂ O ₂ in vitro in MCFs.	43
Figure 18. TET3 is co-localized at DNA DSBs induced by NCS in vitro in MCFs.	44
Figure 19. PLA confirms the recruitment of TET3 at DNA DSBs in vitro in MCFs.	45
Figure 20. ChIP sequencing data showing overlap of TET3 and γ -H2AX globally in HEK293 cells.	46
Figure 21. Establishment of TET3 knockdown in vitro in MCFs.	47
Figure 22. TET3 knockdown results in endogenous DNA DSBs in vitro in MCFs.	48
Figure 23. Effect of TET3 knockdown on HR and NHEJ efficiency in vitro in MCFs.	50
Figure 24. TET3 knockdown results in decreased BrdU incorporation in vitro in MCFs.	52
Figure 25. TET3 knockdown results in impaired recruitment of RAD51 at DNA DSBs in vitro in MCFs.	53
Figure 26. TET3 knockdown does not affect the recruitment of 53bp1 at DNA DSBs in vitro in MCFs.	54
Figure 27. TET3 knockdown results in chromatin compaction in vitro in MCFs.	56

<i>Figure 28. TGF-β treatment in MCFs affects cell count, proliferation, DNA damage and TET3 expression.....</i>	<i>58</i>
<i>Figure 29. TGF-β decreases DNA DSBs in MCFs.</i>	<i>59</i>
<i>Figure 30. TGF-β increases NHEJ mediated DNA repair response in MCFs. ..</i>	<i>61</i>
<i>Figure 31. TGF-β dramatically increases proliferation rate in MCFs which can be rescued by TET3 overexpression.....</i>	<i>63</i>
<i>Figure 32. TGF-β increases H3s10p signalling in vitro in MCFs.....</i>	<i>65</i>
<i>Figure 33. TET3 overexpression results in increased HR repair efficacy in TGF-β treated MCFs.</i>	<i>66</i>
<i>Figure 34. Mouse fibrotic fibroblasts have increased 53bp1 expression in vivo.</i>	<i>67</i>
<i>Figure 35. Human fibrotic fibroblasts have decreased TET3 expression.</i>	<i>68</i>
<i>Figure 36. Schematic representation illustrating the role of TET3 in modulating the DDR response in healthy and fibrotic fibroblasts.....</i>	<i>70</i>
<i>Figure 37. Schematic representation of TET3 interaction partners analysed from the string database.</i>	<i>73</i>

IV. List of tables

<i>Table 1. Cell line used in the entire study.</i>	<i>16</i>
<i>Table 2. List of cell culture media and supplements used in this study.</i>	<i>16</i>
<i>Table 3. List of chemicals and reagents used in this study.</i>	<i>17</i>
<i>Table 4. List of consumables used in the study.</i>	<i>19</i>
<i>Table 5. Recombinant protein used throughout the experiment.</i>	<i>20</i>
<i>Table 6. List of primary antibodies used in this study.</i>	<i>21</i>
<i>Table 7. List of secondary antibodies used in this study.</i>	<i>21</i>
<i>Table 8. List of buffers used in the study.</i>	<i>22</i>
<i>Table 9. List of primers used in the study.</i>	<i>23</i>
<i>Table 10. List of commercially available kits used in the present study.</i>	<i>23</i>
<i>Table 11. List of commercially purchased plasmids used in the present study.</i>	<i>24</i>
<i>Table 12. List of equipment used in the present study.</i>	<i>24</i>
<i>Table 13. List of softwares used in the study.</i>	<i>26</i>

V. Abbreviations

2-OG-2 Oxy Glutarate	CD24-Cell Surface Glycoprotein 24
53BP1-Tumor Suppressor P53-Binding Protein 1	CD44-Cell Surface Glycoprotein 44
5caC-5-Carboxy Cytosine	ChIP-Chromatin
5fC-5-Formyl Cytosine	Immunoprecipitation
5hmC-5 Hydroxymethyl Cytosine	CHK1-Checkpoint Kinase 1
5hmC-5-Hydroxymethyl Cytosine	CHK2-Checkpoint Kinase 2
5mC-5 Methyl Cytosine	Col4a1-Collagen of Basement Membrane, Alpha-1 Chain
5mC-5-Methyl Cytosine	COL4A2-Collagen of Basement Membrane, Alpha-2 Chain
A431-Epidermoid carcinoma 431 cell line number	CpG-Cytosine Purine Guanine
ALK5-Activin A Receptor Type II-Like Protein Kinase Of 53kD	CRISPR-Clustered Regularly Interspaced Short Palindromic Repeats
AME-Adverse Maternal Environment	CTGF-Cellular Communication Network Factor 2
Ang-II-Angiotensin-II	CtIP-CtBP-interacting protein
ANOVA-Analysis of Variance	CVDs-Cardio Vascular Diseases
ATAC-Assay for Transposase-Accessible Chromatin using sequencing	Cys-Cysteine
ATM-Ataxia Telangiectasia Mutated	DAPI-4',6-diamidino-2-phenylindole
ATR-Ataxia Telangiectasia and Rad3-Related Protein	DDR-DNA Damage Repair
BamHI- <i>Bacillus amyloliquefaciens</i> Type II restriction endonucleases	D-loop-Displacement loop
BsmBI- <i>Bacillus stearothermophilus</i> Type II restriction endonucleases	DMEM-Dulbecco's Modified Eagle Medium
BSA-Bovine Serum Albumin V	DNA-Deoxy Ribo Nucleic Acid
BLM-BLM RecQ Like Helicase	DNA2-DNA Replication Helicase/Nuclease 2
BMP-7-Bone Morphogenetic Protein 7	DNA-PKcs-Protein Kinase, DNA-Activated, Catalytic Polypeptide
BRAP2-BRCA1 Associated Protein 2	DNMT1-DNA Methyltransferase 1
BRCA1-Breast and Ovarian Cancer Susceptibility Protein 1	DNMT3a-DNA Methyltransferase 3a
Brca1-Breast Cancer Type 1 Susceptibility Protein	DNMT3B-DNA Methyltransferase 3b
BRCA2-Breast and Ovarian Cancer Susceptibility Protein 2	dNTP- Deoxyribonucleotide Triphosphate
BrdU-5-bromo-2'-deoxyuridine	DPPA3-Developmental Pluripotency Associated 3
Cas9-CRISPR associated protein 9	DSBH-Double Stranded Break Helix
CaCl ₂ -Calcium Chloride	DSBs-Double Stranded Breaks
CCRA2-Cell Cycle and Apoptosis Regulator 2	DTT-Dithiothreitol
	ECM-Extra Cellular Matrix

EGFP-Enhanced Green Fluorescent Protein	KH ₂ PO ₄ -Potassium dihydrogen phosphate
ERK-Extracellular Related Kinase	KD-Knock Down
EXO1-Exonuclease 1	Ki67-proliferation marker protein
EZH2-Enhancer of Zeste 2	Ki-67
Polycomb Repressive Complex 2 Subunit	KU-Thyroid Autoantigen 70kD
FACS-Fluorescence-Activated Cell Sorting	LIG1-Ligase 1
Fe ⁺⁺ -Ferrous ion	LIG4-Ligase 4
G1-Gap 1	M-Molar
G2M-Gap2 Mitotic	MAPK-Mitogen Activated Protein Kinase
GAPDH-Glyceraldehyde-3-Phosphate Dehydrogenase	MCFs-Mouse Cardiac Fibroblasts
GC-Guanine Cytosine	MDA-MB231- M.D. Anderson Metastasis Breast cancer 231
GFP-Green Fluorescent Protein	MEK-Mitogen Activated Protein Kinase
GI-Genomic Instability	mg-Milli Gram
GSH-Glutathione	Mins-Minutes
GSSG-Glutathione Disulfide or Oxidized Glutathione	mL-Milli Litre
gRNA1-Guide RNA 1	MgSO ₄ -Magnesium Sulphate
gRNA2-Guide RNA 2	MOF-Ortholog Of Drosophila Males Absent on The First
GTPase-Guanine Tri Phosphatase	MRE11-Meiotic Recombination 11 Homolog 1
H&E- Haematoxylin/Eosin	MSH2-MutS Homolog 2
H ₂ O ₂ -Hydrogen Peroxide	MSH6-MutS Homolog 6
H3k27me3-Histone Lysine 27 Tri Methylation	MTS-Masson's Trichrome Stain
H3s10p-Histone 3 Serine 10 phosphorylation	MTT-(3-(4,5-dimethylthiazol-2-yl)-2,5-diphenyltetrazolium bromide
HCl-Hydrochloric acid	nM-Nano Molar
HEPES- 4-(2-hydroxyethyl)-1-piperazineethanesulfonic acid)	Na ₂ HPO ₄ ·7H ₂ O-Disodium hydrogen phosphate heptahydrate
Hi-C-High-Throughput Sequencing Capture	NaCl-Sodium Chloride
HMBG1-High Mobility Group Box 1	NaH ₂ PO ₄ -Sodium Dihydrogen Phosphate Monohydrate
HR-Homologous Recombination	NBS1-Nijmegen Breakage Syndrome 1
IDAX-Inhibition of the Dvl And Axin Complex	NCS-Neocarzinostatin
IF-Immunofluorescence	NER-Nucleotide Excision Repair
IL-1β-Interleukin 1 Beta	NHEJ-Non-Homologous End Joining
IL-4-Interleukin 4	nM-Nano Molar
IL-6-Interleukin 6	mM-Milli Molar
IR-Infra Red	ng-Nano Gram
I-Sce1-Intron-encoded endonuclease I-Sce I	NP-40-Nonyl
JNK-Janus Kinase	Phenoxyethoxyethanol

OE-Over Expression
 p300-E1A Binding Protein P300
 p53-Transformation-Related Protein 53
 PARP1-Poly (ADP-Ribose) Polymerase 1
 PBS-Phosphate Buffered Saline
 p-CHK2-Phosphorylated Checkpoint Kinase 2
 PI-Propidium Iodide
 PLA-Proximity Ligation Assay
 Pol λ -DNA Polymerase Lambda
 Pol μ -DNA Polymerase Mu
 PRMT5-Protein Arginine Methyltransferase 5
 PVDF-Poly Vinylidene Difluoride
 RAS-Rat Sarcoma
 RNA-Ribo Nucleic Acid
 RAD51-RecA, E. Coli, Homolog of Recombination Protein A 1
 RAD52-DNA Repair and Recombination Protein RAD52
 Rad54-DNA Repair and Recombination Protein RAD54
 RASAL1-Ras GTPase-Activating-Like Protein
 RASSF1A-Ras Association (RalGDS/AF-6) Domain Family Member 1
 RFP-Red Fluorescent Protein
 ROS-Reactive Oxygen Species
 RPA-Replication Protein A
 RPL4-Ribosomal Protein L4
 RPM-Revolution Per Minute
 S-Synthesis Phase
 SEC-Seconds
 SD-Standard Deviation
 SEM-Standard Error of Mean
 Sin3a-SIN3 Transcription Regulator Family Member A
 SMAD-Small Mothers Against Decapentaplegic
 SMAD1- Small Mothers Against Decapentaplegic 1
 SMAD3-Small Mothers Against Decapentaplegic 3
 SMAD4-Small Mothers Against Decapentaplegic 4
 SMAD5-Small Mothers Against Decapentaplegic 5
 SNIP1-Smad Nuclear-Interacting Protein 1
 SSBs-Single Stranded Breaks
 ssDNA-Single Stranded DNA
 TAK1-Transforming growth factor beta-activated kinase 1
 TBST-Tris-Buffered Saline Tween-20
 TBS-Tris Buffered Saline
 TDG-Thymine DNA Glycosylase
 TET1-Tet methylcytosine dioxygenase 1
 TET2-Tet methylcytosine dioxygenase 2
 TET3 KD-Tet methylcytosine dioxygenase 3 Knockdown
 TET3 OE-Tet methylcytosine dioxygenase 3 Overexpression
 TET3-Tet methylcytosine dioxygenase 3
 Tgfr1/2-Transforming growth factor Beta Receptor one or two
 TGF- β 1-Transforming Growth factor Beta1
 TGF- β 2-Transforming Growth factor Beta2
 TGF- β 3-Transforming Growth factor Beta3
 TGF- β -Transforming Growth Factor Beta
 T β RI-Transforming growth factor Beta Receptor One
 T β RII-Transforming growth factor Beta Receptor Two
 WHO-World Health Organisation
 WB-Western Blot
 XRCC1-X-Ray Repair Cross-Complementing Protein 1
 XRCC4-X-Ray Repair Cross-Complementing Protein 4
 XLF-Non-Homologous End Joining Factor 1

Zn⁺⁺-Zinc divalent ion
α-SMA-Alpha 2 Smooth Muscle
Actin
γ-H2AX-Histone 2AX Serine 139
Phosphorylation

°C-Degrees Celsius
μg-Micro Gram
μL-Micro Litre
μM-Micro Molar
μmol-Micro Mole

Abstract

Activation and proliferation of cardiac fibroblasts are the prime mediators of cardiac fibrosis. Existing studies show that ROS and inflammatory cytokines produced during fibrosis not only signal proliferative stimuli but also contribute to DNA damage. Therefore, as a prerequisite to maintain sustained proliferation in fibroblasts, activation of distinct DNA repair mechanism is essential. We have previously shown a protective epigenetic role of TET3 in organ fibrosis. Here, we demonstrate that TET3 additionally impacts DNA damage response (DDR) mechanisms via orchestrating checkpoint-assisted homologous recombination (HR)-mediated DDR, and that TGF- β , in combination with lack of TET3 in cardiac fibrosis, leads to an increase of a checkpoint-arrest independent non-homologous end joining (NHEJ) DDR. Finally, we provide evidence that overexpression of TET3 reduces the increased proliferation rate of fibrotic fibroblasts by shifting the DDR response from NHEJ to HR.

1. Introduction

1.1 Cardiovascular diseases and cardiac fibrosis

Cardiovascular disease is the leading cause of death worldwide. A recent statistic released by the WHO accounts an estimated 17.9 million deaths from CVDs, representing 48 % of the worldwide mortality (Mendis et al, 2011; WHO, 2018). Notably, almost all forms of CVDs are aggravated by and associated with cardiac fibrosis (Hinderer & Schenke-Layland, 2019). Cardiac fibrosis is a scarring process characterised by excessive accumulation of extracellular matrix (ECM) proteins that can lead to increased myocardial stiffness eventually resulting in impaired systolic and diastolic function in the heart (Ho et al, 2010; Rockey et al, 2015; Travers et al, 2016).

ECM in the heart is primarily composed of collagen I (mostly confers strength) and collagen III (mostly confers elasticity) which predominantly provide the fundamental structural network to deliver strength and elasticity to the myocardium (Berk et al, 2007; Kong et al, 2014). Besides providing strength and elasticity to the myocardium, ECM also serves as a homeostatic buffer for growth factors and cytokines, facilitating intracellular crosstalk within the myocyte and non-myocyte cells (Fan et al, 2012; Li et al, 2018). Increased accumulation of ECM during fibrotic progression causes enhanced stiffening of the heart muscles and impairs normal physiological systolic and diastolic functions in the organ (Kim et al, 2000). Therefore, a proper balance between the deposition and degradation of ECM is essential in healthy hearts.

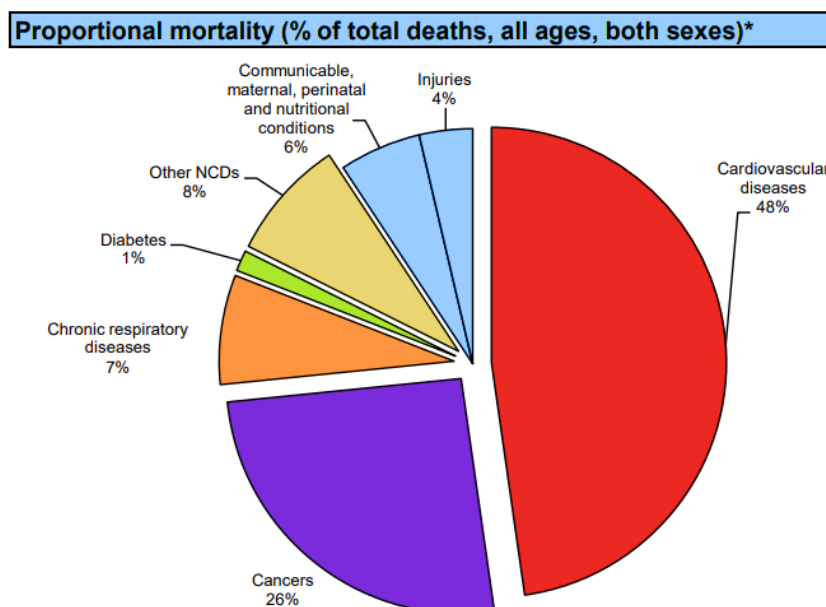


Figure 1. Pie-chart showing overall mortality % (worldwide) in both men and women due to various diseases. Data adapted from WHO (WHO, 2018).

1.1.1 Types of cardiac fibrosis

Fibrosis in the heart has been described to develop in two possible ways (a) reactive (b) reparative/replacement fibrosis (Brilla & Weber, 1992; Liu et al, 2017). Reparative fibrosis occurs in response to injury during myocardial infarction (Lopez et al, 2001). In myocardial infarction dead cells (mostly cardiomyocytes) accumulate due to untimely apoptosis or necrosis in the infarcted area, which are then removed and replaced by excessive deposition of non-myocyte cells to form a scar (Desmoulière et al, 1995; Piek et al, 2016). Excessive apoptosis and necrosis during chronic infarction release a lot of cytokines (such as TGF- β , IL-4 and IL-6) that in the end result in pathological fibrosis in the heart (Chiong et al, 2011; Greulich et al, 2019; Saraste et al, 1997). Although such scarring process is initiated to preserve the structural integrity of the organ, excessive scarring due to chronic injury eventually leads to impaired cardiac function.

In contrast to reparative fibrosis, reactive fibrosis mostly occurs in response to mechanical stress, pressure overload or due to changes in neuro-hormonal signalling cascade but acute cell loss is absent (Liu et al, 2017; Talman & Ruskoaho, 2016). Initiation of reparative fibrosis leads to excessive deposition of extracellular matrix proteins by activated fibroblasts without causing a significant loss of cardiomyocytes.

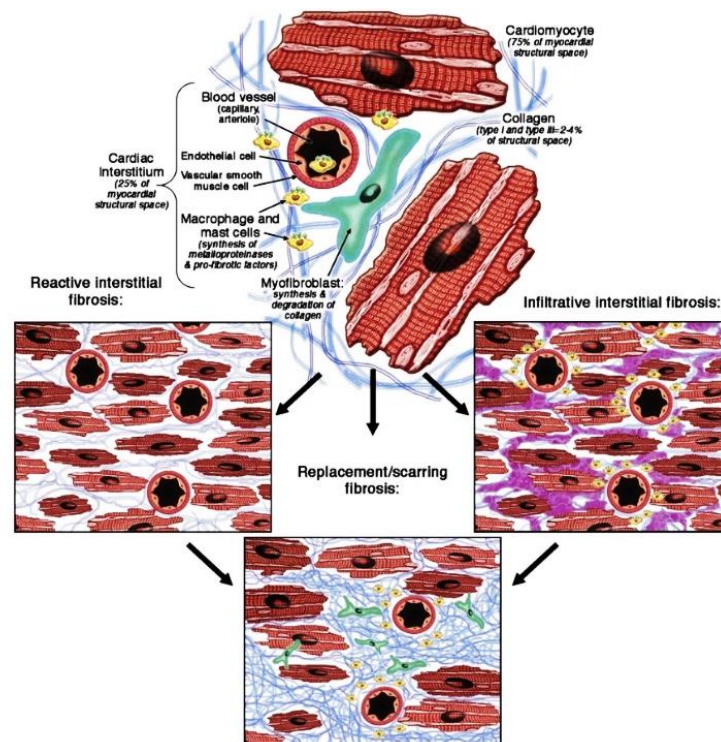


Figure 2. Schematic representation of replacement and repair cardiac fibrosis. Adapted from Mewton et al. (Mewton et al, 2011). Copy right license number 4704831089992.

1.1.2 Cardiac Fibroblasts

The heart as an organ is composed of two major cell types, cardiomyocytes and non-myocytes (Zhou & Pu, 2016). Fibroblasts belong to the non-myocytic population that plays a prime role in fibrogenesis (Humeres & Frangogiannis, 2019; Travers et al, 2016). During pathological remodelling, fibroblasts are activated and undergo transformation to activated fibroblasts (also known as myofibroblasts) (Kong et al, 2014). The activated fibroblast in turn secretes several cytokines, growth factors, reactive oxygen species, ECM proteins and matrix metalloproteinases that disrupt proper function of the heart (Chen & Frangogiannis, 2013; Shinde & Frangogiannis, 2014). Cardiac fibroblasts are diffusely interspersed between cardiomyocytes and recent studies show they play a crucial role in transmission of electrical signals in the myocardium (Zhang et al, 2012). A recent *in vitro* study indicates that cardiac fibroblasts exchange electrical signals between cardiomyocytes via connexin 43, which helps in spontaneous synchronization of beating in distant cardiomyocytes.

Although the actual number of fibroblast population in the heart is still not clear, it is estimated to comprise 11-15 % of the total cell population in the adult mouse heart and about 55-65 % in the adult rat heart (Zhou & Pu, 2016). Lineage tracing studies in pressure overload induced mouse models demonstrate that 15-20 % of the fibrotic fibroblasts in the ventricles are derived primarily by endothelial cells whereas the rest 80-85% of the total fibrotic fibroblasts are derived from either epicardial cells or the resident fibroblasts (Kanisicak et al, 2016; Moore-Morris et al, 2014; Zeisberg et al, 2007). Interestingly, the origin of cardiac fibroblasts in each species are quite distinct, hence its distribution of population in heart is extremely heterogeneous in nature (Zeisberg & Kalluri, 2010).

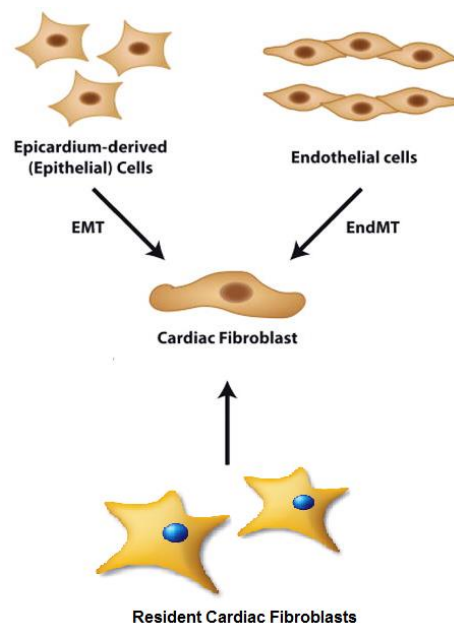


Figure 3. Schematic illustration showing the source of cardiac fibroblasts.

Adapted and modified from Krenning et al. (Krenning et al, 2010). Copy right license number 4704831415631.

1.1.3 The role of TGF- β in fibroblast activation

TGF- β is considered to be one of the critical cytokines released in the fibrotic heart that plays a central role in the activation and proliferation of cardiac fibroblasts (Khalil et al, 2017; Liu et al, 2017). Activated fibroblasts are also known as myofibroblasts whose primary role during fibrotic response is to secrete excessive extracellular matrix proteins, inflammatory cytokines and ROS that casually contributes to more damage in the myocardium (Humeres & Frangogiannis, 2019; Humeres et al, 2016). There are three isoforms of TGF- β in mammals, i.e. TGF- β 1, TGF- β 2 and TGF- β 3, of which TGF- β 1 is the most predominant (Wu et al, 2018). Three separate genes encode the three isoforms but all three genes share a high degree of homology (Frank et al, 1996). All the three isoforms are secreted as an inactive form and are activated after proteolytic cleavage (Shi et al, 2011). Once activated, TGF- β mediates its effect via binding to its receptors T β RI, (also known as ALK5) and T β RII resulting in phosphorylation of Smad2/3 (Hayashi & Sakai, 2012). Activated Smad2/3, in turn, binds to Smad4 resulting in translocation into the nucleus (Chen et al, 2005). Once the phosphorylated smad 2/3/4 complex enters the nucleus and binds to genomic DNA, it facilitates transcription of essential genes involved in fibrogenesis (Khalil et al, 2017). Recent studies have shown that fibroblast-specific deletion of Tgfbr1/2 or Smad3, but not Smad2, results in an attenuated fibrotic response in a pressure overload-induced cardiac fibrosis model. This clearly signifies the importance of activated TGF- β signalling pathway in regulating the fibrotic progression (Khalil et al, 2017). Studies also demonstrate that independent of its smad mediated transcription activities, TGF- β can activate various signalling cascades like TGF- β -activated kinase 1 (TAK1), extracellular signal regulated kinase (Erk), p38 Mitogen activated protein kinase (MAPK), c-Jun-N-terminal kinase (JNK), and GTPase pathways (Zhang, 2009). Previous studies show that transient activation of the RAS/MEK/ERK cascade by TGF- β results in increased CTGF expression, actin stress fiber formation and ECM contraction (Chatzifrangkeskou et al, 2016).

1.2 EPIGENETIC REGULATION OF CARDIAC FIBROSIS

1.2.1 Epigenetics

Studies since the last two decades have highlighted the critical role of epigenetics in deciphering the nature and cause of dynamic heterogeneous changes in gene expression profiles associated with unchanged DNA sequences (Nicoglou & Merlin, 2017). Ongoing studies have shown that epigenetic changes in heart during pathological disease state such as fibrosis can lead to invariant change in gene expression regulated either at DNA, histone or at transcriptome levels (Kmietczyk et al, 2019; Mathiyalagan et al, 2014; Tao et al, 2014). Interestingly, although epigenetic changes are heritable, they are also reversible in nature owing to the presence of

numerous epigenetic writers and erasers (Nicoglou & Merlin, 2017). Numerous emerging studies confirm the role of epigenetic factors in programming the activation and proliferation of cardiac fibroblasts during cardiac fibrosis (Felisbino & McKinsey, 2018). A recent study in a pressure overload induced cardiac fibrosis model highlights the role of histone acetylation in regulating the expression of proliferative genes such as p15 and p57 to maintain a sustained proliferation of cardiac fibroblasts during fibrosis (Williams et al, 2014). Similarly, another study demonstrates the effect of inhibition of p300 histone acetyltransferase in blocking the proliferative response of cardiac fibroblasts during fibrogenesis. Evidence also highlight the role of DNA methylation in cardiac fibrosis (He et al, 2019; Olsen et al, 2017). A previous study by our group has demonstrated that increased hypermethylation of RASAL1 (a key anti-fibrotic gene) leads to aggravation of fibrosis by enhancing the endothelial to mesenchymal transition, resulting in increased activated fibroblast deposition (Xu et al, 2015). In the same study it is reported that treatment of fibrotic hearts with BMP-7 can attenuate the progression of cardiac fibrosis by erasing the methyl mark at the RASAL1 promoter through increased expression of DNA demethylase TET3. Another study in rat cardiac fibroblasts demonstrate that increased fibroblast activation is associated with decreased RASSF1a expression due to promoter methylation of the gene by DNMT1 (Tao et al, 2014). Moreover, the same study reports that fibroblast activation can be blocked by expressing RASSF1a by treating with DNMT inhibitor 5-aza-2'-deoxycytidine. All these studies strongly suggest the involvement of epigenetic signatures in regulating cardiac fibrosis. Altogether from the above studies, DNA methylation and demethylation are emerging as one of the key epigenetic modification that can be exploited therapeutically to restrain or even revert cardiac fibrosis.

1.2.2 TET enzymes

One of the breakthroughs in solving the riddle of active demethylation process came to light in early 2009 with the discovery of TET enzymes, best known for their ability to convert 5mC to 5hmC, 5fc and 5caC (Tahiliani et al, 2009). TET enzymes are called after the ten-eleven translocation (t (10;11) (q22; q23)), found in cases of patients suffering from acute myeloid and lymphocytic leukemia (Tahiliani et al, 2009). Emerging studies have emphasized the role of TET proteins in diverse cellular processes like gene transcription, stem cell differentiation, immune cell maturation, embryonic development, proliferation, DDR and so on, making them a potential gene of interest in the field of development and diseases (Rasmussen & Helin, 2016; Tan & Shi, 2012). However, the molecular mechanism orchestrated in such diverse biological process by the TET proteins is still not precisely understood.

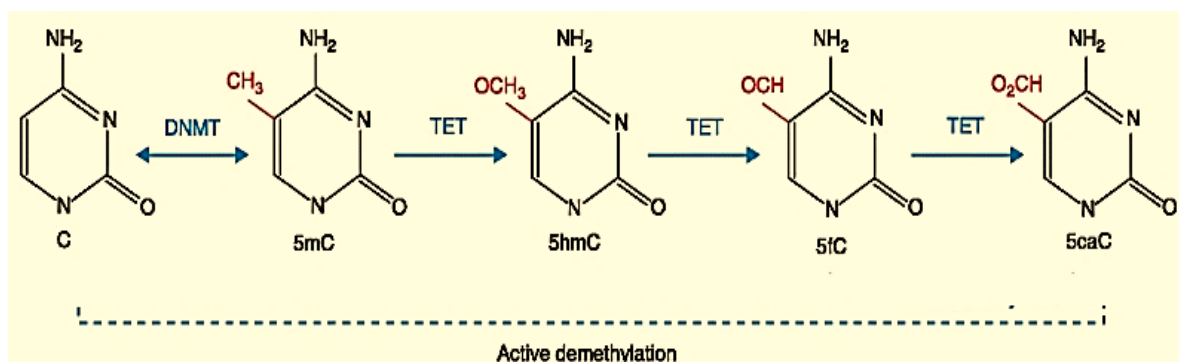


Figure 4. Schematic representation showing active DNA demethylation process catalyzed by the TET enzymes in *Homo sapiens*.

Source image is adapted from Scourzic et al. (Scourzic et al, 2015). Figure was re-created using chem-sketch due to copy right issue.

1.2.3 TET isoforms and mechanism of action

The mammalian TET family consists of three isoforms, namely TET1, TET2 and TET3. The catalytic domain is evolutionarily conserved in all the TET isoforms and harbors a double-stranded β helix domain (DSBH) and a cysteine-rich region before the DSBH (Melamed et al, 2018). The DSBH domain serves as binding site for protein-protein interaction and harbors binding sites for the cofactors 2-oxoglutarate (2-OG) and Fe (II) (Wu & Zhang, 2017). The cysteine-rich domain contains the binding site for the metal Zn^{++} , which provides stability to the overall structure of TET proteins (Wu & Zhang, 2017). Unlike other cysteine-rich domain-containing proteins, the TET proteins cysteine-rich region does not form an independent motif but instead enfolds within the DSBH (Yin & Xu, 2016). The TET proteins employ a flipping mechanism to position the methylated cytosine to their catalytic pocket. Once flipped into a precise position, the target base orients towards the Fe^{++} and 2-OG catalyzing the DNA oxidation reaction. The amino terminus of both TET1 and TET3 contains the CXXC domain, which is involved in binding to methylated CpG sites (Melamed et al, 2018). However, TET2 lacks a conserved CXXC domain, which is hypothesized to be missing due to gene conversion and duplication events during evolution (Akahori et al, 2015). Recent studies demonstrate that TET2 can still bind to the DNA with the help of IDAX domain (Ko et al, 2013). The difference in TET proteins is not confined to its structure but also to their distinct expression pattern around a wide range of tissues (Melamed et al, 2018).

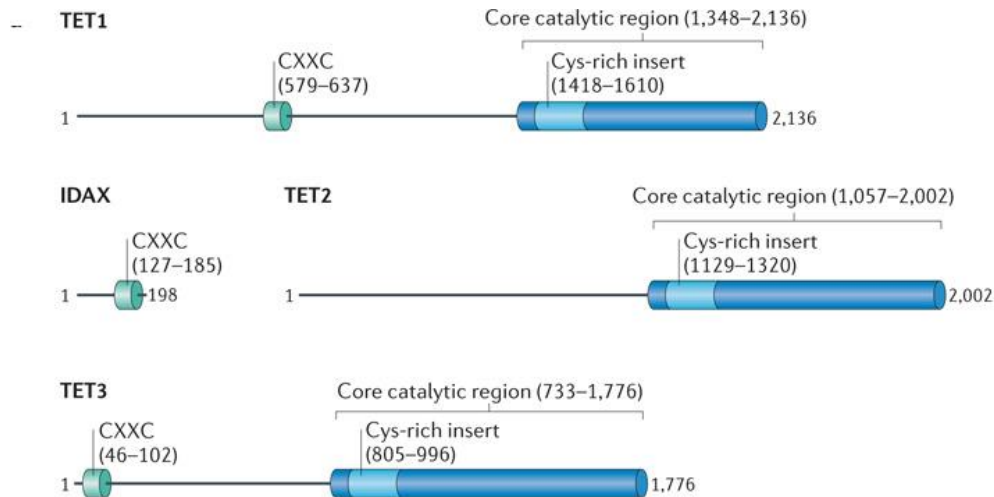


Figure 5. Schematic illustration of TET enzymes in *Homo sapiens*.

Source image is adapted from Pastor et al. (Pastor et al, 2013), Copy right license number 4704840422098. There are three isoforms of TET proteins, namely TET1, TET2 and TET3. All TET isoforms have a conserved catalytic domain in the C-terminus. TET1 and TET3 have CXXC domain in their N-terminus, which is absent in TET2.

1.2.4 Role of TETs in cardiovascular diseases

One of the primary functions of TET enzymes is their ability to hydroxymethylate DNA. Emerging evidence shows that the change in DNA hydroxymethylation pattern is associated with increased cardiac hypertrophy in a pressure overload model of heart failure (Greco et al, 2016). Change in DNA hydroxymethylation pattern suggests an alteration in the expression of TET enzymes. TET enzymes are thus emerging as new players in cardiovascular diseases (Felisbino & McKinsey, 2018). Studies demonstrate that loss of TET2 results in aggravation of inflammation and ameliorates endothelial cell dysfunction in atherosclerotic mouse models (Liu et al, 2013). Another study shows that loss of TET2 in hematopoietic or myeloid cells in pressure overload-induced heart failure models worsens cardiac fibrosis and concomitant increase in the expression of interleukin-1beta (IL-1 β) (Fuster et al, 2017). The findings support that mutations in TET2, in hematopoietic or myeloid cells are associated with increased risk of coronary heart diseases (Fuster et al, 2017).

Additionally, a study by our group demonstrates that BMP7 mediated expression of TET3 can rescue cardiac fibrosis via re-expression of RASAL1 (an essential gene silenced during cardiac fibrosis) in pressure overload-induced mouse model (Xu et al, 2015). Another study shows adverse maternal environment (AME) alters TET expression in the heart and increases the risk of cardiac fibrosis (Spearman et al, 2018). However, it is interesting to note that so far, there are no reports to link the role of TET1 in cardiovascular diseases (Spearman et al, 2018). Since the heart is comprised of a heterogeneous population of cells, it is not entirely clear whether TET isoforms are expressed globally or in a cell type-specific manner. Moreover, recent studies in cancer models demonstrate that all the isoforms of TET orchestrate different functions, so it

would be interesting to understand the role of TET proteins as facilitators or effectors of cardiovascular disease progression (Rawluszko-Wieczorek et al, 2015).

1.3 DNA DAMAGE

Exposure to a variety of endogenous as well as exogenous stimuli poses a constant threat to the genomic DNA to form DNA lesions (Norbury & Hickson, 2001). Depending on the source, the DNA lesions generated can either be single-stranded or double-stranded. DNA is the blueprint of life (Hakem, 2008). Unrepaired DNA lesions can lead to increased replication stress, mutations, decreased proliferation, premature apoptosis, threatening the genomic integrity and hence the survival of the cell itself (Eastman & Barry, 1992). To ensure genomic stability, cells have evolved stringent checkpoints and associated DNA damage repair response (Zhou & Elledge, 2000). The DNA damage repair response is a highly dynamic and complicated process. It is regulated at three fundamental levels by a distinct set of proteins (Maréchal & Zou, 2013).

- (i) Sensors- recognizing the DSBs (e.g. mre11-rad50-nbs1 complex)
- (ii) Transducers- signalling at the DSBs (e.g. ATM and ATR)
- (iii) Effectors and mediators- repair factors recruited at the DSBs (e.g. 53BP1 or RAD51), cell cycle checkpoint kinases activators in response to DSBs (e.g. CHK1 and CHK2).

A flaw in any of these fundamental points may contribute to disease and affects cell survival.

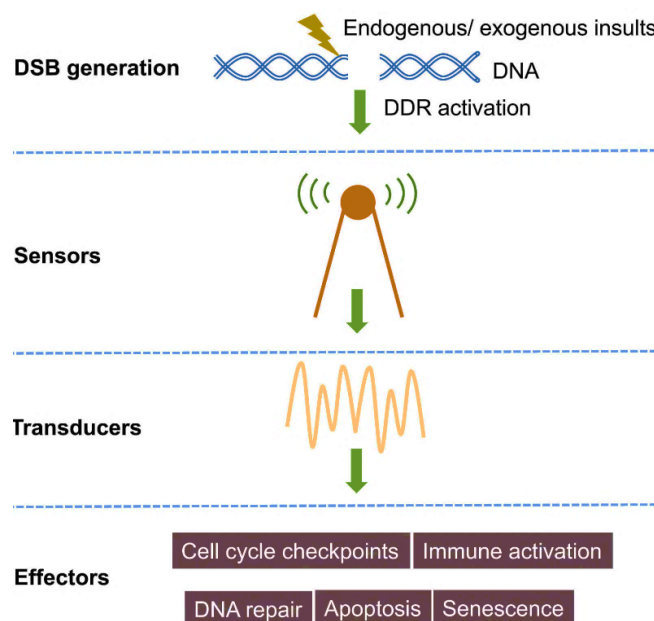


Figure 6. Schematic representation of DNA damage repair response.

Source image is adapted from Srinivas et al. (Srinivas et al, 2019). Copy right license is not required, as the publisher granted the represented image free to be reused.

1.3.1 DNA repair response

Of all the types of DNA lesions encountered by the cells, DSBs poses an extreme threat, and if left unresolved becomes harmful for the survival of the cells (Mehta & Haber, 2014). DSBs in cells are repaired predominantly by the two redundant repair response pathways NHEJ (Non-Homologous-End-Joining) and Homologous recombination (HR) (Kakarougkas & Jeggo, 2014).

1.3.2 Non-Homologous-End-Joining repair response pathway

NHEJ is a template-independent fast DDR response pathway that mediates direct ligation of two broken ends of DNA (Davis & Chen, 2013). NHEJ operates in a template-independent manner; hence, it is actively available to resolve DNA DSBs in all phases of the cell cycle (Davis & Chen, 2013; Delacote & Lopez, 2008). The NHEJ works in four sequential steps described

- i. DNA damage end recognition and assembly of NHEJ repair factors at DSBs.
- ii. Promotion of stability around DSBs.
- iii. Short DNA end processing.
- iv. End ligation of broken and processed DNA ends.

The first step in NHEJ is the recruitment of Ku heterodimers to the sites of DSBs. Ku heterodimers have a very high affinity (binding constant of $2 \times 10^9 \text{ M}^{-1}$) towards binding to broken DNA DSBs ends (Lee et al, 2016). Ku heterodimer are comprised of Ku70 and Ku80 subunits After binding to DNA ends, Ku complex serves as a docking site for the recruitment of nucleases and NHEJ core repair factors (Lee et al, 2016). The next step facilitated by the Ku complex is to promote the stability around DSBs to prevent the untimely collapse of the DNA ends (Krasner et al, 2015). DNA stability at the broken ends, in part by Ku complex, is facilitated by the recruitment of the catalytic subunit of DNA dependent protein kinase (DNA-PKcs) (Lee et al, 2016). Upon binding to DNA DSBs, DNA-PKcs gets auto-phosphorylated, which in turn facilitates the phosphorylation of NHEJ repair factors like 53bp1 (Callén et al, 2009). DNA-Pkcs not only promote phosphorylation of repair proteins but also timely recruitment and release of nucleases such as Artemis to enable proper trimming of broken ends (Jiang et al, 2015). Once the broken DNA ends are processed, DNA polymerases Pol μ or Pol λ are recruited to fill the gap (Ramsden, 2011). The last and essential step in NHEJ is to ligate the processed broken ends. The process initiates via recruitment of scaffolding protein XRCC4 which forms a docking site for the recruitment of DNA ligase IV (Ahnesorg et al, 2006). XRCC4 stabilizes DNA ligase IV by promoting its adenylation (Davis & Chen, 2013). NHEJ pathway is active throughout the cell cycle (Davis & Chen, 2013). However, it is highly favored to operate in G1 cells. NHEJ is a fast repair process but it is error-prone and can also result in increased insertions, deletions and substitutions (Davis & Chen, 2013).

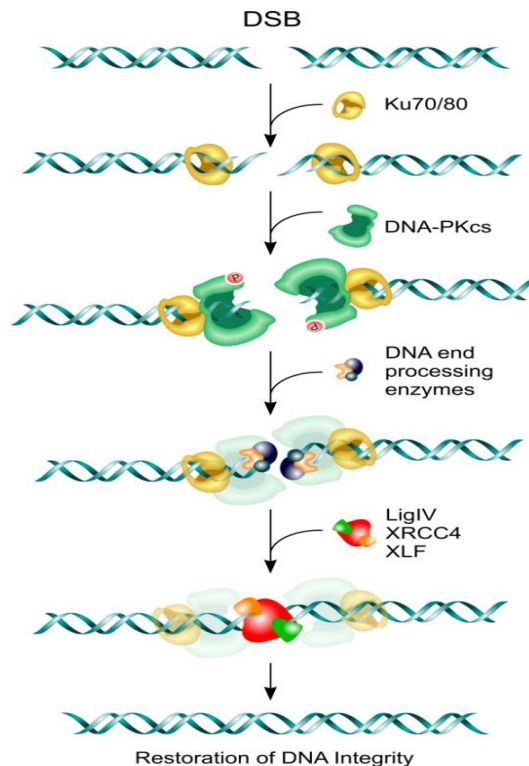


Figure 7. Schematic representation of NHEJ-mediated DNA repair pathway.

Source image is adapted and modified from Iliakis et al. (Iliakis et al, 2015). Copy right license number 1002992-1. In response to DNA DSBs, KU70 heterodimer complex is recruited to the site of DNA damage. KU70 complex in turn recruit's DNA-PKcs and other DNA end processing enzymes that aid in stabilizing the DNA breaks and prepare for repair. DNA polymerases are recruited to fill in the gaps and in the end DNA ligase4 and XRCC4 help in ligating the broken ends.

1.3.3 Homologous-Recombination repair response pathway

HR is a slow, template-dependent high-fidelity DDR response pathway that predominantly operates in the S and G₂/M phases of the cell cycle (Norbury & Hickson, 2001). HR plays a crucial role in maintaining genomic integrity in mitotically active cells (Moynahan & Jasin, 2010). Additionally, HR facilitates recovery from stalled replication forks, implicating their role in avoiding unwanted replication stress (Ait Saada et al, 2018). HR works in four sequential steps described as

- i. Enzymatic resection of DNA DSBs end.
- ii. Recruitment of nucleoprotein filaments to stabilize broken DNA ends.
- iii. Search for homologous daughter strand, followed by invasion to initiate repair of the broken DNA ends.
- iv. Synthesis of DNA repair at the DSBs.
- v. Resolution of repair intermediates to complete the repair at DSBs.

The first step in the HR repair response is the processing of broken DNA ends to generate 3' single-stranded DNA (ssDNA) overhangs. This process is widely known as DNA end resection and is carried out by the action of 4 enzymes (Huertas, 2010).

- (a) MRN complex,
- (b) Exonuclease 1 (EXO1),
- (c) DNA2, and
- (d) CtBP-interacting protein (CtIP).

Once the ssDNA ends are generated, heterotrimeric Replication Protein A (RPA) complex recruits to the 3' ssDNA end to prevent the formation of loops and secondary structures (Polo & Jackson, 2011). Recruitment of RPA complex follows the loading of RecA, E. Coli and Homolog of Recombination Protein A (RAD51). RAD51 is an essential monomeric protein complex that binds to the resected end of ssDNA tails and facilitates sister-chromatid strand invasion (Ma et al, 2017). Completion of strand invasion is followed by the formation of displacement loop (D-loop). In the end, replicative polymerase δ uses the invading strand as a primer to initiate DNA synthesis to fill up the gaps (Delacote & Lopez, 2008).

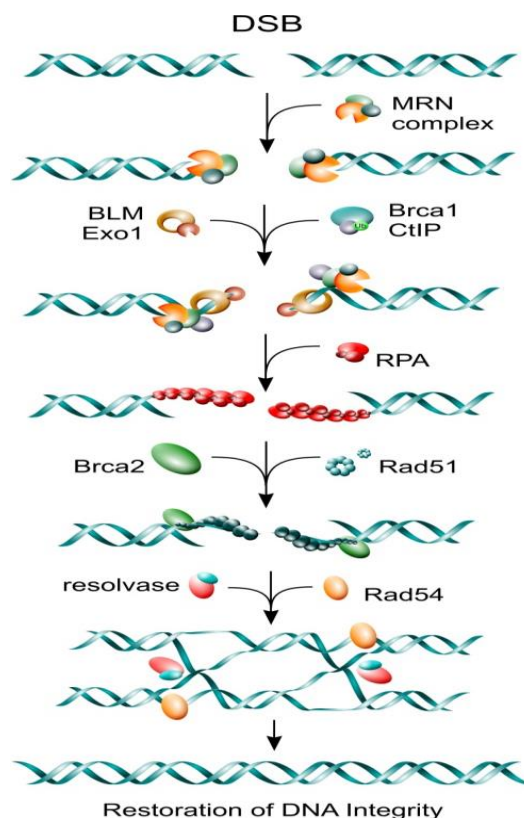


Figure 8. Schematic representation of HR-mediated DNA repair pathway.

Source image is adapted and modified from Iliakis et al. (Iliakis et al, 2015). Copy right license number 1002992-1. In response to HR mediated DNA repair, MRN complex is recruited to the site of DNA DSBs. MRN complex in turn recruits BRCA1, CtIP to process the DNA ends. Such processing of DNA ends is known as DNA end resection and it plays a key role in recruiting RPA1 and RAD51 to mediate homology strand search and initiate DNA repair. In the end, resolvases and DNA ligating enzymes are recruited to complete the ligation process.

1.4 ROLE OF DNA DAMAGE AND REPAIR IN CARDIOVASCULAR DISEASES

Studies highlighting the role of DNA damage as an independent factor for the development of cardiovascular diseases are emerging. In line with these observations, it is reported that Ku70^{-/-} (Ku70 is an essential component of NHEJ DDR response) knockout in mice results in cardiac hypertrophy. Similarly, ATM^{-/-} (the upstream DNA damage sensor kinase) knockout in mice aggravates the progression of cardiac fibrosis (Foster et al, 2012). A recent study in pressure overload-induced mouse model demonstrates loss of XRCC1 and PARP1 in cardiomyocytes causes increased single-stranded break accumulation and acute inflammation in the failing heart (Higo et al, 2017).

Interestingly, the presence of single nucleotide polymorphism in DNA repair genes is also associated with an increased risk of cardiovascular diseases. Such as single nucleotide polymorphism in the RAD52 gene (involved in HR repair) increases the risk of mortality in cardiovascular patients (Lenart et al, 2017). Single nucleotide polymorphism in BRAP2 (a protein involved in HR) is associated with increased risk of myocardial infarction. Similarly, single nucleotide polymorphism in BRAP2 causes right ventricular hypertrophy (Ozaki et al, 2009). A study in anthracycline-induced cardiac failure demonstrates BRCA2 (a protein involved in HR) deficiency promotes cardiomyocyte apoptosis (Singh et al, 2012).

Additionally, failing or aging hearts are also reported to demonstrate a decrease in NHEJ efficacy in cardiac fibroblasts (Vaidya et al, 2014). Loss of function studies show that HMGB1 (a non-histone chromatin protein) is associated with increased clearance of DNA DSBs in a fibrotic heart (Takahashi et al, 2019). An exciting aspect of all of these studies is that the role of DNA damage and repair responses are widely studied mostly in cardiomyocytes. However, the impact of DNA damage on cardiac fibroblasts is not entirely clear. Hence, more investigation is necessary to understand the role of DNA damage and repair in fibroblasts, as these are the principal mediator of cardiac fibrosis.

1.5 ROLE OF TGF- β IN DNA DAMAGE AND REPAIR RESPONSES

TGF- β is a pleiotropic cytokine that coordinates several cellular processes (Liu et al, 2017). TGF- β is also emerging as one of the new players in facilitating DDR responses (Barcellos-Hoff & Cucinotta, 2014). Studies in murine keratinocytes demonstrate loss of TGF- β contributes to the genomic instability independent of p53 activation (Lin et al, 2012). Studies show that loss of TGF- β in a human microvascular endothelial cell line drives centrosome aberration and aneuploidy (Langenkamp & Molema, 2009). Similarly, smad4 deficiency in the presence of TGF- β signalling in murine lung tumors impairs clearance of DNA DSBs (Haeger et al, 2016). Increased

expression of TGF- β in MDA-MB231 cells is reported to decrease HR repair efficacy but results in decreased DNA DSBs due to its effect on downregulating the damage sensors ATM and MSH2 (Pal et al, 2017). Interestingly, in A431 carcinoma cells, TGF- β is reported to increase the cell survival against ionizing radiation-induced DNA DSBs via switching to accelerated NHEJ DDR (Lee et al, 2016). The same study also demonstrates that such accelerated NHEJ in A431 cells is due to increased expression of Lig4, a key NHEJ repair factor (Lee et al, 2016). Apart from its role in HR and NHEJ, studies have also demonstrated active involvement of TGF- β in NER and alt-NHEJ (Liu et al, 2018; Zheng et al, 2019). Altogether these results show that aberrant TGF- β signalling poses a potential threat to genomic instability due to impact on the DNA damage and repair response. Increased expression of TGF- β is known to contribute to activation and proliferation of cardiac fibroblasts during fibrosis (Liu et al, 2017). However, the contribution of TGF- β in facilitating the DDR response in the fibrotic fibroblast has not been studied.

1.6 ROLE OF TETs IN DNA DAMAGE AND REPAIR RESPONSES

TET (TET1/2/3) proteins are emerging players in orchestrating the DNA damage and repair responses in eukaryotic cells (Chen et al, 2018; Kuhns et al, 2019; Zhang et al, 2017). A study in glial cells shows loss of TET1 results in activation of G2M arrest and harbors endogenous increase in DNA DSBs even in the absence of genotoxic stress (Coulter et al, 2017; Kuhns et al, 2019). A study in mouse embryonic stem cells demonstrates that TET1 forms a complex with Sin3a and MOF to regulate the expression of DNA repair genes (Zhong et al, 2017). Notably, the same study reports that loss of TET1 also leads to increased DNA DSBs in the absence of external DNA damage, which is consistent with the previous observation in human glial cells (Coulter et al, 2017; Zhong et al, 2017). Loss of TET1 results in a decrease in both HR and NHEJ efficacy, suggesting their role in DNA DSBs repair response pathways (Zhong et al, 2017). In p53 mutated lung cancer cell lines, knockdown of TET1 is reported to result in increased DNA damage, slower cell growth, and increased genomic instability (Filipczak et al, 2019). In mouse Purkinje cells ATM-mediated stabilization of TET1 is reported to contribute to efficient repair of DNA DSBs (Jiang et al, 2015).

In myeloid malignancies, TET2 mediated hydroxymethylation results in recruitment of MSH6 (a protein involved in DNA mismatch repair) to the DNA damage sites (Greenberg et al, 2017). Moreover, a study shows loss of TET2 causes defects in chromosome segregation and decrease of BRCA2 (involved in HR repair) mRNA expression (Kafer et al, 2016). In human bone osteosarcoma epithelial cell lines TET2 interacts with SMAD nuclear interacting protein 1 (SNIP1) to regulate the expression of DNA damage repair genes (Chen et al, 2018). Additionally, a recent report demonstrates that ATR mediated stabilization of TET3 is involved in DNA repair (Jiang et al, 2017). The same study further reports that TET3 facilitates DNA repair via its catalytic activity to form new 5hmC marks at sites of DNA damage and its loss

harbors increased endogenous DNA damage. However; the study sheds no light on whether TET3 is recruited directly to the DNA damage sites or its involvement in the choice of DNA repair (Jiang et al, 2017). A TET2 and TET3 double knock out in myeloid cells is also reported to increase DNA DSBs in the absence of external damage (An et al, 2015). The same study also demonstrates change in expression of DNA repair genes in the state of TET2 and TET3 double knockout. Altogether, these studies clearly show an association between the interplay of TETs and DNA damage repair response proteins in facilitating or fine-tuning the DNA repair to ensure genomic instability. However, how the cells decide to use the TET isoforms in different phases of DNA repair is not entirely clear and needs further investigations.

1.7 AIMS OF THESIS

The fibrotic microenvironment regularly produces ROS and cytokines that continuously damage the DNA resulting in production of SSBs or DSBs. DSBs are highly deleterious lesions and so far, their effect on cardiac fibrosis are not entirely clear. Notably, in response to DSBs most cells are programmed to halt the cell cycle until the DNA lesions are resolved. However, cardiac fibroblasts proliferate in an increased DNA DSBs niche during fibrosis. Therefore, it is important to understand how fibroblasts are able to proliferate despite increased DNA damage. The fibrotic progression is also associated with change in epigenetic marks. In line with these observations, our group has previously observed that TET3 can ameliorate fibrotic progression in both murine models of cardiac and renal fibrosis. Recent studies are highlighting a role of TET3 in DNA damage and repair response. These observations lead us to hypothesize that TET3 may prevent aberrant proliferation of fibroblasts via regulating the DDR response. In line with these ideas, the present study aims to investigate:

1. a potential association of TET3 and DNA damage in healthy and fibrotic cardiac fibroblasts
2. the role of TET3 in engaging the choice of DNA repair in healthy and fibrotic cardiac fibroblasts
3. how loss of TET3 in the pro-fibrotic niche impacts proliferation of cardiac fibroblasts

2. MATERIALS AND METHODS

2.1 Materials

2.1.1 Cell line

Table 1. Cell line used in the entire study.

<u>Cell Line</u>	<u>Cell Type</u>	<u>Characteristics</u>	<u>Source</u>
MCFs	Mouse Cardiac Fibroblast	Primary	Science cell#M630057

2.1.2 Cell culture media and additives

Table 2. List of cell culture media and supplements used in this study.

<u>Name</u>	<u>Source</u>	<u>Order No.</u>
DMEM High glucose	Gibco	12491-015
DMEM Low glucose	Gibco	D5796
Fetal calf serum	Sigma-Aldrich	F4135-500ML
L-Glutamine (200 mM)	Gibco	25030081
Penicillin/Streptomycin Solution	Gibco	15140-122
Phosphate buffered saline	Gibco	14190-094
Pyruvate	Sigma-Aldrich	28374849
Trysin-EDTA 0,25%	Sigma-Aldrich	T4049-100ML

2.1.3 Chemicals and reagents

All chemical and reagents used throughout the experiments are enlisted in Table 3.

Table 3. List of chemicals and reagents used in this study.

Name	Source	Order No.
37% HCL	Merck	100317
Agarose	Sigma Aldrich	A4718
Low melting agarose	Sigma Aldrich	A0169
CaCl ₂	Sigma Aldrich	21049
DTT	Invitrogen	Y00147
Ethanol	ROTH	5054.1
Fast SYBR green	Applied Biosystems	4385612
β-mercaptoethanol	ROTH	4227.3
Hepes	Merck	391340
Isoflurane	Abbvie	B506
Isopropanol	ROTH	6752.2
Luria Broth Base	Thermo-scientific	12780052
Luria Broth Agar	Thermo-scientific	22700025
Magnesium chloride	Sigma-Aldrich	M8787
Nuclease free water	Qiagen	129114
OligoDT primers	Invitrogen	58862
Methanol	ROTH	8388.2

MgSO ₄	Merck	7487-88-9
NaCl	Merck	7647-14-5
Na ₂ HPO ₄ ·7H ₂ O	Merck	7782-85-6
NaH ₂ PO ₄	Merck	10049-21-5
NaHCO ₃	Merck	144-55-8
KH ₂ PO ₄	Merck	7778-77-0
Bovine serum albumin	Sigma-Aldrich	A9418
Trizol	Ambion	15596-026
Tween-20	Sigma-Aldrich	P1379
Triton-X 100	Sigma-Aldrich	T8787
Glycine	Carl Roth	3908
Weigert's iron hematoxylin solution	Sigma-Aldrich	HT1079
Xylol	ROTH	9713-3
RNaseZap	Ambion	AM9782
Ponceau reagent	ROTH	3469.1
SDS loading buffer	Novex	96868
NP-40 Lysis buffer	Invitrogen	FNN0021
NuPAGE SDS Sample buffer (4x)	Novex	NP0007
10x PBS	Thermo-Scientific	70011044
4% PFA	ROTH	664666
Blocking buffer	ROTH	33285
Target retrieval		

solution 10x pH6	Dako	S1699
Dimethyl sulfoxide	Sigma-Aldrich	D84118
ULTRA Tablets, Mini, EDTA-free, EASY pack	ROCHE	5892791001
Superscript® II Reverse Transcriptase	Invitrogen	100004925
dNTP mix	Invitrogen	18427-013
5X First strand buffer	Invitrogen	y02321
RNase out	Invitrogen	100000840
NCS	Sigma-Aldrich	69856
H ₂ O ₂	Sigma-Aldrich	H1009
5X First strand buffer	Invitrogen	y02321
Bovine serum albumin	Sigma-Aldrich	A9418
Fast SYBR green	Applied Biosystems	4385612
MTT	Sigma-Aldrich	11465007001
Dimethyl sulfoxide	Sigma-Aldrich	D84118
PVDF membrane	ThermoFisher Scientific	88518

2.1.4 Consumables

Table 4. List of consumables used in the study.

Name	Source	Order No.
6-well plates	Thermo Fischer	140675
8-well chambered slides	Ibidi	80841

24-well plates	Thermo Fisher Scientific	12475
96-well plates	Thermo Fisher Scientific	269620
Black coated 96-well plates	Thermo Fisher Scientific	15119
T-25 Flask	Thermo Fisher Scientific	174951
T-75 Flask	Thermo Fisher Scientific	174952
12 well 4-12 % SDS PAGE gel	Thermo Fisher Scientific	NP0321
Falcon Tubes 15 mL	Thermo Fisher Scientific	352095
Falcon Tubes 50 mL	Thermo Fisher Scientific	10788561
FACS Tubes	STEMcell Technologies	38030
Eppendorf Tubes 1.5 mL	Eppendorf	0030 120.086
Eppendorf Tubes 2.0 mL	Eppendorf	0030 120.094
Pipette Tips 1.0 mL	Sarstedt	70.762.211
Pipette Tips 200 µL	Sarstedt	70.760.452
Pipette Tips 10 µL	Sarstedt	70.1130.105
Serological pipettes 5 mL	Sarstedt	86.1253.001
Serological pipettes 10 mL	Sarstedt	86.1253.001
Serological pipettes 25 mL	Sarstedt	86.1685.001
Scalpel	Fisher Scientific	10567364

2.1.5 Recombinant proteins

Table 5. Recombinant protein used throughout the experiment.

<u>Name</u>	<u>Source</u>	<u>Order No.</u>
-------------	---------------	------------------

TGF- β	R&D Systems	240-B-010/CF
--------------	-------------	--------------

2.1.6 Antibodies

Table 6. List of primary antibodies used in this study.

<u>Name</u>	<u>Source</u>	<u>Dilution (in use)</u>	<u>Order No.</u>
53bp1	Santacruz	1:1000 (IF)	H-300
GAPDH	Santacruz	1:1000 (WB)	6C5
H3s10p	Cell signalling	1:50 (IF, FACS)	29237
Ki67	Abcam	1:50 (IF)	ab15580
RAD51	Santacruz	1:10 (IF)	H-92
TET3	Genetex	1:25 (IHC, IF) 1:1000 (WB)	GTX121453
α -SMA	Sigma-Aldrich	1:1000 (IF)	A5228
γ -H2AX	Millipore	1:1000 (IF, IHC)	JBW301

Table 7. List of secondary antibodies used in this study.

<u>Name</u>	<u>Source</u>	<u>Dilution (in use)</u>	<u>Order No.</u>
Alexa Fluor $\text{\textcircled{R}}$ 488 donkey anti-mouse	Life Technologies	1:500	A21235
Alexa Fluor $\text{\textcircled{R}}$ 488 donkey anti-rabbit	Life Technologies	1:500	A21206
Alexa Fluor $\text{\textcircled{R}}$ 568 donkey anti-mouse	Life Technologies	1:500	A-31571

Alexa Fluor ® 568 donkey anti-rabbit	Life Technologies	1:500	A-32795
Alexa Fluor ® 647 goat anti-mouse	Life Technologies	1:500	A32728
Polyclonal Rabbit Anti-Rabbit Immunoglobulins	DAKO	1:200	P0448
Polyclonal Rabbit Anti-Mouse Immunoglobulins	DAKO	1:2500	P0161

2.1.7 Buffers

Table 8. List of buffers used in the study.

Buffers	Recipe
2 % BSA in 1X PBS	2g of BSA in 100 ml of PBS
10 % BSA in 1X PBS	10g of BSA in 100 ml of PBS
PBS	137 mM NaCl 2.7 mM KCl 4.3 mM Na ₂ HPO ₄ ·7H ₂ O 1.4 mM KH ₂ PO ₄ , pH 7.4
Krebs-Hepes Buffer	140 mM NaCl 3.6 mM KCl 0.5 mM NaH ₂ PO ₄ 0.2 mM MgSO ₄ 1.5mM CaCl ₂ 10 mM Hepes (pH 7.4) 2 mM NaHCO ₃
PBST	137 mM NaCl 2.7 mM KCl 4.3 mM Na ₂ HPO ₄ ·7H ₂ O 1.4 mM KH ₂ PO ₄ , pH 7.4 0.1% Tween-20
TBS	20 mM Tris 150 mM NaCL, pH 7.4
TBST	20 mM Tris 150 mM NaCL 0.1% Tween-20, pH 7.4

2.1.8 Primers

Table 9. List of primers used in the study.

Gene	Forward	Reverse	Concentration (In use)
RPL4	CCTTACGCCAAGACTATGCGCA	CCTTCTCGGATTTGGTTGCCAG	4 μ M
TET1	ACACAGTGGTGCTAATGCAG	AGCATGAACGGGAGAATCGG	4 μ M
TET2	ACCTGGCTACTGTCATTGCTCC	TGCAGTGACTCCTGAGAATGGC	4 μ M
TET3	TGCGATTGTGTCGAACAAATAGT	TCCATACCGATCCTCCATGAG	4 μ M
TET3 gRNA1	GAT CGA TGG CCA GCA CGG ATG AGT TG	AAA ACA ACT CAT CCG TGC TGG CCA TC	10 μ M
TET3 gRNA2	GAT CGT GTC TTC CCC TCC CAG TTC CG	AAA ACG GAA CTG GGA GGG GAA GAC AC	10 μ M

2.1.9 Commercial Kits

Table 10. List of commercially available kits used in the present study.

Name	Source	Order No.
Amplex Red kit	Sigma-Aldrich	A12222
Annexin V apoptosis kit	Abcam	ab14085
BrdU assay kit	Roche	11647229001
GSH/GSSG activity kit	Abcam	ab138881
Midi-prep Kit	Qiagen	12145
Mini-prep Kit	Qiagen	2716
Pierce BCA Protein Assay Kit	Thermo Scientific	23225
PLA assay kit	Sigma Aldrich	DUO92101
Pure Link RNA mini Kit	Ambion	23225
TET activity kit	Abcam	ab156913

Vectastain Universal Elite ABC kit	Vector Laboratories	99585
------------------------------------	---------------------	-------

2.1.10 Plasmids

Table 11. List of commercially purchased plasmids used in the present study.

<u>Plasmid</u>	<u>Source</u>	<u>Order No.</u>	<u>Concentration</u>
CRISPR/Cas9	Origene	GE100010	2.5 µg
EGFP	Origene	45567	2.5 µg
I-Sce-1	Addgene	26477	2.5 µg
mouse TET3	Addgene	60940	2.5 µg
pDR-GFP	Addgene	26475	2.5 µg
pLCN-DSB	Addgene	98895	2.5 µg
RFP	Addgene	54608	2.5 µg

2.1.11 Equipment

Table 12. List of equipment used in the present study.

<u>Name</u>	<u>Use</u>	<u>Company</u>
Cell line tissue culture	S1	Biowizard Kojair
Autoclave	Sterilization	Fernwald
Bioanalyzer 2000	Visualisation of DNA	Agilent
Bright light microscopy	Visualisation of cells	Olympus
Cell Culture Centrifugation	Centrifugation	Hettich
ChemiDOC™	Visualisation of protein	Biorad

Confocal Microscopy	Visualisation of fluorescence	Leica
Drier	Drying autoclaved materials	Memmert GmbH, Schwabach
FACS Aria II	FACS	Becton Dickinson
Fluorescence camera Color View	Visualisation of fluorescent cells	Olympus
Ice maker	Smashed ice production	AF80 Scotsman-ice
Light Microscope	Bright field visualisation of cells	Leica RM 2165
Magnetic stirrer	Stirring	IKAMAG RCT IKA
Microtome	Tissue sectioning	Leica
Mikroskop Axiovert S100 TV	Visualisation of cells	ZEISS
Nanodrop2000	DNA/RNA/protein concentration measurement	Thermo Scientific
Pipettes	Pipetting	Eppendorf AG
Refrigerator -20°C	Cold storage	Liebherer, Bulle
Refrigerator 4°C	Cold storage	Liebherer, Bulle
Roller mixer	Rolling of tubes	Bibby Scientific, Stuart®
Sonicators	Sonication	Newtown, USA
StepONE Plus Real-Time PCR System	Real time PCR	Applied Biosystems
The Belly Dancer-Stovall	Shaking	Life science incorporated, Greenboro
Thermocycler Mastercycler	PCR	Eppendorf AG
Thermomixer	Heating block	Thermo Scientific
Tissue lyser	Tissue Lysis	Qiagen
Vortex Genie	Vortexing	Bender & Hobein AG

Xcell SureLock Electrophoresis Cell	Running protein samples	Invitrogen
--	-------------------------	------------

2.1.12 Softwares

Table 13. List of softwares used in the study.

<u>Software</u>	<u>Application</u>	<u>Source</u>
Adobe Illustrator	Preparation of figures	Adobe Products
Cistrome Data Browser	Downloading ChiP sequencing files	cistrome.org/db
EaSeq	ChIP sequencing analysis	easeq.net
Endnote 4	References	Thomson Reuters
Flowing Software 2	FACS analysis	Perttu Terhu, Turku Centre of Biotechnology, FI
Grammarly	English Grammar checking	Grammarly
Image J	Western Blot quantification	Imagej.nih.gov
PRSIM	Statistics	Graph Pad 8
Transcriptome Analysis Console	Microarray analysis	Thermo Fisher Scientific
Windows Office Package 2010	Writing Thesis	Windows, Washington, USA

2.2 METHODS

2.2.1 Human myocardial tissue sections

All patient samples are collected from the Department of Cardiology, UMG Gottingen, in accordance with ethical rules and regulations of the Institutional Review Board of the University of Göttingen and the responsible government authority of Lower Saxony (Germany).

2.2.2 Animal welfare and ethics statement

All experimental animal studies were conducted in accordance with the guidelines of the experimental protocols and ethical rules approved by the Institutional Review Board of the University of Göttingen and the responsible government authority of Lower Saxony (Germany). The animal protocols used in these experiments conformed to the guidelines in Directive 2010/63/EU of the European Parliament on the protection of animals.

2.2.3 Fibrosis induction using angiotensin II osmotic minipump in mice

The angiotensin II model was implemented as described. Briefly, 14- to 16-week-old C57/BL/6N mice with body weights between 25 g and 30 g were used for angiotensin II (Ang-II) pump implantation experiments. Ang-II (1.5 mg/kg per day), or PBS as the control, was administered to the animals, using an osmotic minipump (ALZET Model 1002), for 4 weeks.

2.2.4 Cell culture

Mouse primary cardiac fibroblasts (MCFs) were obtained from Cell-Science. The cells were cultured using 1.5 g Glucose Dulbecco's Modified Eagle Medium (DMEM) supplemented with 10% fetal bovine serum, sodium pyruvate (1 mM), nonessential amino acids (0.1 mM), penicillin (100 units/ml), and streptomycin (0.1 mg/ml). The cells were maintained at 37°C in 5% CO₂ and cultured until passage 4. All the experiments were conducted in either the second or the third passage. Mycoplasma contamination was routinely checked during the entire course of the experiment.

2.2.5 Neocarzinostatin (NCS) and transforming growth factor beta (TGF-β) treatment

The MCFs cells were treated with either 100 ng/ml of neocarzinostatin (NCS, Stock 0.5 mg/mL) or 15 ng/mL of transforming growth factor beta (TGF-β) or 100 μM of H₂O₂ (H₂O₂, Stock- 9.8 M) in all subsequent cell culture experiments.

2.2.6 Generation of clustered regularly interspaced short palindromic repeats/CRISPR-associated protein 9 (CRISPR/Cas9) Tet methylcytosine dioxygenase 3 (*TET3*) knockdown constructs

The clustered regularly interspaced short palindromic repeats/CRISPR-associated protein 9 (CRISPR/Cas9) backbone was used to generate tet methylcytosine dioxygenase 3 (*TET3*) gene knockdown constructs in the MCFs. Guided RNAs targeting exon 10 and exon 11 of the *TET3* gene were designed, and off-target binding effects were minimized on the basis of scores obtained on the online tool Blueheronbio (OriGene, Herford, Germany). The single-guide RNA (sgRNA) sequences were inserted into the pLenti-Cas9-Guide plasmid (OriGene GE100010, Herford, Germany) with BamHI and BsmBI restriction sites to generate p-Lenti-Cas-sgRNA m*TET3* constructs and confirmed by DNA sequencing. The deletion of the flanked exon was predicted to lead to a frameshift mutation, eventually resulting in the generation of a premature spliced transcript, leading to decreased protein expression.

2.2.7 Plasmid isolation using midi-prep kit

The HiSpeed® Plasmid Midi Kit from QIAGEN (Hilden, Germany) was used for the isolation of the plasmid. Bacterial cells cultured overnight were centrifuged at 4600 RPM for 20 mins. The supernatant was discarded in bacterial waste, and the pellets were resuspended in 6 ml Buffer P1, which had been stored at 4°C. Next, 6 ml of Buffer P2 was added and incubated for 5 minutes at room temperature. Another 6 ml of Buffer P3 was subsequently added, and the tubes were inverted several times. Afterward, the liquid was transferred to barrel tubes (part of the kit) and incubated for 10 minutes. During this incubation step, the HiSpeed® Tips were equilibrated with 4 ml of ABT-buffer. At this point, the lysate was filtered into the equilibrated Tip and was washed with 20 ml of Buffer QC. The elution was then performed with 56°C-prewarmed QF Buffer. The DNA was precipitated with 3.5 ml of isopropanol after 5 minutes of incubation. The eluate was filtered through the QIA precipitator; it was then washed twice with 80% ethanol. After the outlet nozzle was dried for 3 minutes, the plasmid was eluted in 800 µl of nuclease-free water. Finally, the DNA concentration was measured by Nano Drop.

2.2.8 *In vitro* transfection

The night before transfection, 50000 cells per well were seeded in a 6-well culture plate in an antibiotic-free DMEM (Gibco, Carlsbad, USA) well supplemented with 10% heat-inactivated fetal bovine serum (FBS, Sigma-Aldrich, St. Louis, USA). For the knockdown experiments, 2.5 µg of pLenti-cas9 *TET3* plasmid DNA was transfected; for over-expression, 2.5 µg of mouse *TET3* plasmid DNA was transfected using Lipofectamine 2000 reagent (Invitrogen, Carlsbad, USA). A total of 4 hours after transfection, the medium in each well was replaced by a fresh antibiotic-free medium and allowed to incubate for the next 48 hours.

2.2.9 Histology

Paraffin-embedded specimens were sectioned at 3 μm ; Masson's trichrome stain (MTS) was performed as per the established protocol in lab (Tampe et al, 2015). For morphometric analysis of interstitial fibrosis, fibrotic areas were assessed using cell Sens (Olympus, Tokyo, Japan) software. A total of 10 visual fields were randomly selected for each MTS stained section at 200x magnification, and the relative interstitial fibrotic area was evaluated using a 10 mm² graticule.

2.2.10 Immunohistochemistry

Formalin-fixed, paraffin-embedded mouse heart sections were de-paraffinized in xylene and rehydrated in ethanol containing distilled water. Masson's trichrome staining and fibrotic area quantification were performed as previously described in our publications. The sections were stained using the polyclonal antibody against *TET3* (GeneTex, Irvine, California, United States). The Vectastain Universal Elite ABC Kit (Vector Laboratories, Burlingame, California, United States) was used for performing peroxidase labelling. The area of interest was visualized using AEC Substrate-Chromogen (Dako, Glostrup, Denmark) according to the manufacturer's protocol, and nuclear staining was performed using Mayer's Hematoxylin Solution (Sigma-Aldrich, St. Louis, Missouri, United States) as previously described.

2.2.11 Single-cell, neutral gel electrophoresis

Neutral comet assay was performed on the whole mouse hearts and *in vitro* in mouse cardiac fibroblasts (MCFs). Briefly, isolated cells from the mouse hearts or MCFs were mixed with 1% low-melting agarose gel. The resulting solution was then poured on a chilled precoated agarose glass slide. The cells were then lysed overnight at 4°C in lysis solution (Trevigen, 4250-010-01). The next day, the slides were run in the freshly prepared neutral running buffer (Trevigen, 4250-050-K) for 30 minutes at 12 V. Post-electrophoresis, SYBR Safe was added to visualize the comet tails using a fluorescent microscope.

2.2.12 Amplex Red assay

The H₂O₂ concentration in the mouse hearts was measured using the Amplex Ultrared dye according to the manufacturer's instructions. In brief, the mouse hearts were minced into small pieces (20 mg) and incubated with Amplex Red and Krebs Hepes Buffer at a concentration of 100 $\mu\text{mol/L}$ and horseradish peroxidase at a concentration of 1 U/mL for 60 min in the dark. The supernatant was collected immediately after incubation and transferred to a black-coated 96-well plate, and fluorescence was measured at 560nm.

2.2.13 Protein extraction and quantification

Proteins were extracted from the cells by using 100 μ L of NP-40 buffer, pre-added with protease inhibitor tablets (ROCHE). The extracted proteins were sonicated at 40 amplitude for 10 minutes, with 15 seconds on and off-cycle. After that, the samples were centrifuged at 13000 RPM at 4 °C. The supernatant was collected in a fresh 1.5 mL Eppendorf tube for further use.

The extracted proteins were quantified using bicinchoninic acid (BCA) protein estimation kit. This method relies on an alkaline medium where the reduction of cuprous ion to cupric ion takes place in the presence of protein. As a result of such a reaction, a purple-coloured product is formed due to the chelation of two molecules of BCA with one molecule of cuprous ion. The concentration of the protein is thus quantified as a measure of absorbance at 562nm.

2.2.14 TET and glutathione/glutathione disulfide (GSH/GSSG) activity assays

Both activity assays were performed in the mouse hearts as per the manufacturer's instructions (ab156913, ab138881). Briefly, 20 μ g of tissue were collected and minced into small pieces with the help of a surgical scalpel. For testing both TET and GSH/GSSH activity, the small tissue pieces were first lysed for 1 hour at 4 °C in nuclear lysis solution, provided in the respective kits. After completion of lysis, for analyzing TET activity assay, 2 μ L of 0.5X TET Substrate was added and incubated at 37°C for 90 min. Then, 50 μ L of the capture antibody were added to the samples (1:1000 from stock). The samples were further incubated at 37°C for 60 minutes. Thereafter, samples were washed thrice with 1X wash buffer and then incubated with 50 μ L of the Diluted Detection Antibody. The samples were further washed thrice with 1X wash buffer. After that, 100 μ L of developer solution was added, and the samples were incubated for 15 minutes. In the end, 50 μ L of stop solution was added, and absorbance was measured using ELISA plate reader at 450 nm.

For GSH/GSSG assay, 50 μ L of GSH Assay mixture were added into each GSH standard and sample well. For total GSH + GSSG (reduced and oxidized), 50 μ L of total glutathione Assay mixture were added into each GSSG standard and sample. After that, the samples are incubated at room temperature 45 minutes in the dark. In the end, absorbance was measured using ELISA plate reader at 490 nm.

2.2.15 Immunofluorescence

A total of 10000 cells per chamber were seeded in the 8-well chambered slides. Before fixing, the slides were washed twice with 1X PBS. Fixing was performed using 4% paraformaldehyde (PFA) for 15 minutes at room temperature. Post-fixation cells were permeabilized with 0.1% phosphate-buffered saline with Tween 20 (PBST) (1XPBS + Triton X 100) for 7 minutes; they were then washed twice in 1X PBS. The cells were

blocked with 5% bovine serum albumin (BSA) in PBST for 1 hour at room temperature. Post-blocking, the cells were incubated with respective primary antibodies dissolved in 1% BSA in PBST overnight at 4°C. The next day, the cells were washed thrice with 1X PBS and thereafter incubated with secondary antibody dissolved in 1% BSA in PBST for 1 hour. The cells were rewashed thrice with 1X PBS and mounted with 4',6-diamidino-2-phenylindole (DAPI) to be visualized under the microscope.

2.2.16 Confocal image analysis

All images were photographed using an LSM780 confocal microscope. Triple-stained images were taken using settings in the frame with either Alexa green 488, Alexa red 568, or Alexa infrared 647 lasers. All the images represented were processed using ZEN blue software (ZEISS, Oberkochen, Germany), keeping the parameters constant. The nuclei of all the represented images were visualized with the DAPI channel.

2.2.17 RNA isolation

For the purpose of isolating the RNA from the samples, 700 µl trizol was first added, and the cells were completely resuspended. They were incubated for 15 minutes on ice. Afterward, 250 µl of chloroform was added, and the tubes were shaken at least 7 times. They were then incubated for 7 minutes at room temperature. The phases were separated during centrifugation for 20 minutes with 15000 RPM at 4°C. The aqueous phase was then separated, and an equal amount of 70% ethanol was added. The resulting solution was transferred to spin cartridges, which are part of the Pure Link™ RNA Mini Kit. The cartridges were centrifuged for 2 minutes with 15000 RPM at 4°C to fix the RNA on the filter; they were then washed with wash buffer I and centrifuged for 30 seconds. The RNA was washed 2 more times with wash buffer II and centrifuged for 30 seconds. The filter was dried by centrifugation for 2 minutes with no solution added. Additionally, it was dried for 2 minutes by passive evaporation. After 2 minutes of incubation, the RNA was eluted with 30 µl of 56°C-prewarmed nuclease-free water by centrifugation for 2 minutes in fresh Eppendorf tubes. Finally, the RNA concentration was measured by Nano Drop.

2.2.18 Complementary DNA synthesis

To analyze the isolated cellular transcripts, the RNA was converted into complementary DNA (cDNA). First, the isolated RNA was diluted in nuclease-free water to yield a final RNA amount of 1 µg. Next, 1 µl of 10x reaction buffer and 1 µl deoxyribonuclease I (DNase I) were added to the diluted RNA, which was then incubated for 15 minutes at room temperature. At the end, 1 µl of stop solution was added. Afterward, the samples were heated to 70°C for 10 minutes; they were then cooled on ice. In the next step, 1 µl of 10mM deoxyribonucleoside triphosphate (dNTP) and 1 µl of 100 µM oligo(dT) per sample were added and incubated for 5 minutes at 65°C. Next, 4 µl 5x first-strand buffer, 2 µl of 0.1 M dithiothreitol (DTT), and 1 µl RNaseOUT (20U/µL) were added, and the RNA was incubated for 2 minutes at 42°C.

Finally, 1 μL of Superscript® Reverse Transcriptase (20U/ μL) was added per sample. The reaction was left at 42°C for 50 minutes and at 70°C for 15 minutes. The cDNA was frozen at -80°C before use.

2.2.19 Real-time quantitative polymerase chain reaction (RT-qPCR)

Real-time quantitative polymerase chain reaction (RT qPCR) was performed using SYBR Green Master Mix on Applied Biosystems StepOne software v2.3. Briefly, the RNA was isolated from the tissues or the cells using the PureLink RNA isolation kit, and cDNA was synthesized using the Invitrogen cDNA synthesis protocol. Validated primers were used to analyze the change in gene expression. The forward and reverse primers of each gene were mixed in nuclease-free water (primer concentrations are provided in Table 9). A master mix containing 6 μL of nuclease-free water, 2 μL of primer mix, and 10 μL of SYBR Green per sample was prepared, and 18 μL of the mix was added per well. Finally, 2 μL of cDNA in 1:20 dilution was added. After the plate had been closed airtight with Micro Amp™ Optical Adhesive Film, the samples were vortexed and centrifuged.

The following program was used:

95°C	10 min	}	1 cycle
95°C	20 sec	}	40 cycles
60°C	30 sec	}	

The relative expression levels were calculated using the following equation: 2-delta-delta Ct.

2.2.20 Western blot

Briefly, the cells were homogenized in nonyl phenoxyethoxyethanol (NP-40) lysis buffer (Life Technologies, Carlsbad, USA) supplemented with protease inhibitor cocktail (Roche, Basel, Switzerland) for 30 minutes on ice. Protein lysates were then sonicated and measured using a bicinchoninic acid (BCA) kit. Next, 50 μg of protein samples were loaded in a 4% to 12% Bis-Tris polyacrylamide gel electrophoresis system (Novex, Carlsbad, USA) and transferred onto a nitrocellulose membrane (GE Healthcare, Freiburg, Germany). The membranes were blocked with 5% bovine serum albumin in tris-buffered saline with Tween 20 (TBST) (tris-buffered saline (TBS) pH 7.2, 0.1% Tween 20) and then combined with the *TET3* antibody in 2% BSA in TBST overnight at 4°C. The next day, the membrane was washed 3 times in TBST and then incubated with the secondary antibody. Luminescence was detected using chemiluminescent substrate (Cell Signalling, Danvers, USA) on a ChemiDoc XRS system (Bio-Rad, Hercules, USA). The same membranes were restriped to show glyceraldehyde 3-phosphate dehydrogenase (GAPDH) as a loading control.

2.2.21 Flow cytometry

Briefly, the cells were washed with PBS twice before detachment with trypsin (1:3 dilution, incubation for 2 to 4 minutes at 37°C). An equal amount of culture media was added to stop the reaction. The cell solution was centrifuged for 10 minutes with 1.200 RPM, and the supernatant was discarded. Afterward, the cells were washed twice with ice-cold PBS; this involved carefully suspending them in 1 ml of PBS before centrifuging them with 1.200 RPM for 10 minutes. In a final step, the cells were suspended in 500 µl of ice-cold PBS. A total of 5 ml of 70% ethanol was added dropwise with constant vortexing. The cells were in single suspension after this procedure; they were frozen at -80°C overnight for at least 1 hour. In the next step, the suspension was centrifuged again for 10 minutes with 4600 RPM at 4°C. The supernatant was discarded, and the precipitate was resuspended in 500 µl of ice-cold PBS. The solution was transferred into Eppendorf tubes. Afterward, 500 µl of propidium iodide and 2 µl of ribonuclease A (RNase A) were added and mixed conscientiously. The suspension was incubated for 30 minutes at 37°C. Within 1 hour, the measurement was taken with BD Accuri TM C6 (BD Biosciences, San Jose, California, United States).

2.2.22 Proximity ligation assay

The cells were seeded at a density of 10^4 cells per well in an 8-chambered slide. The cells were fixed and permeabilized as described before in immunofluorescent studies. After permeabilization, the cells were incubated with blocking buffer provided in the mouse/rabbit red starter Duolink kit (Olink, Uppsala, Sweden) for 2 hours at 37°C in a humidified chamber. The primary antibodies were then conjugated with the probes provided within the kit and incubated for 1 hour at room temperature at 37°C in a humidified chamber. They were then washed 3 times in Buffer A (provided in the kit). The cells were then combined with amplification buffer and enzymes as per the manufacturer's protocol and incubated for 90 minutes at 37°C in a darkened humidified chamber. Finally, the cells were washed with 1x Buffer B (supplied with the kit) for 10 minutes; this was followed by a 1-minute wash with 0.01X Buffer B. Finally, the cells were mounted using the DAPI conjugated mountant supplied with the kit. The red blobs indicated the proximity between 2 cellular-bound antibodies.

2.2.23 Non-homologous end joining (NHEJ) and homologous recombination (HR) reporter plasmids

The MCFs were stably transfected with 2.5 µg of circular pLCN-DSB or pDR-GFP (Addgene, Cambridge, USA) (Pierce et al., 1999; Seluanov et al., 2004). Resistant colonies were selected with 5 µg/mL of puromycin (ThermoFisher Scientific Scientific, Waltham, USA). Transfection with I-SceI (pCBASceI, Addgene, Cambridge, USA) introduced a double-strand break (DSB) at genomic I-SceI sites of the reporter plasmid, which helped to restore the green fluorescent protein/enhanced green fluorescent protein (GFP/EGFP) signal, visualizing non-homologous end joining (NHEJ)/homologous recombination (HR) repair events.

2.2.24 Cell counting assay

Briefly, the cells were counted using the trypan blue assay. The rate of proliferation was calculated as $R_p = \ln(N(t)/N(0))/t$, where $N(t)$ = the number of cells at time t , $N(0)$ = the number of cells at time 0, and t = time (in days).

2.2.25 MTT cell proliferation assay

Briefly, 1000 cells were plated in a 96 well chambered plate and 20 μ l of 5 mg/ml MTT was added to each well. One set of wells with MTT but without cells was taken as negative control. After addition of MTT, cells were left to incubate at 37°C for 4 hours. After incubation, media was removed and 100 μ l of DMSO was added. Briefly, 10 minutes within incubation, cells were measured for proliferation at 495 nm using an ELISA plate reader.

2.2.26 Analysis of publicly available microarray datasets

Datasets provided publicly were analyzed according to general recommendations, using Transcriptome Analysis Console software (Thermo Scientific, Waltham, Massachusetts, United States). Human transcriptome array data were shown as log₂ median-centered intensities extracted from database accession numbers **GSE57345**.

2.2.27 BrdU DNA end resection assay

Briefly, control, TET3 knockdown and TET3 rescued MCFs were incubated with 20 mM of BrdU for 24 hours. Cells were fixed with 90 % ethanol in 1X PBS for 20 minutes. After fixation, cells were washed thrice with 0.1% PBST and then denatured with 2N HCl for 35 min. Cells were subsequently blocked with 10% FBS in 1X PBS for 1 hour at room temperature and thereafter washed thrice with 1X PBS. Subsequently, anti-BrdU secondary antibody from the BrdU kit was added and absorbance was measured in an ELISA plate reader at 370nm.

2.2.28 Statistics

Statistical analysis was performed using Graph Pad Prism 8 software. For comparing between two groups Welch unpaired two tailed Student's t-test was performed. For comparison of more than two groups, one-way ANOVA Bonferroni and Sidak test analysis was performed. Statistical significances are represented in the graphs as * $p \leq 0.05$, ** $p \leq 0.01$, *** $p \leq 0.001$.

3. Results

3.1 Mouse fibrotic hearts accumulate ROS and oxidative stress

The fibrotic microenvironment is highly dynamic, and studies have shown that the increased ROS generation aggravates fibrosis (An et al, 2015). Chronic accumulation of ROS causes oxidative stress in the fibrotic hearts and leads to cytokine production and DNA damage (Mondal et al, 2013; Takimoto & Kass, 2007). H_2O_2 is one of the most prominent ROS that causes significant damage to fibrotic hearts (Guo et al, 2014; Qin et al, 2010; Steinhorn et al, 2018). The glutathione redox couple is the key buffer system that scavenges the H_2O_2 produced in the fibrotic heart (Swain et al, 2016). Increased ROS accumulation causes a shift in the ratio of reduced/oxidized glutathione (GSH/GSSG) (Sag et al, 2014). In line with these observations, we investigated the production of ROS (H_2O_2) and induction of oxidative stress in an angiotensin-II treated murine model of cardiac fibrosis. We confirmed fibrosis induction using Masson's trichrome staining (MTS) (**Figure 9A**). Our results show a 1.7-fold increase in collagen deposition in fibrotic mouse hearts as compared to healthy control hearts (**Figure 9B**). We then confirmed a 3.7-fold increase in ROS generation using Amplex Red assay and a 1.67-fold decrease in the GSH/GSSG ratio, confirming accumulation of oxidative stress in fibrotic hearts (**Figure 9C-D**). Our results demonstrate that fibrotic mouse hearts have a significant increase in ROS and a decrease in the GSH/GSSG ratio compared to healthy mouse hearts.

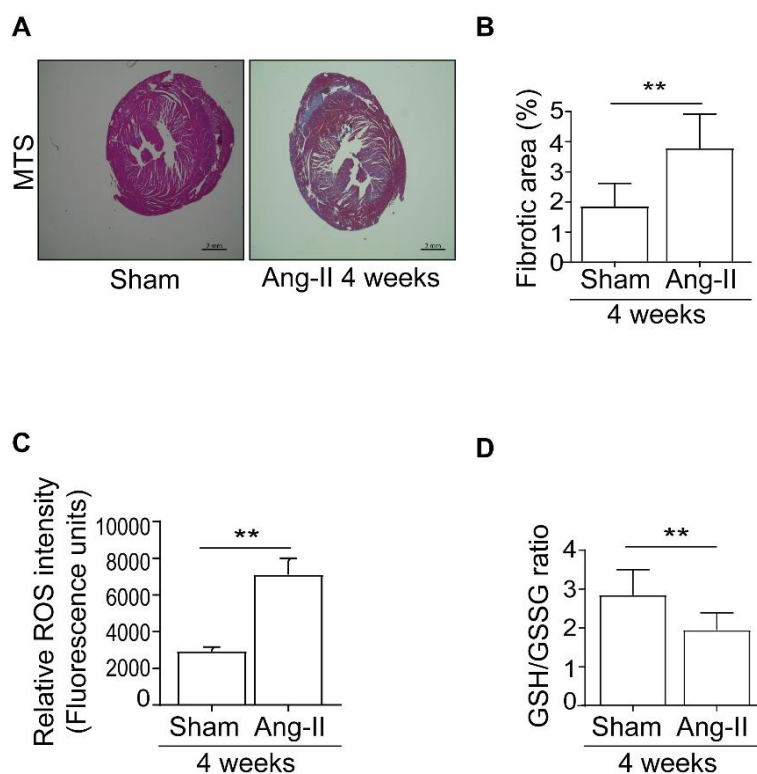


Figure 9. Mouse fibrotic hearts have increased ROS and oxidative stress.

(A) MTS staining showing collagen deposition (stained blue) in 4 weeks of sham and angiotensin-II treated mouse hearts. (B) Graph representing % of the fibrotic area in 4 weeks of sham and angiotensin-

II treated mouse hearts. **(C)** Fluorescence measurement showing ROS intensity using Amplex Red assay in 4 weeks of sham and angiotensin-II treated mouse hearts. **(D)** Graph representing the change in GSH/GSSG ratio as an indicator of oxidative stress in 4 weeks of sham and angiotensin-II treated mouse hearts. Summarised quantitative findings are shown as mean \pm SEM from 3 shams, and 3 Angiotensin-II treated mouse hearts. Statistical significance was calculated using Welch unpaired two tailed Student's t-test, and P-values correspond to $**p \leq 0.01$. Scale bars represent 2 mm.

3.2 Mouse fibrotic hearts have increased DNA damage

Increased ROS and oxidative stress during cardiac fibrosis causes DNA lesions (Chen et al, 2019; Panth et al, 2016). Studies have confirmed that ROS-induced oxidative stress can cause both DNA SSBs and DSBs (AbdulSalam et al, 2016). The involvement of SSBs in heart failure is well understood, whereas the effect of DSBs in fibrotic progression is not clear (Higo et al, 2017). To confirm increased production of DSBs during fibrosis, we used γ -H2AX (a marker of DNA DSBs) staining. Immunohistochemical analysis shows significant production of DSBs in both myocyte and non-myocyte cell populations in the fibrotic mouse hearts (**Figure 10**).

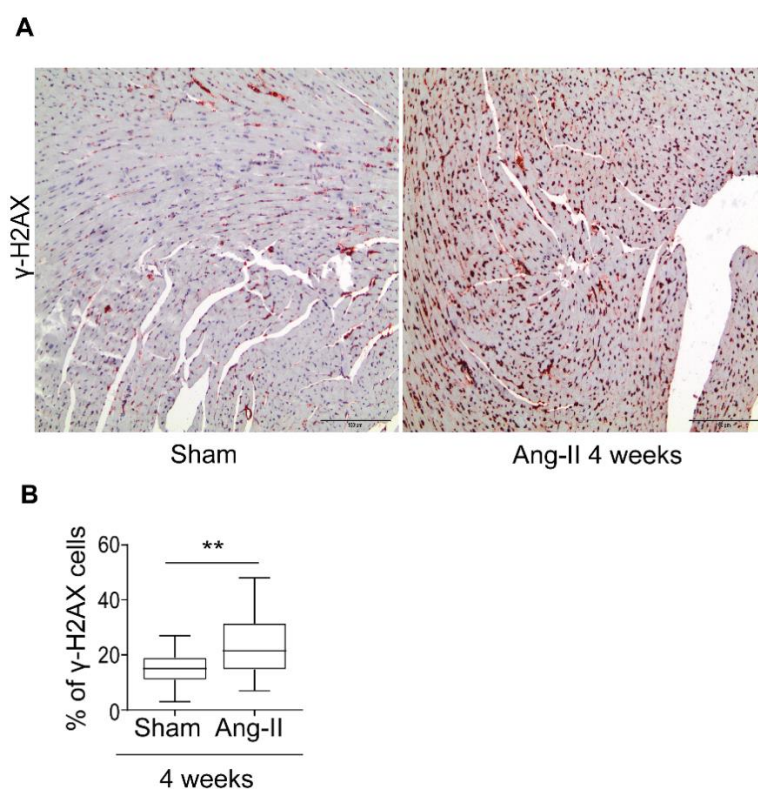


Figure 10. Mouse fibrotic hearts have increased DNA damage.

(A and B) Immunohistochemistry representative images and the respective graph shows the expression pattern of γ -H2AX in 4 weeks of sham and angiotensin-II treated mouse hearts. Summarised quantitative findings are shown as mean \pm SEM from 3 shams, and 3 angiotensin-II treated mouse hearts. Statistical significance was calculated using Welch unpaired two tailed Student's t-test, and P-values correspond to $**p \leq 0.01$. Scale bars represent 100 μ m.

3.3 Mouse fibrotic fibroblasts show increased proliferation despite DNA damage

Our immunohistochemical staining results demonstrate an increase in DNA DSBs in the non-myocyte cell population. Since fibroblasts comprise the most significant non-myocytic cell population besides endothelial cells, we then assessed the presence of DNA DSBs in fibroblasts (Zhou & Pu, 2016). To confirm the accumulation of DNA DSBs in fibroblasts, we used γ -H2AX and α -SMA (a fibroblast marker) double immunofluorescent staining. Our results show an increase in the percentage of γ -H2AX and α -SMA double-positive cells of total α -SMA positive cells in fibrotic mouse hearts as compared to healthy sham hearts (**Figure 11**).

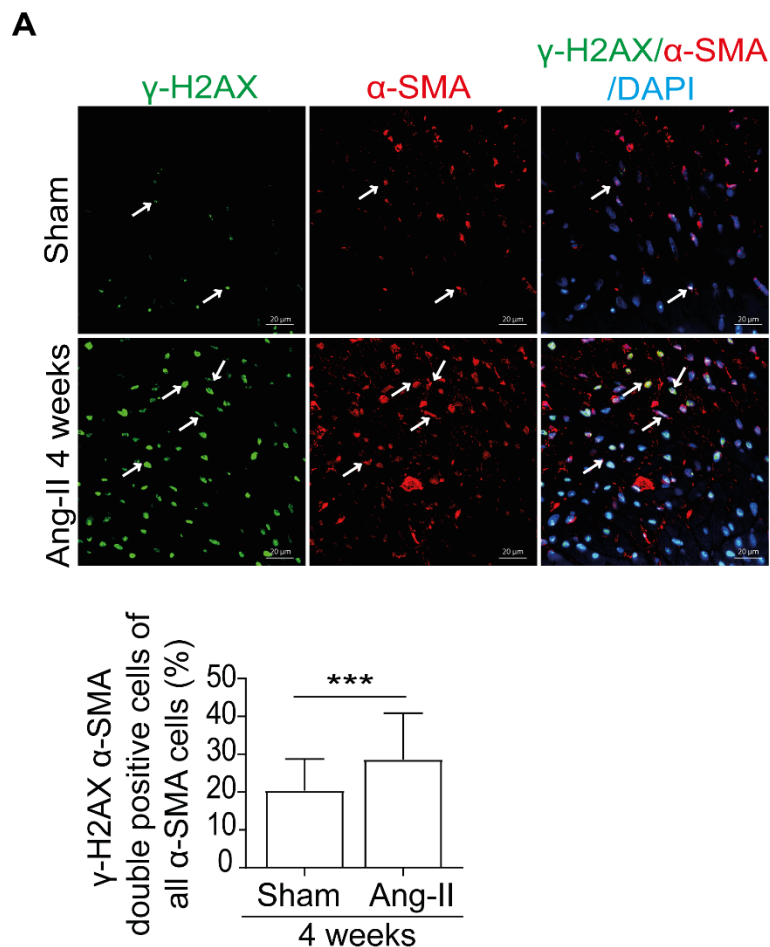


Figure 11. Mouse fibrotic fibroblasts have increased DNA DSBs.

Confocal representative images and the respective graph shows double staining of γ -H2AX and α -SMA in 4 weeks of sham and angiotensin-II treated mouse hearts. Summarised quantitative findings are shown as mean \pm SEM from 3 shams, and 3 angiotensin-II treated mouse hearts. Statistical significance was calculated using Welch unpaired two tailed Student's t-test, and P-values correspond to *** $p \leq 0.001$. Scale bars represent 20 μ m. White arrow marks indicate γ H2AX⁺, α -SMA⁺, and γ -H2AX/ α -SMA⁺⁺ cells at the indicated stages.

Similarly, to assess increased proliferation in cardiac fibroblasts, we used Ki67 and α -SMA double immunofluorescent staining. As expected, our results show an increase in Ki67 and α -SMA double-positive cells in the fibroblast population (**Figure 12**).

Altogether, these results demonstrate that the fibrotic fibroblasts can proliferate despite increased DNA damage.

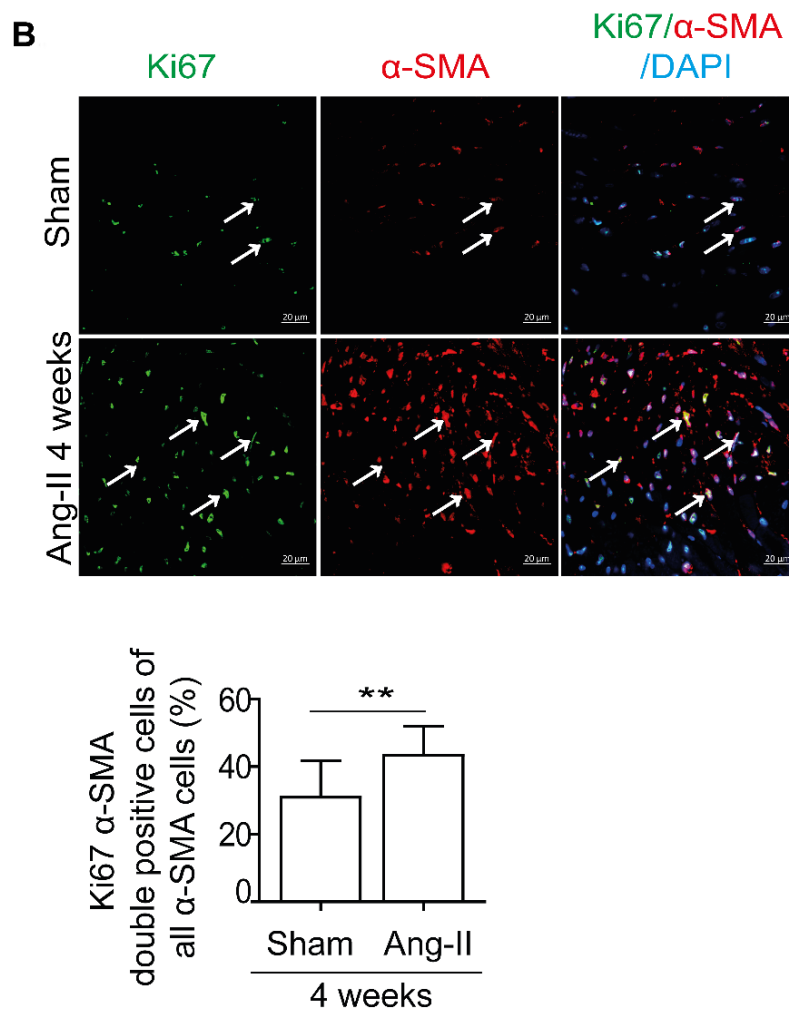


Figure 12. Mouse fibrotic fibroblasts have increased Ki67 expression.

Confocal representative images and the respective graph shows double staining of Ki67 and α -SMA in 4 weeks of Sham and angiotensin-II treated mouse hearts. Summarised quantitative findings are shown as mean \pm SEM from 3 shams, and 3 angiotensin-II treated mouse hearts. Statistical significance was calculated using Welch unpaired two tailed Student's t-test, and P-values correspond to ** $p \leq 0.01$. Scale bars represent 20 μ m. White arrow marks indicate Ki67⁺, α -SMA⁺, and Ki67/ α -SMA⁺⁺ cells at the indicated stages.

3.4 Mouse fibrotic hearts lose TET3 expression

Studies from our lab have shown that loss of TET3 is associated with aggravated organ fibrosis (Tampe et al, 2015; Xu et al, 2015; Xu et al, 2018). In line with these observations, we first confirmed the loss of TET3 in angiotensin-II treated mouse fibrotic hearts. Immunohistochemistry scoring and mRNA expression analysis demonstrate that TET3 is significantly downregulated in fibrotic mouse hearts as compared to control mouse hearts (**Figure 13A-C**). Additionally, immunohistochemistry scoring shows a reduction of TET3 in non-cardiomyocytes (i.e.

fibroblasts and endothelial cells). Interestingly, our results also demonstrate an overall decrease in catalytic activity of TET enzymes in general in the fibrotic hearts (**Figure 13D**).

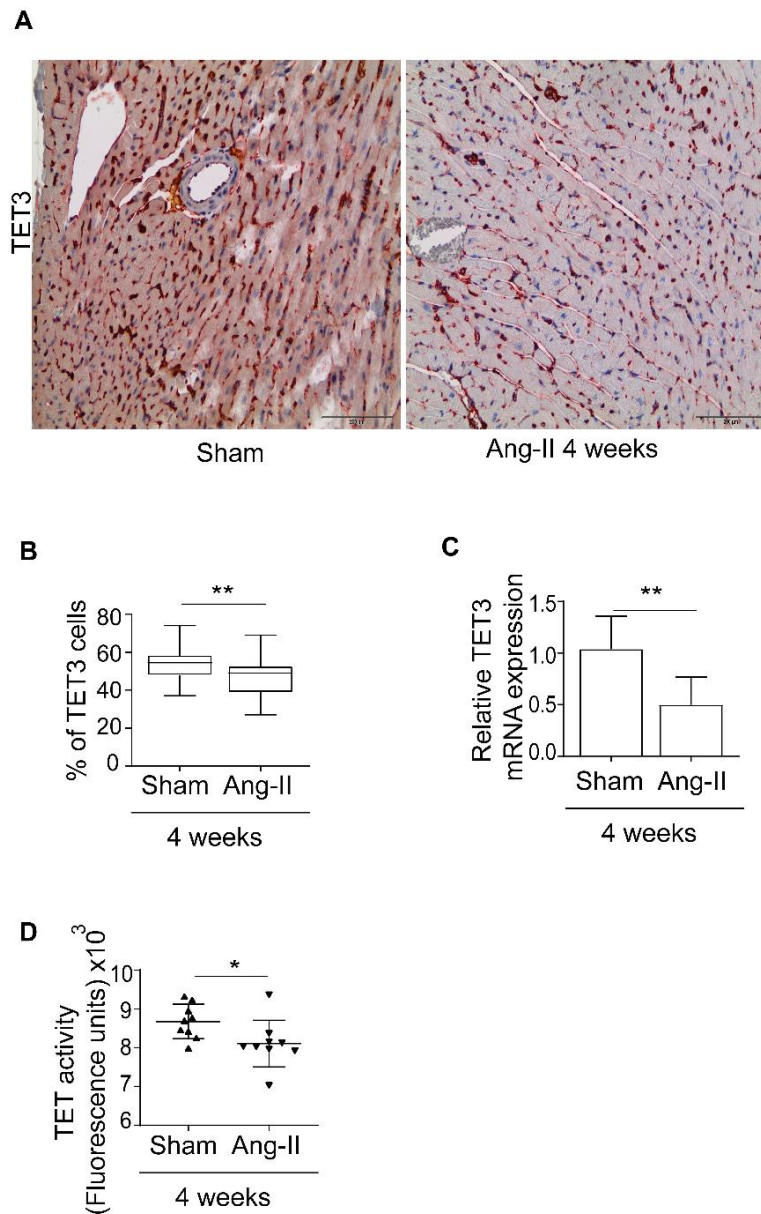


Figure 13. Mouse fibrotic hearts have decreased TET3 expression and reduced TET activity.

(**A and B**) Immunohistochemistry representative images and associated graph shows the expression pattern of TET3 in 4 weeks of sham and angiotensin-II treated mouse hearts. Summarised quantitative findings are shown as mean \pm SEM. (**C**) Relative mRNA expression of TET3 in sham and angiotensin-II mouse fibrotic hearts. Summarised quantitative findings are shown as mean \pm SD. (**D**) The bar graph shows decreased TET activity in sham and angiotensin-II mouse fibrotic hearts. Summarised quantitative findings are shown as mean \pm SD. Statistical significance was calculated using Welch unpaired two tailed Student's t-test, and P-values correspond to * $p \leq 0.05$, ** $p \leq 0.01$, *** $p \leq 0.001$. Scale bars represent 100 μm .

3.5 Mouse fibrotic fibroblasts show decreased TET3 expression

In mouse hearts, cardiac fibroblasts comprise around 56% of the total non-myocyte cell population (Zhou & Pu, 2016). Thus, we then assessed the expression of TET3 in cardiac fibroblasts. Expression of TET3 in fibroblasts is confirmed by co-immunofluorescent staining with α -SMA. By counting the total percentage of TET3 and α -SMA double-positive cells out of the total α -SMA positive cells, our results demonstrate that TET3 expression is significantly downregulated in angiotensin-II treated murine fibrotic fibroblasts as compared to sham fibroblasts (**Figure 14**).

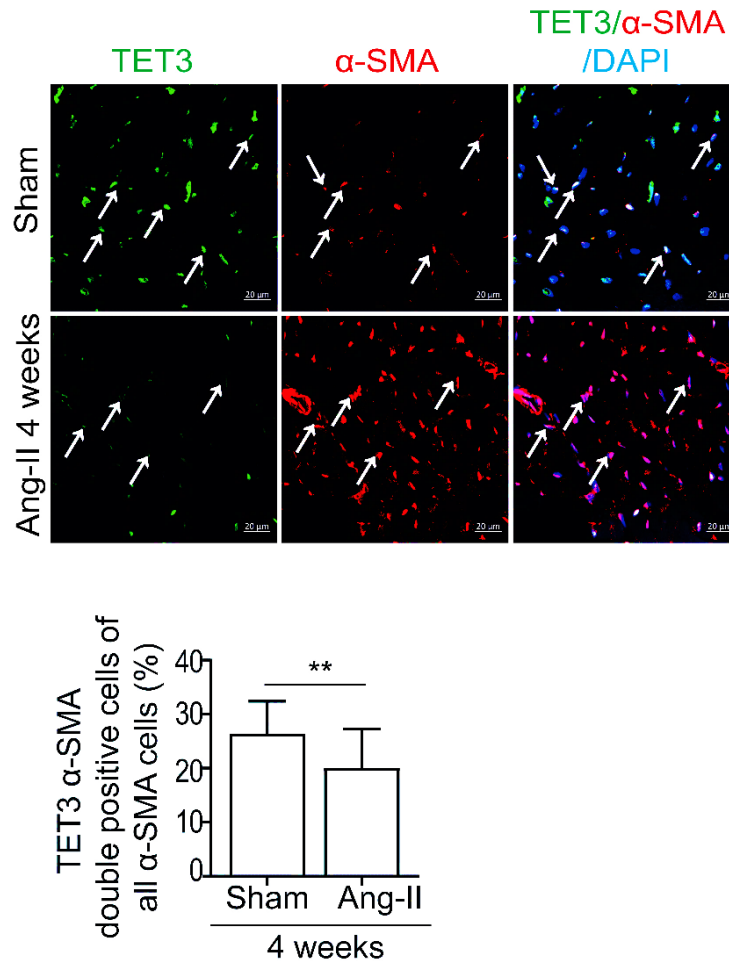


Figure 14. Mouse fibrotic fibroblasts have decreased TET3 expression.

Confocal representative images and respective graph shows double staining of TET3 and α -SMA in 4 weeks of sham and angiotensin-II treated mouse hearts. Summarised quantitative findings are shown as mean \pm SEM from 3 shams, and 3 Angiotensin-II treated mouse hearts. Statistical significance was calculated using Welch unpaired two tailed Student's t-test, and P values correspond to $**p \leq 0.01$. Scale bars represent 10 μ m. White arrow marks indicate TET3⁺, α -SMA⁺ and TET3/ α -SMA⁺⁺ cells at the indicated stages.

3.6 Ischemic human hearts show decreased TET3 expression

Our *in vivo* data demonstrates downregulation of TET3 in fibrotic mouse hearts. Hence, our next aim was to evaluate the clinical significance of TET3 in healthy and diseased human hearts. Therefore, we continue examining the expression profile of TET3 from a publicly available microarray (**GSE57345**) dataset consisting of gene expression profile collected from healthy and diseased human hearts. The RNA samples analysed in the microarray were obtained from Myocardial Applied Genomics Network (MAGNet) consortium (www.med.upenn.edu/magnet/) and comprise information on TET3 expression in 135 ischemic left ventricles and 96 non-failing left ventricles.

Consistent with our *in vivo* results in mouse hearts, we also demonstrate a significant decrease in TET3 expression ($p = .00000142$) in human patient cohorts consisting of 135 ischemic left ventricles and 96 non-failing left ventricles (**Figure 15A**). An increase in fibrosis is associated with increased COL4A1 and COL4A2 production. Our results demonstrate a strong negative correlation between expression of TET3 and COL4A1, suggesting that increased collagen production is associated with decreased TET3 expression (**Figure 15B**). Altogether, the microarray data analysed from the cohort of 231 human patients suggest that TET3 downregulation is associated with increased collagen expression.

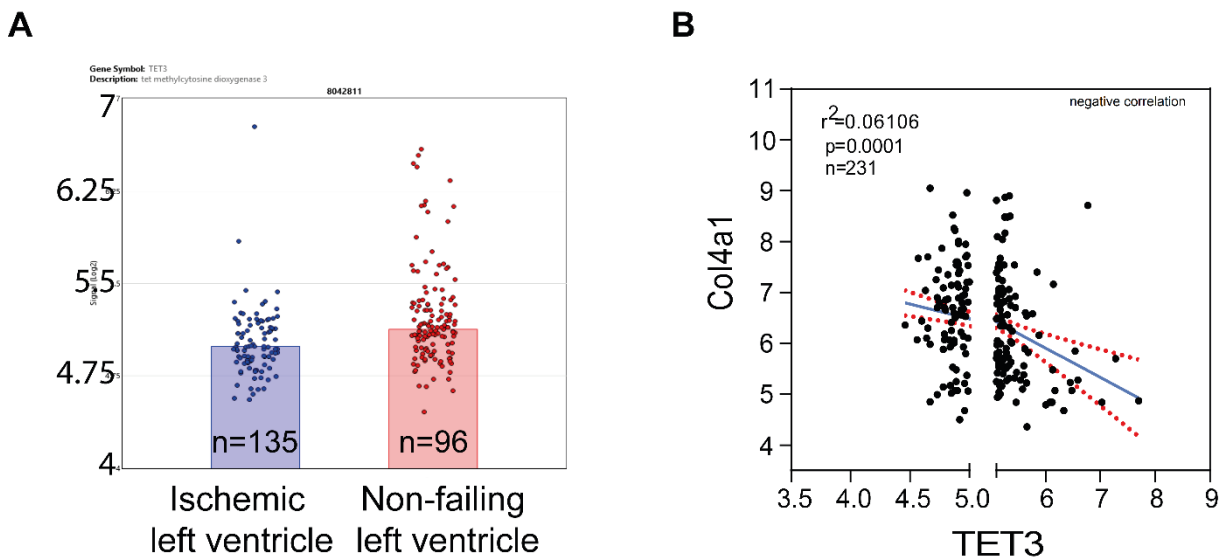


Figure 15. Ischemic human hearts have decreased TET3 expression.

(A) TET3 normalized signal intensity in 135 ischemic and 96 non-failing left ventricles. (B) Correlation graph showing negative association between TET3 and Col4a1 in 135 ischemic and 96 non-failing left ventricles. Pearson correlation coefficient analysis is shown as r^2 in the represented graph.

3.7 TET3 is positively associated with RAD51 and negatively associated with 53BP1 expression in ischemic human hearts

Recent studies have highlighted the role of TET3 in DNA damage and repair response (Jiang et al, 2017), and likewise, our *in vivo* data demonstrate an increase in DNA DSBs in the fibrotic mouse hearts. Therefore, TET3 may be involved in DNA repair responses. Consistent with this idea, we observe a strong positive correlation between the expression of TET3 and RAD51 ($p = .0004$; a marker for HR) and a negative correlation with 53BP1 ($p = .0005$; a marker for NHEJ) in the same patient cohort, suggesting that TET3 might be involved in the DNA damage repair response (**Figure 16**).

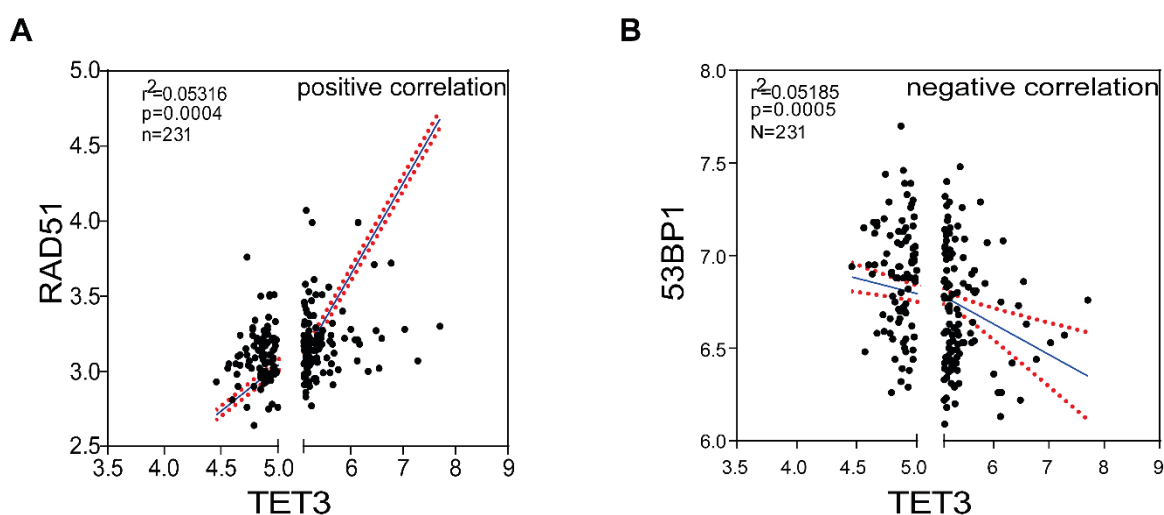


Figure 16. TET3 is positively associated with RAD51 expression and negatively associated with 53BP1 expression in ischemic human hearts.

(A) Co-relation graph showing positive association between TET3 and RAD51 in 135 ischemic and 96 non-failing left ventricles. (B) Co-relation graph showing negative association between TET3 and 53bp1 in 135 ischemic and 96 non-failing left ventricles. Pearson correlation coefficient analysis is shown as r^2 in the represented graph.

3.8 TET3 is recruited to the DNA DSBs *in vitro* in MCFs when challenged with H₂O₂

TET3 dynamics at DNA DSB sites remain unclear. Existing studies account for H₂O₂ as one of the critical molecules contributing to DNA damage in hearts (Ye et al, 2016). Therefore, we examined the recruitment of TET3 to H₂O₂-induced DNA lesions in an *in vitro* model of mouse cardiac fibroblasts (MCFs) at 1, 2, 4, 6 and 12 hours after a one-time exposure to H₂O₂ (**Figure 17A**). Using γ -H2AX and TET3 co-staining, we demonstrated that TET3 co-localizes as distinct small foci at the sites of DNA DSBs. Our results show that colocalization of TET3 at DNA lesions is highest one hour after H₂O₂ treatment, followed by a decline. Over the course of the experiment, we observed that DNA damage production by H₂O₂ is discontinuous; it shows a bimodal DNA damage accumulation that increases twelve hours after H₂O₂ treatment (**Figure 17B**). The above results suggest that H₂O₂-induced DNA DSBs occur continuously, so using the present experimental setup makes it difficult to understand the dynamics of

recruitment of TET3 at DSBs. Therefore, we continued to search for a drug that induces DNA DSBs at only one time point to study the recruitment of TET3 at γ -H2AX sites.

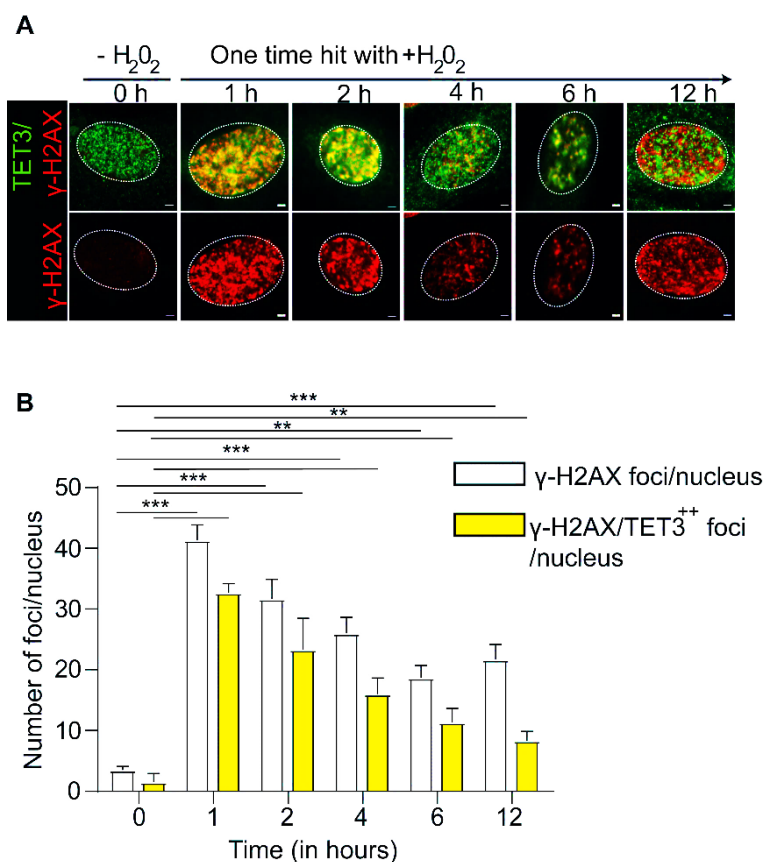


Figure 17. TET3 is co-localized at DNA DSBs induced by H₂O₂ in vitro in MCFs.

(A) Representative confocal images show TET3 (green), and γ -H2AX (red) co-localization in control and H₂O₂ treated MCFs. (B) The bar graph represents the number of TET3, and γ -H2AX co-localized foci (yellow) in H₂O₂ treated MCFs at indicative time points. For counting, 150 cells were considered from 3 independent experiments. Summarised quantitative findings are shown as mean \pm SD. Statistical significance was calculated using one-way ANOVA Bonferroni and Sidak analysis, n.s. represents non-significant and P-values correspond to * $p \leq 0.05$, ** $p \leq 0.01$, *** $p \leq 0.001$. Scale bars represent 10 μ m.

3.9 TET3 is recruited to the DNA DSBs in vitro in MCFs when challenged with NCS

The unsteady nature of H₂O₂-induced DNA DSBs in MCFs, which occurs because a one-time H₂O₂ treatment leads to continuous endogenous H₂O₂ release, introduces a limitation to the study of recruitment of TET3 at γ -H2AX foci, so we used neocarzinostatin (NCS) to induce DNA DSBs. NCS has a short half-life, so a one-time treatment at a dose of 100 ng/ml creates a burst of DSBs that is resolved within 12 hours (Kuo et al, 1984). Induction of DNA DSBs by NCS thus provides a method for the study of recruitment of TET3 at the γ -H2AX foci. Using confocal microscopy and double immunofluorescent staining, we found that TET3 is recruited to the DNA DSBs upon treatment with NCS as discrete small foci following kinetics similar to that of γ -H2AX (Figure 18A). By counting the number of TET3 and γ H2AX double-positive

PLA probes are present at a distance of about 40 nM, it starts hybridizing to form a circular DNA in the presence of DNA ligases. Finally, upon the addition of DNA polymerases, these short circular DNAs are further amplified. And in the end, they are visualized using a fluorescent-labelled complementary oligonucleotide probe as bright red blobs.

Based on this assay, we made use of rabbit TET3 and mouse γ -H2AX antibodies to confirm the recruitment of TET3 at the DSBs. As a negative control, we used no probes to ensure no false positive results. Previous studies have confirmed the recruitment of 53BP1 at γ -H2AX sites using PLA (Rassoolzadeh et al, 2015). Using this information from the literature, we made use of rabbit 53BP1 and mouse γ H2AX antibodies as positive controls to test our experimental setup (**Figure 19A-B**). In agreement with our confocal double staining results, these results showed increased recruitment of TET3 at γ -H2AX sites. These were visualized as distinct blobs after one hour of NCS and H₂O₂ treatment in MCFs, whereas cells without DNA damage induction produced no such PLA blobs (**Figure 19A**).

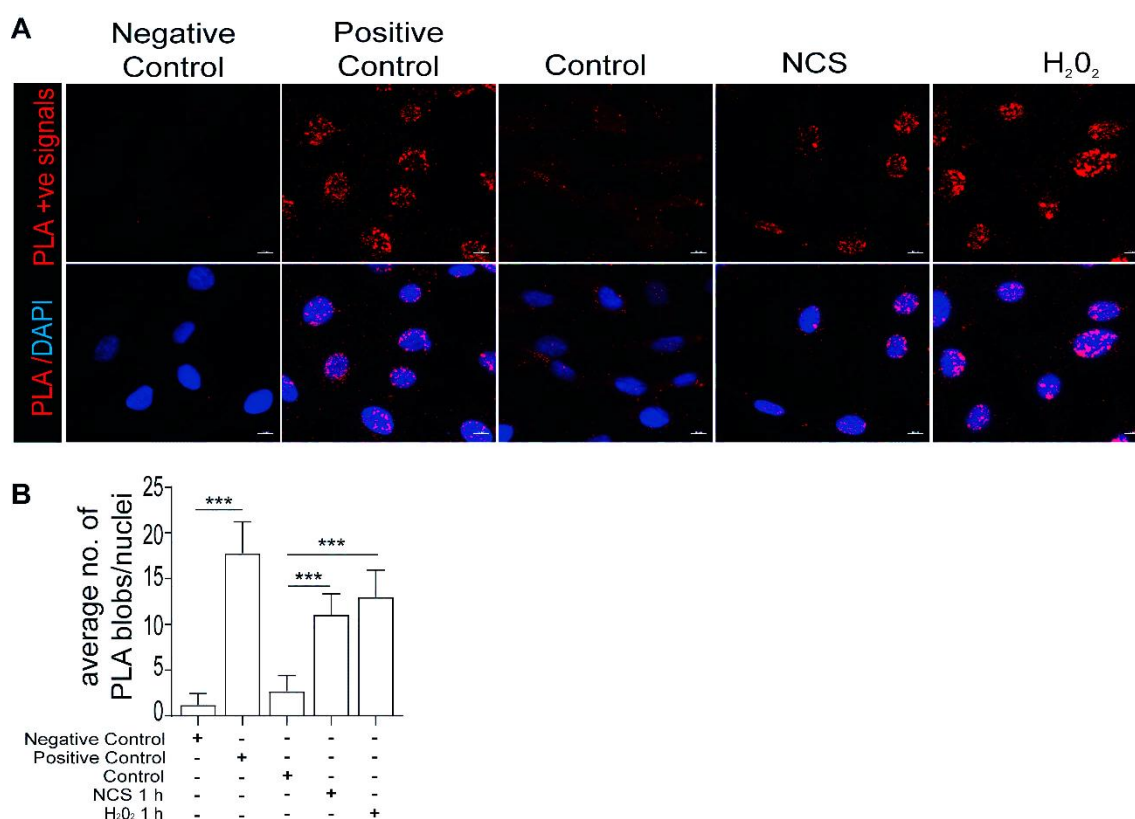


Figure 19. PLA confirms the recruitment of TET3 at DNA DSBs in vitro in MCFs.

(**A and B**) Representative images and analysis of Proximity ligation assay confirming the colocalization of TET3 at γ -H2AX foci upon induction of DNA damage. Negative control represents no antibody treatment, and positive control represents 53BP1 and γ H2AX. For counting, 150 cells were considered from 3 independent experiments. Summarised quantitative findings are shown as mean \pm SD. Statistical significance was calculated using one-way ANOVA Bonferroni and Sidak analysis, and P-values correspond to * $p \leq 0.05$, ** $p \leq 0.01$, *** $p \leq 0.001$. Scale bars represent 10 μ m.

3.11 ChIP sequencing analysis shows TET3 overlaps at DNA DSBs in HEK293T cells

To confirm TET3 recruitment at DNA DSBs is not limited to MCFs, we analyzed ChIP-sequencing data from publicly available database. Mining through the database, we found two ChIP seq data sets in HEK293 cells for TET3 and γ -H2AX. We extracted the processed bigwig files from the database and used easeq analysis software to overlap the TET3 and γ -H2AX ChIP seq peaks ([GSM897577](#), [GSE75170](#)). Because our PLA results show TET3 recruits at DNA DSBs, we hypothesized we would be able to visualize an overlap in TET3 and γ -H2AX peaks in HEK293 cells. In agreement with our results in MCFs, we demonstrate a 36.97 % overlap between the TET3 and γ -H2AX binding sites in HEK cells (**Figure 20**). These results further strengthen that indeed TET3 gets recruited at the DNA DSBs. Moreover, the present sequencing overlaps also suggest that recruitment of TET3 at DNA DSBs is not limited to MCFs.

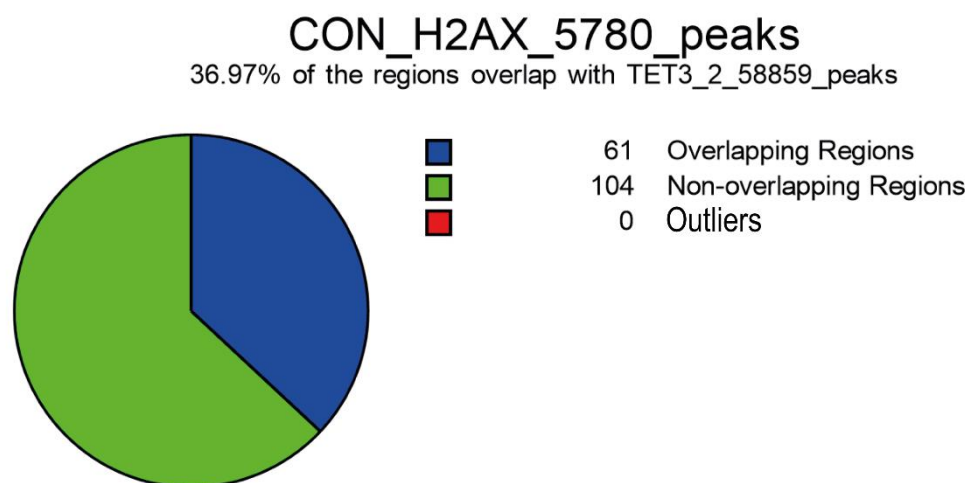


Figure 20. ChIP sequencing data showing overlap of TET3 and γ -H2AX globally in HEK293 cells.

3.12 Loss of TET3 is associated with spontaneous DNA damage in MCFs

Our *in vitro* data shows that TET3 is recruited to the DNA DSBs in healthy MCFs, implicating its possible role in facilitating DDR response. Therefore, to assess the role of TET3 in DDR, a CRISPR/Cas9-based knockdown construct was generated using two guide RNAs targeting exon 10 and exon 11 (**Figure 21A**). The guide RNA sequences used in the experiment were designed to have minimal off-target effects and maximum on-target effect. Our mRNA expression data shows that both designed guide RNAs are equally effective in downregulating TET3 (**Figure 21B-C**). However, the Western blot data shows that guide RNA2 targeting exon 11 is most effective in downregulating TET3 expression (**Figure 21D-E**).

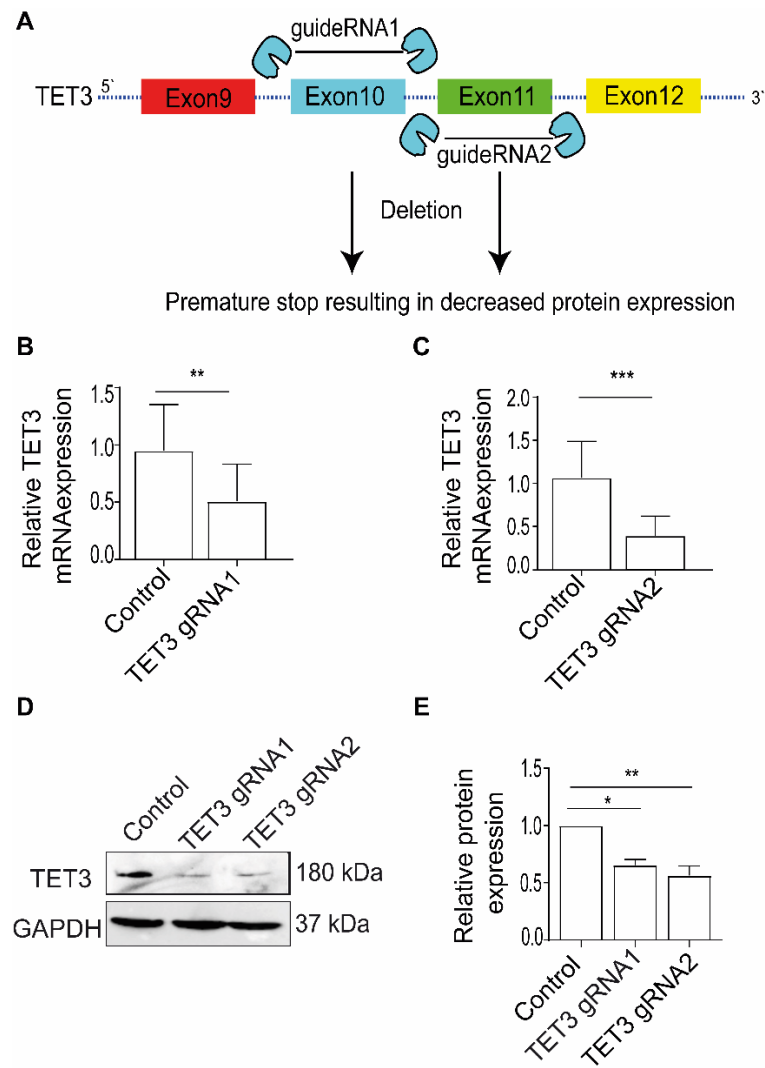


Figure 21. Establishment of TET3 knockdown in vitro in MCFs.

(A) Schematic representation of CRISPR/Cas9 mediated TET3 knockdown. (B and C) Relative mRNA expression showing TET3 expression after TET3 knockdown by guide RNA 1 and guide RNA 2. (D and E) Western blot and the associated graph is representing TET3 downregulation upon targeted by guide RNA1 and guide RNA2. All experiments were done in triplicates. Summarised quantitative findings are shown as mean \pm SD. For comparing between two groups, Welch unpaired two tailed Student's t-test was performed. For comparison between more than two groups, one-way ANOVA Bonferroni and Sidak analysis was performed. P-values correspond to * $p \leq 0.05$, ** $p \leq 0.01$, *** $p \leq 0.001$.

To assess the role of TET3 in DDR response, we performed TET3 knockdown in MCFs and examined changes in γ -H2AX foci accumulation as compared to the untreated and empty CRISPR/Cas9 transfected cells. Our results show that knockdown of TET3 by both guide RNAs causes production of endogenous DSBs. Notably, no statistically significant difference was observed in the generation of DSBs between guide RNA1 and 2. But as our Western blot data shows that guide RNA2 is more effective in knocking down TET3, we elected to use guide RNA2 for all future experiments (Figure 21A).

TET proteins share a high degree of sequence homology, so it is possible that knockdown of TET3 can also impact TET1 and TET2 expression. To clarify this, we performed mRNA expression analysis on all TET isoforms upon TET3 knockdown

using guide RNA2. Our results demonstrate that knockdown of TET3 does not result in alteration of TET1 and TET2 expression levels (**Figure 22B-C**). Next, we performed neutral comet assay using guide RNA2 to confirm the accumulation of DNA DSBs in MCFs. Our results demonstrate a significant increase in the tail moment (head DNA% \times length of tail) in TET3 knockdown MCFs, confirming the presence of endogenous DNA DSBs (**Figure 22D-E**). Altogether, our results confirm that knockdown of TET3 results in the accumulation of endogenous DNA DSBs independently of TET1 and TET2, as both genes remain unaltered upon TET3 knockdown.

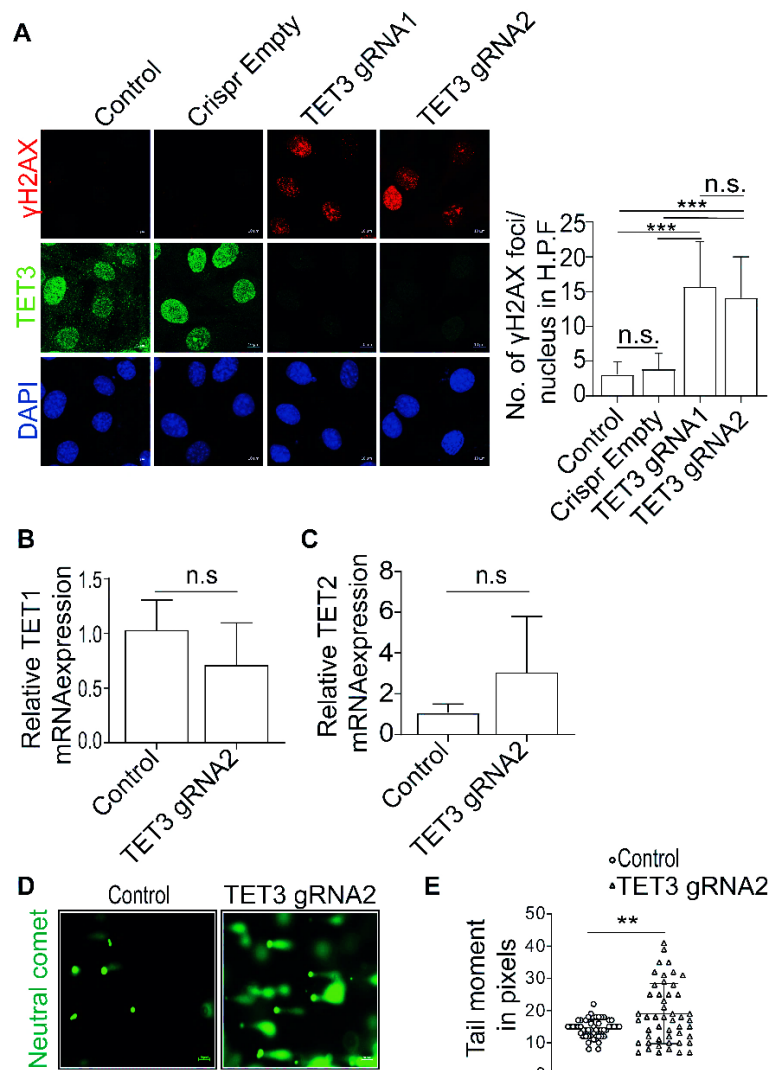


Figure 22. TET3 knockdown results in endogenous DNA DSBs in vitro in MCFs.

(A) Representative confocal images and analysis shows increased γ -H2AX foci induction upon TET3 knockdown. (B and C) Relative mRNA expression showing the effect of TET3 knockdown on TET1 and TET2 expression. (D and E) Neutral comet assay confirming the accumulation of DNA DSBs upon TET3 knockdown. All experiments were done in triplicates, and 150 cells were counted from 3 independent experiments. Summarised quantitative findings are shown as mean \pm SD. For comparing between two groups, Welch unpaired two tailed Student's t-test was performed. For comparison between more than two groups, one-way ANOVA Bonferroni and Sidak analysis was performed. n.s. represents non-significant and P-values correspond to ** $p \leq 0.01$, *** $p \leq 0.001$.

3.13 Knockdown of TET3 results in decreased HR but unchanged NHEJ efficacy in MCFs

DSBs are repaired via two major pathways: the fast but error-prone non-homologous end-joining (NHEJ) and the slow but error-free homologous recombination (HR) (Iyama & Wilson, 2013). As knockdown of TET3 results in accumulation of endogenous DNA DSBs, we decided to assess its role in DNA DSB repair response. For this purpose, we made use of two DNA repair reporters: DRGFP HR (to detect HR efficiency) and pLCN-DSB (to detect NHEJ efficiency).

DR-GFP reporter constructs consist of two differentially mutated fluorescent GFP genes arranged as direct repeats and separated by the presence of the puromycin antibiotic marker (Pierce et al, 1999). One of the mutated GFP genes harbors a recognition site for the rare endonuclease I-Sce1, and the other GFP gene harbors an internal 5'- and 3'-truncated fragment proficient at correcting the mutation in the GFP upon successful completion of HR.

pLCN-DSB reporter constructs consist of non-functional GFP cassettes separated by a neomycin resistance marker (Arnoult et al, 2017). The non-functional GFP cassette consists of two inverted I-Sce1 sites, which upon cleavage result in functional restoration of the GFP signal after successful completion of NHEJ. The restored GFP signal using either of these reporter constructs can be measured by FACS.

After using the HR and NHEJ reporter constructs in MCFs, we observed a significant reduction in HR repair efficiency (**Figure 23A**) upon knockdown of TET3, whereas NHEJ repair efficiency remained unaffected (**Figure 23B**). This result suggests that TET3 is necessary for an integer HR response.

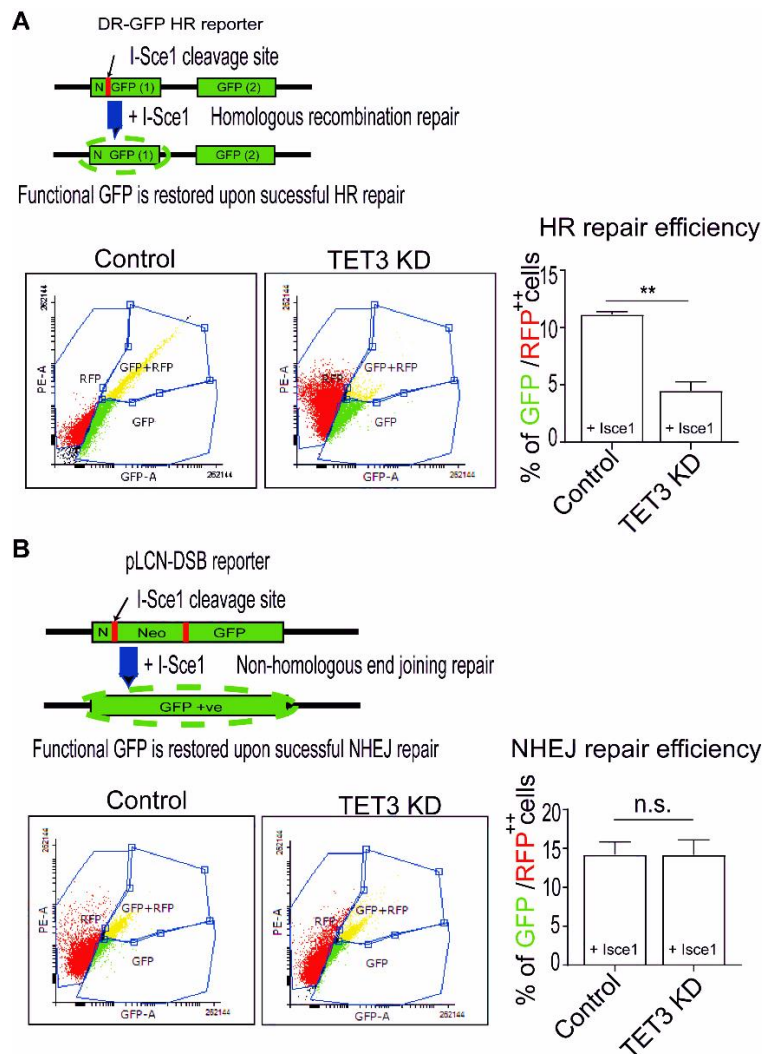


Figure 23. Effect of TET3 knockdown on HR and NHEJ efficiency in vitro in MCFs.

(A) MCFs integrated with a DR-GFP HR reporter substrate were transfected with TET3 knockdown construct and I-SceI and analyzed for change in HR efficiency by scoring % of GFP/RFP double-positive cells using flow cytometry. The associated graph represents HR efficacy in the ratio % of GFP/RFP double-positive cells. (B) MCFs integrated with a pLCN-DSB NHEJ reporter substrate were transfected with TET3 knockdown construct and I-SceI and analyzed for change in NHEJ efficiency by scoring % of GFP/RFP double-positive cells using flow cytometry. RFP was used in all the experiments to ensure transfection efficiency. All experiments were done in triplicates. Summarised quantitative findings are shown as mean \pm SD. Statistical significance was calculated using Welch unpaired two tailed Student's t-test, n.s. represents non-significant and P-values correspond to $**p \leq 0.01$.

3.14 Knockdown of TET3 results in decreased DNA end resection in MCFs

The readout from our reporter constructs demonstrates that TET3 knockdown MCFs have decreased HR efficacy. Diminished HR efficacy can result from either in-efficient DNA end resection or an improper resolution of D-loops by DNA resolvases (Kakarougkas & Jeggo, 2014). Inappropriate resolution of D-loops leads to genomic instability, increased anaphasic bridges, and micronuclei formation (Daley et al, 2014; Falquet & Rass, 2017). As in our results no such abnormal features were observed upon TET3 knockdown, we hypothesized that decreased DNA end resection could be the prime factor contributing to reduced HR efficiency. So, to understand whether the

observed decreased HR efficacy is due to limited or diminished DNA end resection, we performed a bromodeoxyuridine (BrdU)-based pulse chase assay. BrdU is a thymine analogue, which under DNA denaturing conditions incorporates into the single-stranded DNA (ssDNA) actively generated during DNA end resection (Mukherjee et al, 2015). While BrdU incorporation under physiological condition reflects cell proliferation (as traditional assays rely on DNA replication to allow BrdU to get integrated into the DNA), under denaturing conditions, BrdU incorporation is associated with DNA end resection because denaturation halts and dissociates DNA replication machinery, and hence, BrdU can only get incorporated if ssDNA is available. Using anti-BrdU antibodies, the overall change in fluorescence intensity of BrdU incorporation can be measured. A change in BrdU incorporation, thus, serves as a direct readout for DNA end resection (Mukherjee et al, 2015).

To test this concept, we first established that our TET3 rescue experiment is working. Briefly, 2 days after TET3 knockdown, we again re-transfected MCFs with 2.5 µg of TET3 overexpression plasmid. The knockdown cells rescued with TET3 overexpression construct are then left for 36 hours to recover. After 36 hours of recovery, the cells are collected and immediately processed for collecting the total protein lysate. Immunoblot analysis using 50 µg of protein illustrate that the knockdown and rescue experiment worked in the present experimental setup. Image J quantification of the blots clearly show an increase in TET3 protein expression upon rescue with over expression construct. Moreover, in the present experimental setup we are able to demonstrate a constant decrease in TET3 expression upon knockdown, showing robustness of our Crispr/Cas9 targeted TET3 knockdown construct. We then continued to assess the planned DNA end resection study using BrdU assay and our results show that TET3 knockdown in MCFs causes a decrease in BrdU fluorescence intensity that can be partly rescued upon re-expression of TET3. Decreased BrdU incorporation thus reflects a decrease in DNA end resection mechanism in TET3 knockdown MCFs (**Figure 24**).

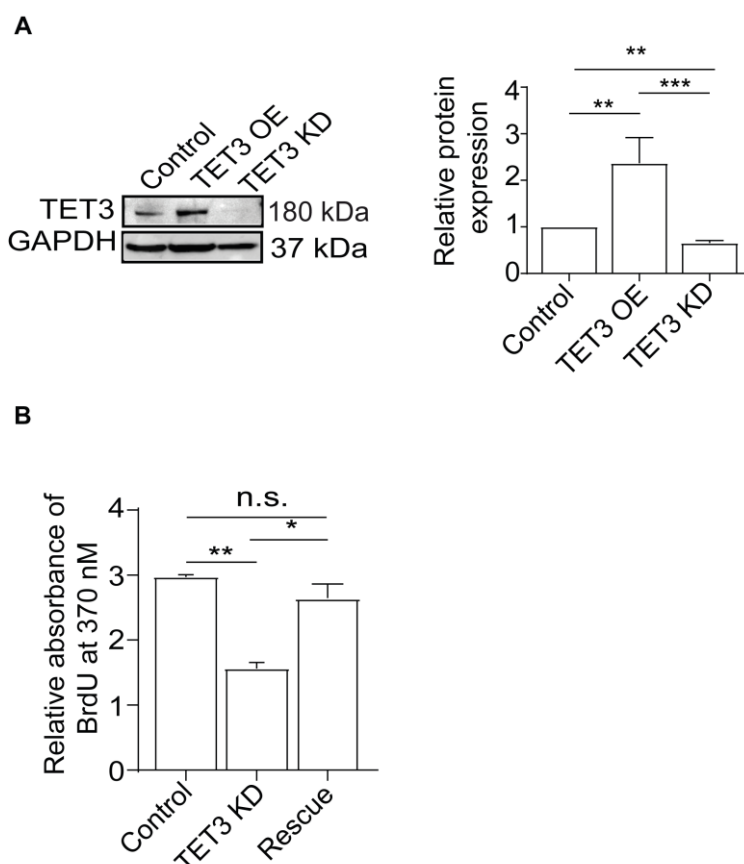


Figure 24. TET3 knockdown results in decreased BrdU incorporation in vitro in MCFs.

(A) Western blot and the associated graph are representing TET3 downregulation and overexpression in MCFs. (B) The bar graph represents decrease in BrdU incorporation due to inefficient DNA end resection. All experiments were done in triplicates. Summarised quantitative findings are shown as mean \pm SD. Statistical significance was calculated using Welch unpaired two tailed Student's t-test, n.s. represents non-significant and P-values correspond to * $p \leq 0.05$, ** $p \leq 0.01$, *** $p \leq 0.001$.

3.15 Knockdown of TET3 results in impaired recruitment of RAD51 to DNA DSBs in MCFs

To gain further insight into the role of TET3 in DNA end resection, we continued to study the recruitment of RAD51 at the DNA DSBs in TET3 knockdown and rescued MCFs. RAD51 is an essential monomeric protein complex, which binds to the end of resected single-stranded DNA tails and facilitates sister chromatid strand invasion (Ivanov et al, 2003; Sullivan & Bernstein, 2018). Previous studies have shown that RAD51 is recruited to sites of DNA damage when regions of ssDNA are exposed (Ma et al, 2017; Špírek et al, 2018). Hence, it serves as a direct readout for understanding the ongoing DNA end resection during HR. To confirm this, we performed staining for γ -H2AX in combination with RAD51 upon TET3 knockdown or rescue in NCS-treated MCFs. Our data demonstrate that upon NCS-induced DNA damage, RAD51 recruits to DSBs (Figure 25A). Interestingly, our results show that TET3 knockdown in MCFs results in increased RAD51 expression. Unlike in control MCFs, however, the recruitment of RAD51 to DNA DSBs is severely reduced in TET3 knockdown cells, despite an increase in DNA DSBs. Moreover, this effect continues to persist in TET3 knockdown MCFs challenged with NCS. These results suggest that although RAD51

results from our reporter constructs, we observed no significant change in 53BP1 foci at DNA DSBs in TET3 knockdown and rescued MCFs, suggesting that TET3 is involved only in the HR-mediated DDR response. Notably, although NHEJ is operational in TET3 knockdown MCFs, our data illustrates DNA DSBs is not resolved completely. We hypothesized there could be two possible reasons for such discrepancy. First, since the amount of DSBs is higher in TET3 knockdown MCFs even in absence of exogenous DNA damage causing agents, these cells just take longer time to repair. Second, the DSBs produced in cardiac fibroblasts in absence of TET3 could have more incompatible DNA ends, hence simple re-ligation of these broken ends is not feasible by NHEJ. This idea is well supported by the recent finding by Chang et.al, where they illustrate the importance of DNA DSBs ends in limiting the chances of NHEJ mediated DDR response (Chang et al, 2016). (**Figure 26A-B**).

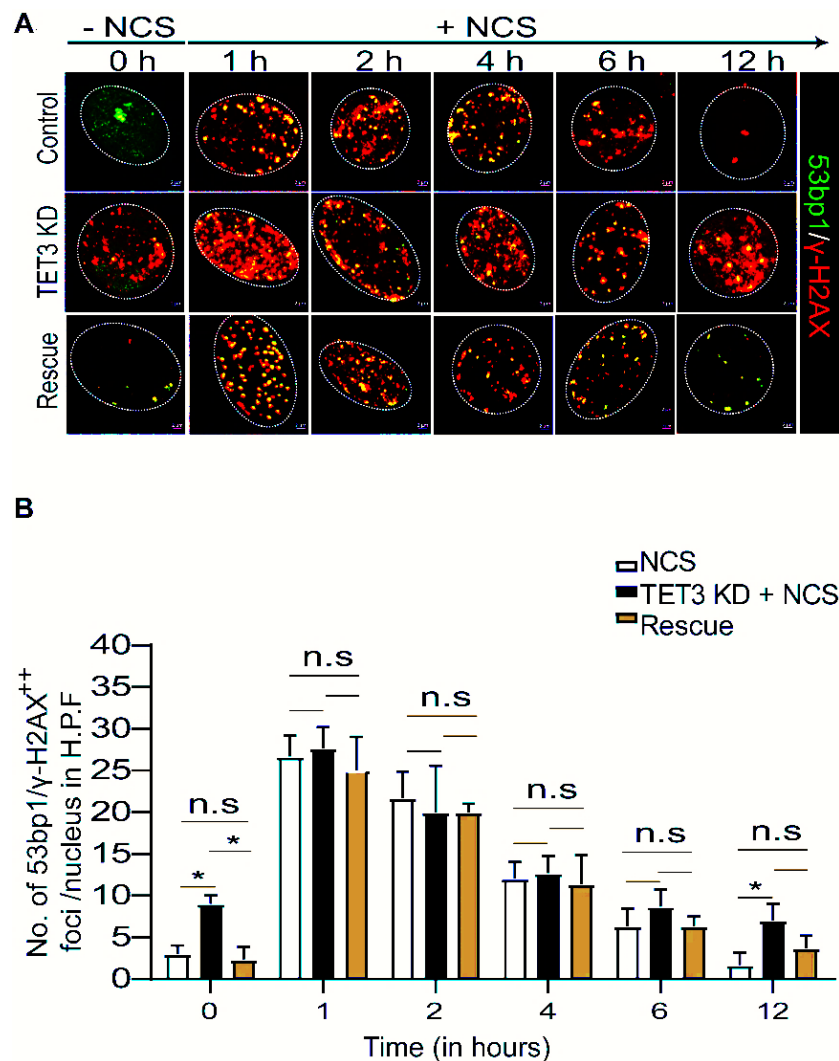


Figure 26. *TET3* knockdown does not affect the recruitment of 53bp1 at DNA DSBs in vitro in MCFs.

(**A and B**) Representative confocal images and an associated histogram shows 53bp1 (green) and γ -H2AX (red) colocalization (yellow) in MCFs in control, TET3 knockdown, and rescued cells (n=100 cells were analyzed in each condition from 3 different experiments). Summarised quantitative findings are shown as mean \pm SD. Statistical significance was calculated using one-way ANOVA Bonferroni and Sidak analysis, n.s. represents non-significant and P-values correspond to *p \leq 0.05, **p \leq 0.01, *** p \leq 0.001.

3.17 Knockdown of TET3 results in decreased global chromatin accessibility

Compaction and decompaction of chromatin play a key role in facilitating DDR response (Burgess et al, 2014; Hauer & Gasser, 2017). Recent investigations demonstrate that compacted chromatin causes efficient activation of the upstream DDR signalling (ATM/ATR) kinases but not its downstream components (Burgess et al, 2014). This establishes that a compacted chromatin state can result in an attenuated DDR response in cells. Additionally, studies have also linked the state of chromatin to the facilitation of the correct choice of DNA repair (Lemaitre et al, 2014; Stadler & Richly, 2017). Studies demonstrate that chromatin compaction restricts the mobility of the HR repair by disturbing nucleosome eviction during active DNA end resection and strand invasion (Oliveira et al, 2014; Yang et al, 2013). Additionally, studies suggest that DNA damage in compacted chromatin is favorably repaired by NHEJ (Noon et al, 2010), as this repair response operates via simple re-ligation of the broken ends.

Previous studies have shown that compacted chromatin limits the efficacy of HR (Sonoda et al, 2006). In line with these observations, our previous data have shown that loss of TET3 results in decreased HR efficacy in MCFs due to impaired DNA end resection and improper loading of RAD51 to the DNA DSBs. So, we hypothesized that this effect in TET3 knockdown cells could be a result of chromatin compaction.

To test this hypothesis, we used DAPI staining, which allows to analyse the intensity distribution within the nucleus as a measure of compaction using confocal microscopy (**Figure 27A**). Our results show that TET3-deficient MCFs have more compacted chromatin than healthy MCFs. Additionally, by re-expressing TET3 in the knockdown MCFs, we can relax the chromatin to be comparable to healthy MCFs (**Figure 27B**). This data demonstrates that the loss of TET3 results in compaction of chromatin which may then contribute to limiting HR efficacy.

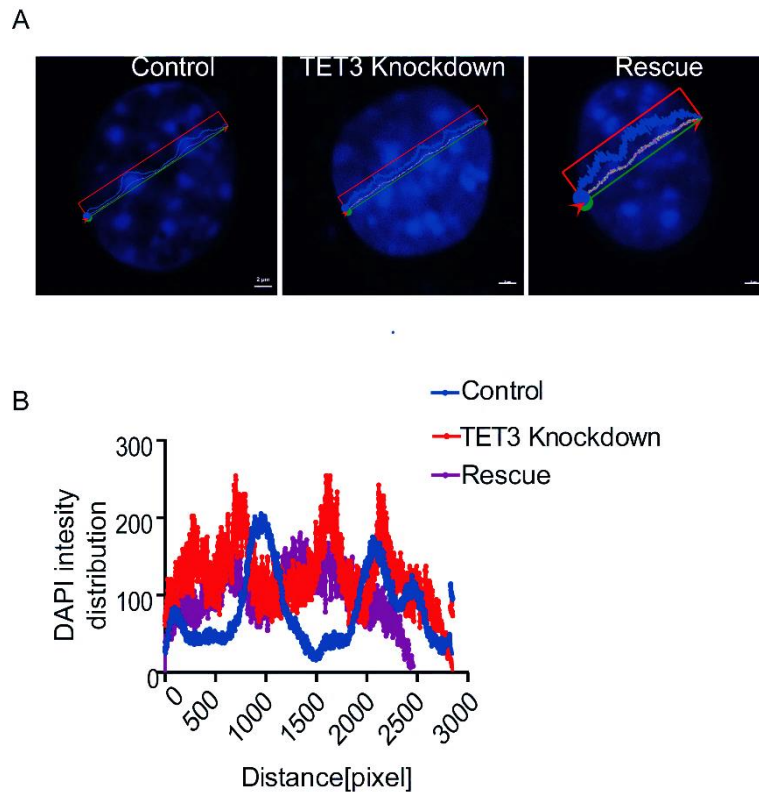


Figure 27. TET3 knockdown results in chromatin compaction in vitro in MCFs.

(A and B) DAPI intensity distribution and representation analyzed by confocal microscopy in Control, TET3 knockdown and rescued cells.

3.18 TGF- β treatment results in decreased TET3 expression but increased proliferation in MCFs

TGF- β is a highly pleiotropic cytokine that is widely known to induce fibroblast proliferation. Studies in murine keratinocytes and human epidermoid carcinoma cells have shown the involvement of TGF- β in the maintenance of genomic stability and DDR responses (Kim et al, 2015; Lee et al, 2016). In line with these observations, it is plausible that TGF- β could promote the proliferation of fibrotic fibroblasts by resolving the DNA damage. Our results demonstrate that TET3 deficient fibroblasts proliferate at a slower rate and have endogenous DNA damage. Thus, we hypothesised that TGF- β might be involved in resolving the DNA DSBs, helping TET3-deficient fibroblasts proliferate.

In order to test the role of TGF- β in promoting proliferation, we treated MCFs with 15 ng/mL of TGF- β and counted the cell doubling rate as well proliferation on every alternate day for ten days. Our results show that TGF- β caused both rapid increase in cell number and proliferation. However, upon removal of TGF- β on day five, we observed both decrease in cell number as well as proliferation. Altogether, our results show that exposure to TGF- β results in increased cell proliferation which then decreases upon removal of TGF- β after 5 days (**Figure 28A-B**).

Having confirmed that TGF- β promotes cell proliferation, we then assessed whether it facilitates resolving DNA DSBs. To address this, we performed γ -H2AX staining on every alternate day for ten days in MCFs. Interestingly, our results show that exposure to TGF- β for 5 days results in the formation of DNA DSBs (**Figure 28C-D**). Moreover, upon removal of TGF- β , we observed increased accumulation of DNA DSBs (**Figure 28C-D**). From these results, it can be understood that the presence of TGF- β helps in resolving DNA damage which helps the cells to proliferate. Removal of TGF- β on day 5 fails to resolve the DNA damage, which in turn results in decreased cell proliferation.

Our *in vivo* data demonstrates that fibrotic fibroblasts have decreased TET3 expression. We attempted to mimic the fibrotic state in MCFs upon TGF- β treatment and predicted that prolonged exposure would result in decreased TET3 expression. From our TET3 fluorescence staining and mRNA expression analysis, we confirmed downregulation of TET3 upon TGF- β treatment in MCFs. Moreover, upon removal of TGF- β on day 5, expression of TET3 remained downregulated (**Figure 28E**).

Recent studies also demonstrate that TGF- β can drive changes in epigenetic writers. While we cannot exclude that even longer exposure to TGF- β also leads to persistently increased proliferation, we suspect that the observed decrease in TET3 expression could be a result of the change in epigenetic balance at either the methylation or histone modification level.

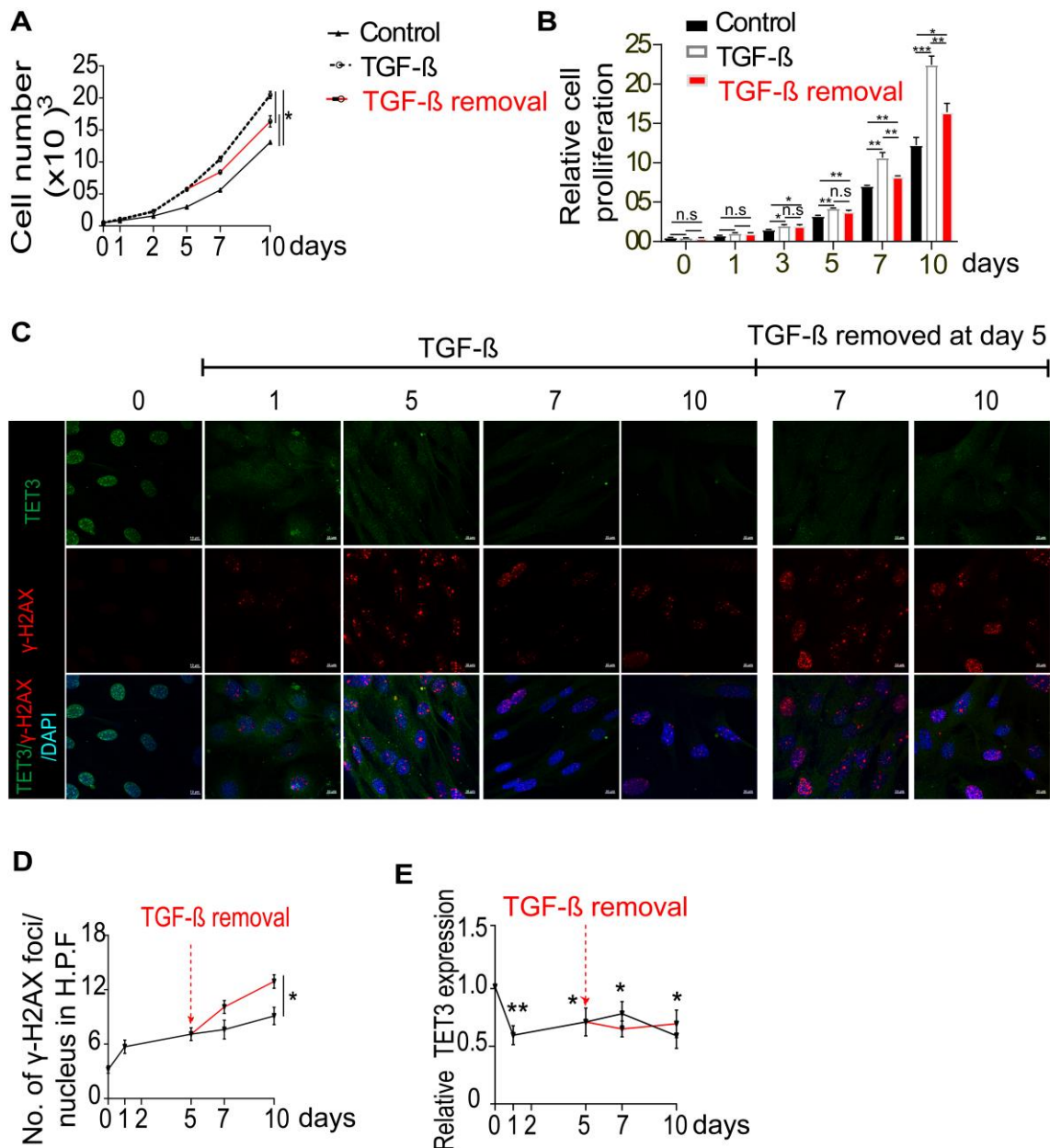


Figure 28. TGF-β treatment in MCFs affects cell count, proliferation, DNA damage and TET3 expression.

(A) The representative graph shows the effect of TGF-β on cell number in MCFs at indicative days. (B) The representative graph shows relative cell proliferation in control and TGF-β treated MCFs at indicative days. Summarised quantitative findings are shown as mean ± SD. (C and D) Representative confocal images and the associated graph shows the effect of TGF-β on γ-H2AX and TET3 expression in MCFs at indicative days. Summarised quantitative findings are shown as mean ± SEM. (E) Relative TET3 mRNA expression upon TGF-β treatment in MCFs at indicative days. Summarised quantitative findings are shown as mean ± SD. All the represented experiments are done in triplicates, and statistical significance was calculated using one-way ANOVA Bonferroni and Sidak analysis, and P-values correspond to *p ≤ 0.05, **p ≤ 0.01, ***p ≤ 0.001.

3.19 TGF- β treatment results in decreased DSBs in MCFs

Next, we continued to investigate how cardiac fibroblasts manage to proliferate during fibrosis despite the presence of DNA damage. To understand this, we mimicked fibrotic conditions by treating NCS treated MCFs and TET3 knockdown MCFs with TGF- β (**Figure 29A**). Consistent with previous studies, by counting the number of γ -H2AX foci per nucleus, we observed that pre-treatment with TGF- β in MCFs exposed to NCS (both under wildtype and TET3 knockdown conditions), leads to a decreased accumulation of DNA DSBs after 1 hour, which continuously declines further until 12 hours after NCS exposure (**Figure 29B-C**).

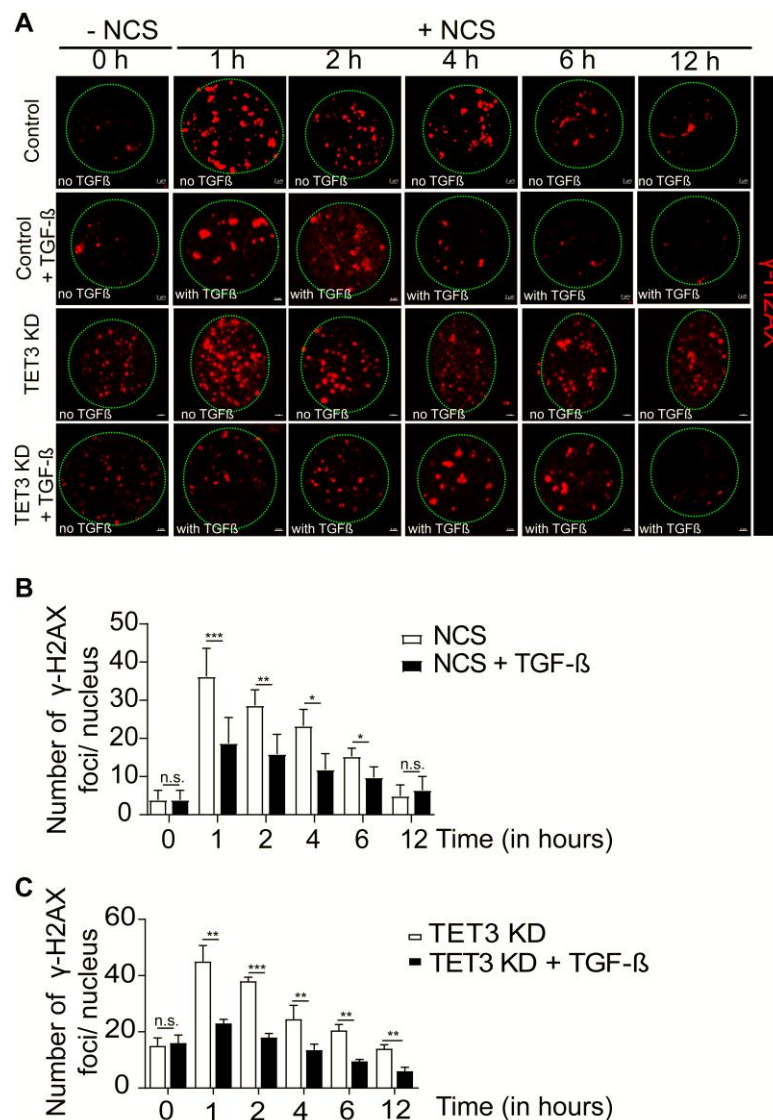


Figure 29. TGF- β decreases DNA DSBs in MCFs.

(A, B and C) Representative confocal images and an associated histogram is showing DNA damage recovery analyzed by resolving of γ -H2AX (red) in the presence or absence of TGF- β at indicated conditions (n=100 cells were analyzed in each condition from 3 different experiments). Summarised quantitative findings are shown as mean \pm SD. Statistical significance was calculated using Welch unpaired two tailed Student's t-test, n.s. represents non-significant and P-values correspond to *p \leq 0.05, **p \leq 0.01, *** p \leq 0.001.

3.20 TGF- β treatment activates increased NHEJ repair

Our previous data show that TGF- β pre-treatment results in decreased γ -H2AX foci (both in control and in TET3 knockdown MCFs), even when challenged with exogenous DNA DSBs inducing drug NCS. This suggests the possibility that treatment with TGF- β in MCFs either limits sensing of DNA DSBs or improves DNA repair capacity. To clarify this, we continued to use the HR and NHEJ DNA repair constructs and analysed the effect on DNA repair efficacies in the presence or absence of TGF- β in control and TET3 knockdown MCFs. Our results show that pre-treatment of TGF- β over 24 hours results in a marked decrease in HR efficiency when analysed by the presence of the percentage of GFP and RFP double-positive cells by FACS (**Figure 30A**). This result is in line with a previously published study in CD44+/CD24–cancer cells in which TGF- β signalling was reported to decrease HR efficacy (Pal et al, 2017). We reported that TGF- β also downregulates TET3 expression, which is involved in the HR repair. In line with these observations, our results show that TGF- β , in combination with reduced TET3 expression also shows a decreased HR efficiency (**Figure 30A-B**). However, we noticed that the combination of TGF- β and TET3 knockdown does not show an additive decrease in HR efficacy but instead is maintained at more or less the same levels, (**Figure 30A**), which is likely due to the fact that TGF- β treatment per se leads to decreased expression of TET3 as previously shown.

After having established that TGF- β downregulates HR efficacy, we continued to investigate whether an increase in NHEJ results in improved DNA repair capacity. Using NHEJ reporter construct analysis, we demonstrate that indeed TGF- β upregulates NHEJ repair efficiency and this increase is maintained in TET3 knockdown cells treated in combination with TGF- β (**Figure 30C-D**). From these results, we conclude that the decrease in DSBs observed upon TGF- β treatment in MCFs is a result of enhanced NHEJ repair efficiency.

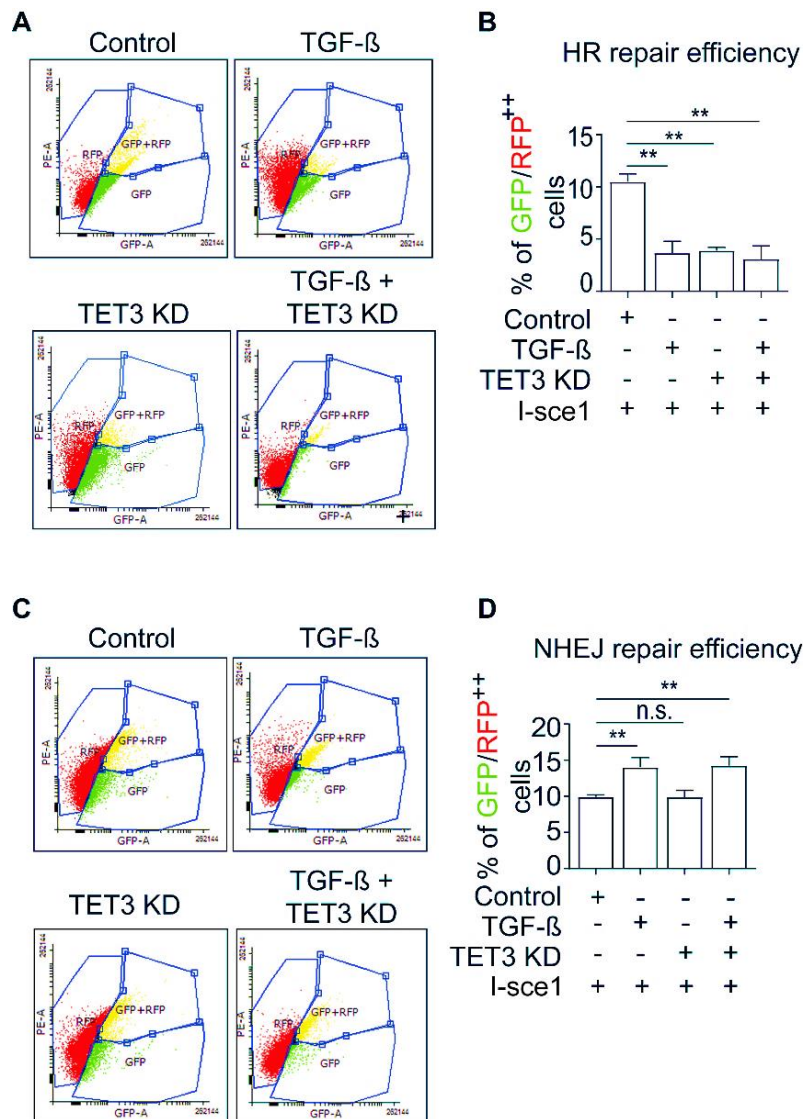


Figure 30. TGF-β increases NHEJ mediated DNA repair response in MCFs.

(A and B) MCFs integrated with a DR-GFP HR reporter substrate were transfected in indicated conditions in combination with I-Sce-1 and analyzed for change in HR efficiency by scoring % of GFP/RFP double-positive cells using flow cytometry. (C and D) MCFs integrated with a pLCN-DSB NHEJ reporter substrate were transfected in indicated conditions in combination with I-Sce-1 and analyzed for change in NHEJ efficiency by scoring % of GFP/RFP double-positive cells using flow cytometry. RFP was used in all the experiments to ensure transfection efficiency. All experiments were done in triplicates. Summarised quantitative findings are shown as mean \pm SD. Statistical significance was calculated using Welch unpaired two tailed Student's t-test, n.s. represents non-significant and P-values correspond to * $p \leq 0.05$, ** $p \leq 0.01$, *** $p \leq 0.001$.

3.21 TGF-β treatment promotes proliferation in cardiac fibroblasts which can be rescued by TET3 overexpression

Our previous results demonstrate that TGF-β treatment results in decreased TET3 expression and an increased number of cells and proliferation. Additionally, our results show that TGF-β increases NHEJ efficacy and that the loss of TET3 decreases HR efficacy. Furthermore, existing studies in the literature demonstrate that the activation

of HR requires the engagement of the G₂M phase arrest. Thus, we hypothesized that overexpression of TET3 in TGF- β treated fibroblasts would result in decreased cell proliferation due to the activation of the checkpoint arrest-assisted HR-mediated DNA repair. Moreover, as TGF- β treatment per se results in decreased TET3 expression, hence, we also hypothesized that the cell proliferation rate would be unchanged in TGF- β treated MCFs with or without CRISPR mediated TET3 knockdown.

To examine our hypothesis, as previously described, we used TGF- β to mimic a fibrotic environment and then compared the change in the number of cells and proliferation over 7 days between TET3 knockdown MCFs combined with TGF- β , with the change in the number of cells and proliferation in TGF- β -treated MCFs. Our cell counting and proliferation results show that TET3 knockdown MCFs treated with TGF- β show no significant change in cell numbers and the proliferation rate compared to the TGF- β -treated MCFs (**Figure 31A-B**).

However, TGF- β -treated MCFs and TET3 knockdown MCFs treated with TGF- β show an increased proliferation rate compared to the control MCFs (**Figure 31B**). Notably, our previous results also demonstrate that NHEJ repair efficiency is maintained at a steady state in TGF- β treated MCFs and TET3 knockdown cells treated in combination with TGF- β . These results demonstrate that the loss of TET3 has no additive effect on the change in cell number and proliferation state in TGF- β -treated MCFs.

Next, we continued investigating our hypothesis that TET3 overexpression in TGF- β -treated MCFs should likely result in decreased cell proliferation. As expected, our results show that the re-expression of TET3 in fibrotic conditions restrains not only cell numbers but also proliferation (**Figure 31**). Existing studies demonstrate that increased DNA end resection due to HR leads to apoptosis in proliferating cells (van den Berg et al, 2019). Therefore, it is highly likely that an increase in TET3 expression in proliferating TGF- β -treated MCFs results in a decrease in the cell number due to additionally increased apoptosis induced by DNA end resection.

So far, from our results, we confirm that TET3 overexpression leads to a decrease in cell proliferation in TGF- β -treated MCFs. Moreover, our data also suggests that cell proliferation is, in part, regulated by the choice of engaged DNA repair. Thus, we continued investigating whether this restrained cell proliferation observed upon TET3 overexpression, as per our hypothesis is, in part, a consequence of increased HR-mediated repair in proliferating MCFs. As, proper engagement of HR requires activation of cell cycle checkpoints, we decided to first look into the H3s10p status and later on into the change in DNA repair efficacies.

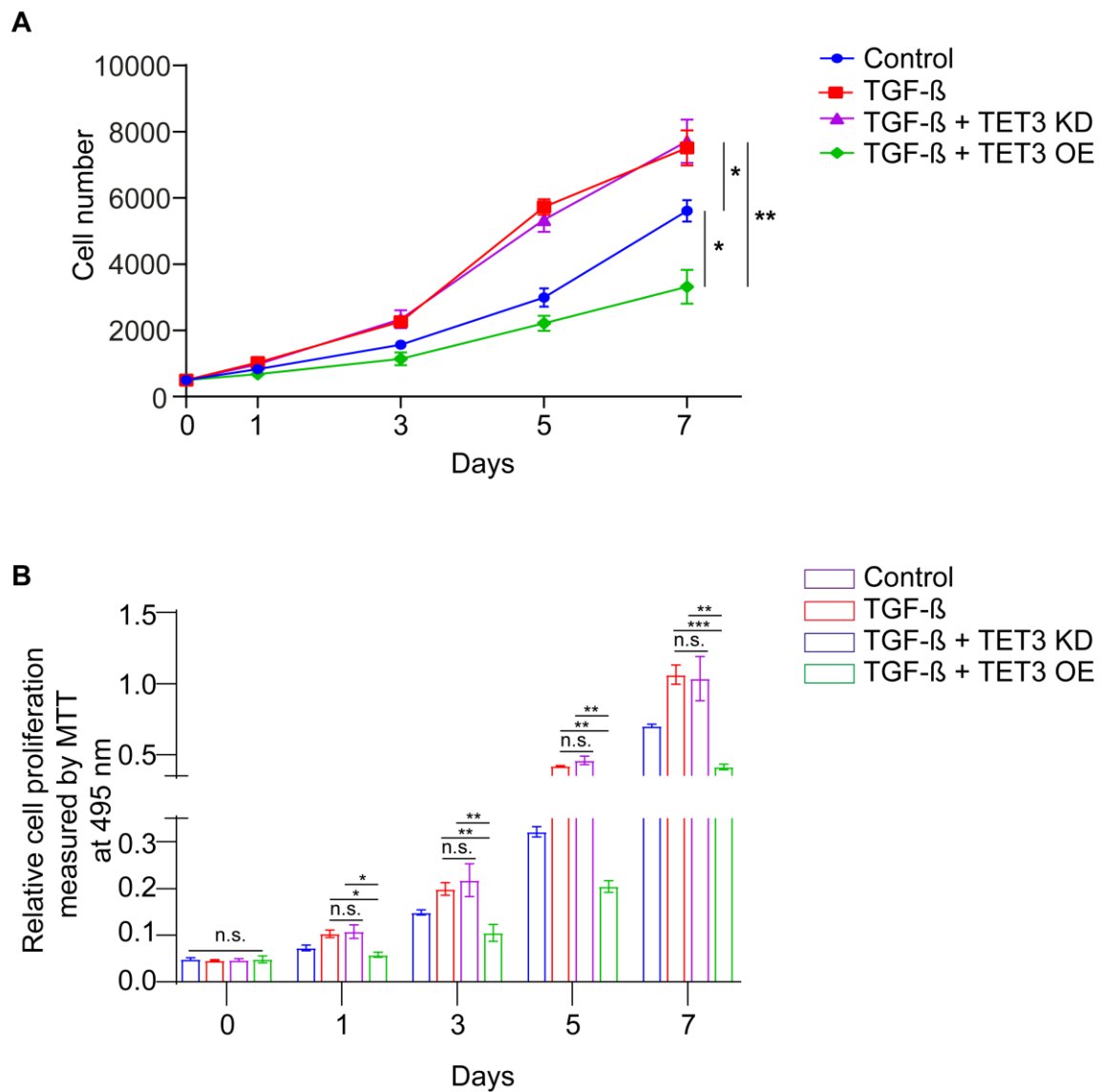


Figure 31. TGF- β dramatically increases proliferation rate in MCFs which can be rescued by TET3 overexpression.

(A) The representative graph shows the effect of TGF- β on cell number in control, TET3 knockdown, and overexpressed MCFs over 7 days. (B) The representative graph shows the effect on cell proliferation in MCFs pre-treated with TGF- β in control, TET3 knockdown, and overexpressed cells. Summarised quantitative findings are shown as mean \pm SD. All experiments were done in triplicates, and statistical significance was calculated using one-way ANOVA analysis, n.s. represents non-significant and P-values correspond to * $p \leq 0.05$, ** $p \leq 0.01$, *** $p \leq 0.001$.

3.22 TGF- β treatment results in increased H3s10p in MCFs

Phosphorylation of histone at serine 10 is a sensitive marker for detecting cells committed to the mitotic phase (Hans & Dimitrov, 2001); (Dong & Bode, 2006). Studies have shown that an increase in the H3s10p signal characterizes a cell's commitment to proliferate. Moreover, H3s10p provides a positive feedback signal for the clearance from checkpoint activation and thus prepares the cells to engage through anaphase and undergo proliferation (Monier et al, 2007). Therefore, as per the literature, a decrease in H3s10p indicates the activation of the G2/M checkpoint, while

an increase in H3s10p indicates clearance of G2M arrest and commitment to proliferation.

In line with these observations, studies have also shown that the presence of DSBs results in decreased H3s10p activation (Hilmi et al, 2017), which allows proper engagement of HR-mediated DNA repair. Based on our previously observed cell proliferation data, we next continued by assessing the activation of H3s10p in the control and TGF- β treated MCFs.

Our results demonstrate that, upon induction of DNA DSBs, MCFs activate the proper G2/M arrest marked by a decreased H3s10p activation (**Figure 32A-B**). This result suggests that, in healthy fibroblasts, the commitment to proliferation is affected by the presence of DSBs due to the efficient activation of HR.

Interestingly, in our previous data, we observed that TGF- β treatment in MCFs results in decreased DNA DSBs via increased NHEJ. As per previous studies, it is well known that the engagement of NHEJ does not require the cells to be arrested in the G2M phase. Thus, we expected TGF- β -treated MCFs to have increased H3s10p status. Indeed, our results show that MCFs treated with TGF- β have increased H3s10p (**Figure 32C-D**), suggesting increased commitment to cell proliferation. This result agrees with our results of increased cell proliferation in TGF- β -treated MCFs, compared to untreated MCFs.

However, we noticed that the combination of TGF- β and TET3 knockdown does not show an additive increase in H3s10p but instead is maintained at more or less the same levels, (**Figure 32C-D**), which is likely because TGF- β treatment per se leads to decreased TET3 expression. These results agree with the cell proliferation data, wherein we reported that the loss of TET3 has no additive effect on the proliferation of TGF- β -treated MCFs.

However, in the present study, we observed that TET3 facilitates HR-mediated DNA repair, which requires the G2M checkpoint arrest to operate. Notably, from our previous data, we confirmed that overexpression of TET3 results in restraining the cell proliferation in TGF- β -treated MCFs. In line with these observations, we hypothesized that the overexpression of TET3 in TGF- β -treated MCFs could result in decreased H3s10p due to increased G2M arrest favoring HR-mediated DNA repair. Indeed, our results demonstrate that, upon re-expression of TET3, TGF- β -treated MCFs dramatically reduce H3s10p (**Figure 32E-F**), suggesting the activation of HR.

Altogether, our results suggest that the restraint in cell proliferation upon TET3 overexpression in TGF- β -treated MCFs may be, in part, a consequence of the activation of a slow G2M checkpoint-dependent HR. So, we continued by assessing the change in HR repair efficacy, to test if indeed the decreased cell proliferation is partly a consequence of TET3 mediated shift in DNA repair.

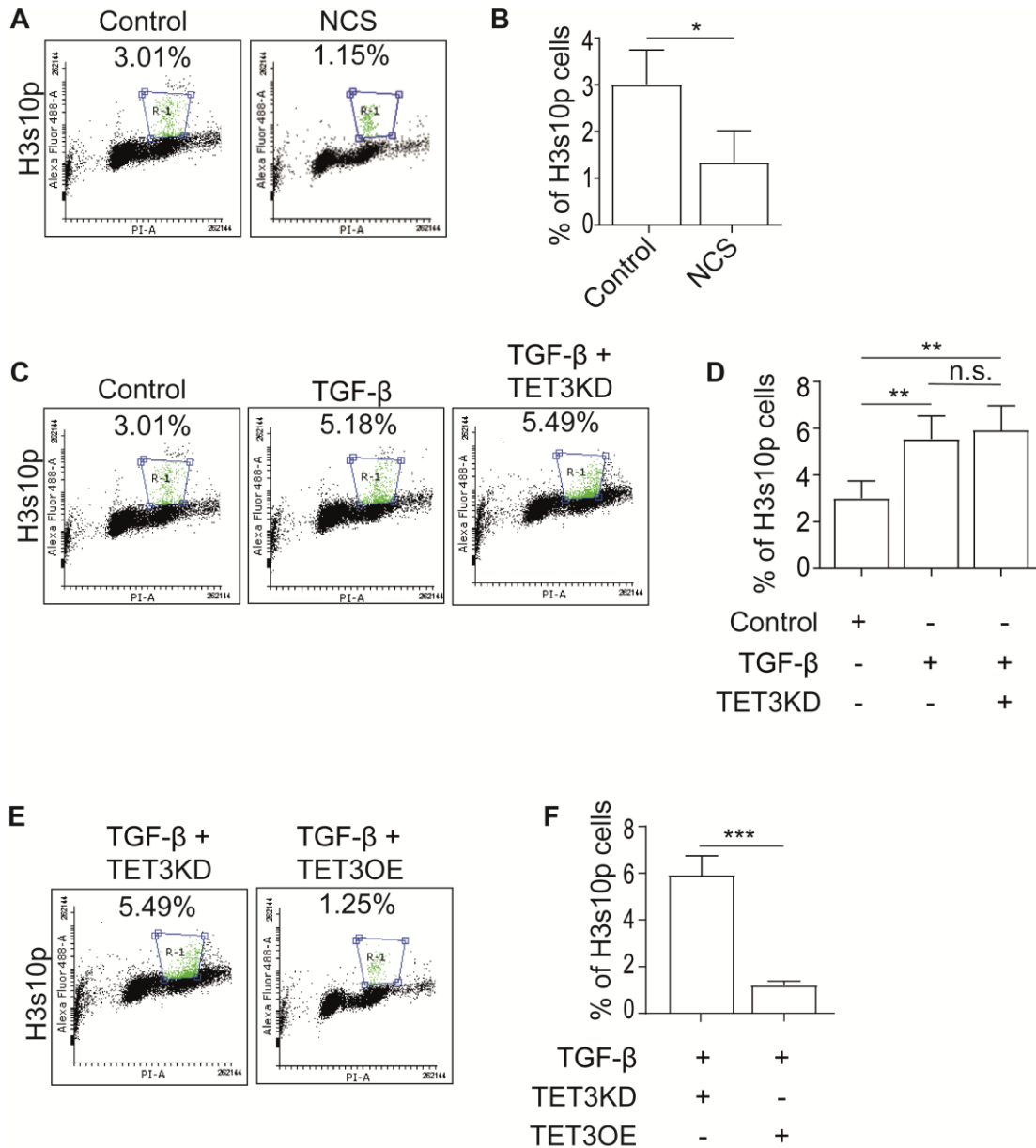


Figure 32. TGF-β increases H3s10p signalling in vitro in MCFs.

(A-F) Flow cytometry analysis of histone H3 on Ser-10 (pH3) representing the mitotic index in Control, NCS, TGF-β or TGF-β with either TET3 knockdown or TET3 overexpressed MCFs at indicated time points (n=10,000 cells analyzed in each condition from 3 different experiments. Summarised quantitative findings are shown as mean ± SD. All experiments were done in triplicates. Statistical significance was calculated using either unpaired nonparametric two-tailed student t-test or one-way ANOVA Bonferroni and Sidak analysis, n.s. represents non-significant and P-values correspond to * p ≤ 0.05, ** p ≤ 0.01, and *** P ≤ 0.001.

3.23 TET3 overexpression in TGF-β treated MCFs results in an increased HR repair

The results from our cell proliferation data indicate that overexpression of TET3 causes decreased cell proliferation in TGF-β-treated MCFs. As TET3 is involved in the HR-mediated DNA repair response, we hypothesized that the observed restraint in the increase in cell numbers and proliferation can be associated with an increased HR. To

understand this idea, we again used HR repair reporter constructs and checked the change in HR efficacy in the TET3 overexpressed condition. Analyzing the percentage of GFP and RFP double-positive cells by FACS, we demonstrated an increase in HR efficiency on TET3 overexpression in TGF- β -treated MCFs (**Figure 33**). Studies have shown that an increased HR repair response provides negative feedback to cell proliferation (Yoon et al, 2014). Consistent with these studies, our results demonstrate an increase in HR upon TET3 overexpression, likely restraining cell proliferation. Surprisingly, our results demonstrate that TET3 overexpression in TGF- β -treated MCFs also results in decreased NHEJ. A recent study shows that increased DNA end resection or hyper-recombination events due to HR lead to a decreased NHEJ-mediated DNA repair efficacy (Lopez-Saavedra et al, 2016). Our present results are in line with these studies and show that the balance of DNA repair is crucial for the cell survival. Thus, from the observed results, we demonstrate that presence of TET3 indeed has an effect on cell proliferation in fibrotic fibroblasts, partly via regulating the choice of DNA repair.

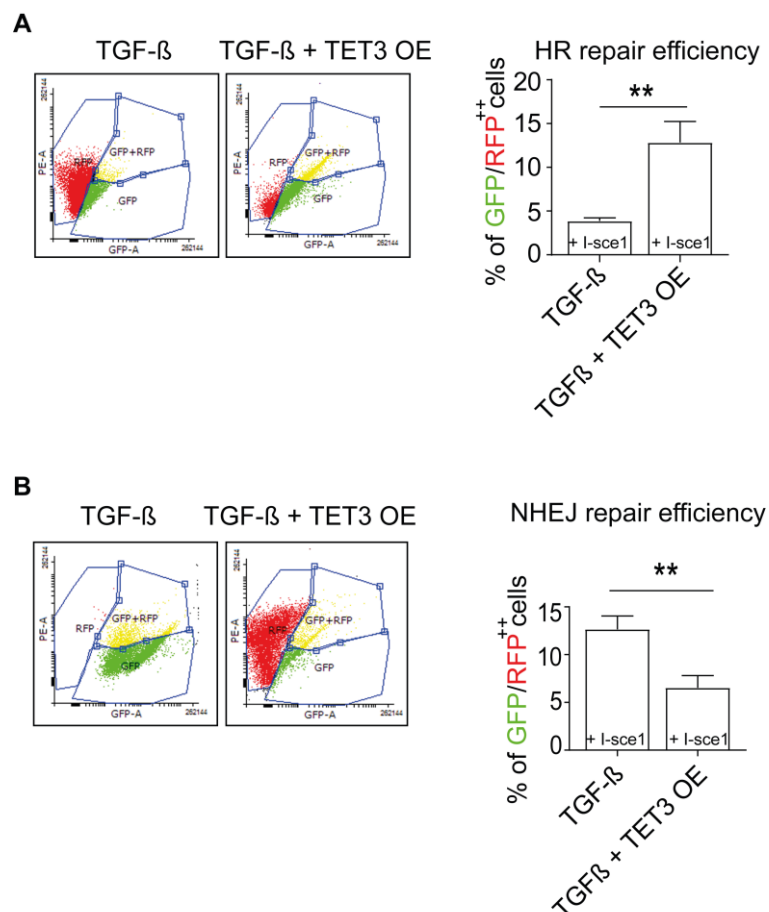


Figure 33. TET3 overexpression results in increased HR repair efficacy in TGF- β treated MCFs.

(A and B) DNA repair constructs showing HR and NHEJ repair efficiency in TGF- β pre-treated MCFs with or without TET3 overexpression conditions (n=10,000 cells analyzed in each condition). RFP was used in all the experiments to ensure transfection efficiency. All experiments were done in triplicates. Summarised quantitative findings are shown as mean \pm SD. Statistical testing was done using Welch unpaired two tailed Student's t-test. Significant P-values are represented in the graphs **p \leq 0. 01.

3.24 Mouse fibrotic fibroblasts have increased NHEJ mediated repair *in vivo*

Thus far, we conclude that the loss of TET3 results in TGF- β -treated MCFs favoring NHEJ-mediated DNA repair, which in turn provides a proliferative advantage to the TGF- β -treated MCFs. In line with these findings, we want to establish that our *in vitro* results can be recapitulated in our *in vivo* mouse fibrotic model. Therefore, to evaluate the significance of our observed *in vitro* results, we continued to assess the expression of 53bp1 (a core NHEJ repair factor) in the fibrotic fibroblasts of our angiotensin-II-treated mouse hearts. Using 53bp1 and α -SMA double immunofluorescent staining, we confirmed increased 53bp1 expression in fibrotic fibroblasts of our angiotensin-II-treated mouse hearts, suggesting increased NHEJ repair (**Figure 34**). Previously, our *in vivo* results demonstrated increased expression of Ki67 in fibrotic fibroblasts. In line with all of these observations, our results altogether demonstrate that the loss of TET3 favors increased NHEJ repair response in fibrotic fibroblasts to provide a proliferative advantage in an abundant DNA damage niche.

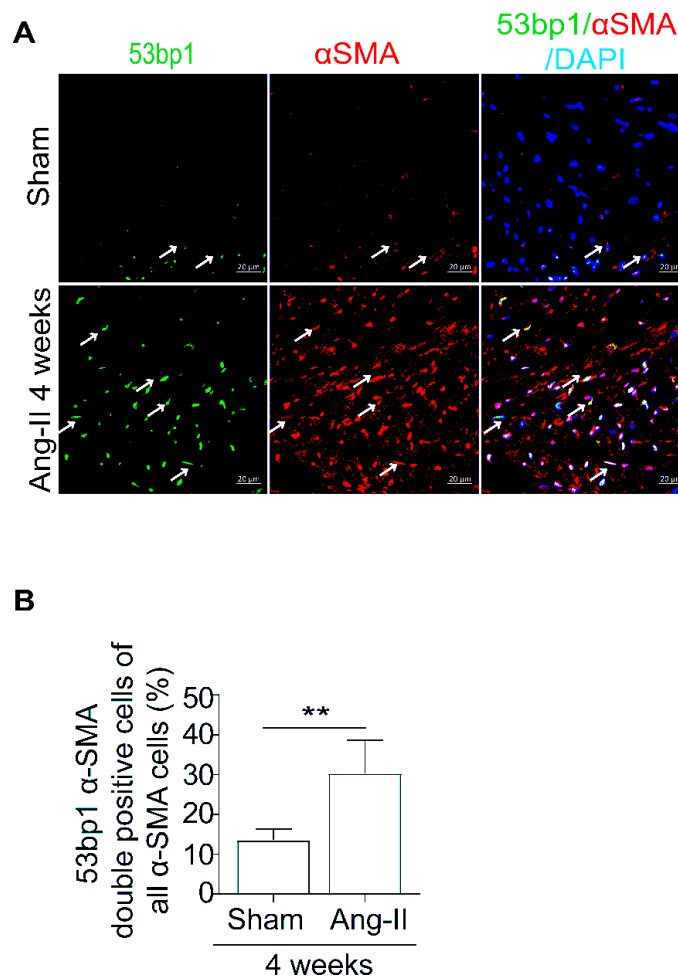


Figure 34. Mouse fibrotic fibroblasts have increased 53bp1 expression *in vivo*.

(A and B) Confocal representative images and the respective graph shows double staining of 53bp1 and α -SMA in 4 weeks of sham and angiotensin-II treated mouse hearts. The arrow marks represent the fibroblasts positive or negative for 53bp1 in 4 weeks of sham and angiotensin-II treated mouse hearts. Summarised quantitative findings are shown as mean \pm SEM from 3 shams, and 3 Angiotensin-II treated mouse hearts. Statistical significance was calculated using Welch unpaired two tailed Student's t-test, and P-values correspond to $**p \leq 0.01$. Scale bars represent 10 μ m.

3.25 Human fibrotic hearts lose TET3 expression

Our *in vitro* and *in vivo* data in mouse cardiac fibroblasts show that the expression of TET3 is downregulated during fibrosis. Additionally, the microarray data of ischemic human hearts also demonstrated a significant decrease in TET3 expression. Therefore, to evaluate the clinical significance of the proposed study during cardiac fibrosis in human patients, we continued by assessing the expression pattern of TET3 in fibroblasts of non-fibrotic and fibrotic human heart biopsies obtained from patients with aortic stenosis. Masson's trichrome staining was performed to confirm and quantify the fibrosis in human hearts (**Figure 35A-B**). Next, using hematoxylin/eosin (H&E) staining, we confirmed the change in morphology of fibrotic and non-fibrotic human hearts (**Figure 35A**). The expression of TET3 in fibroblasts is confirmed by co-immunofluorescent staining with α -SMA (**Figure 35C**). By counting the total percentage of TET3 and α -SMA double-positive cells out of the total α -SMA positive cells, we demonstrate that TET3 expression is downregulated in fibroblasts of fibrotic human hearts (**Figure 35D**), suggesting TET3 plays a role in the maintenance of low fibroblast numbers in healthy human hearts.

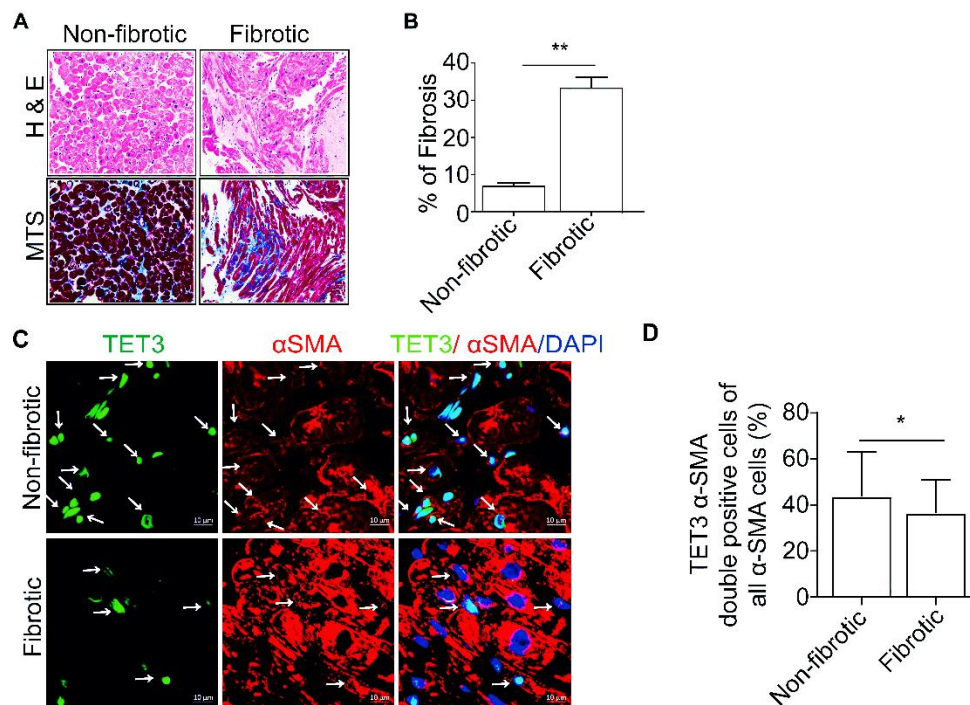


Figure 35. Human fibrotic fibroblasts have decreased TET3 expression.

(A) MTS and H&E staining in non-fibrotic and fibrotic human hearts. **(B)** Graph representing % of the fibrotic area in non-fibrotic and fibrotic human hearts. **(C and D)** Confocal representative images and the respective graph shows double staining of TET3 and α -SMA in non-fibrotic and fibrotic human hearts. Arrows mark fibroblasts positive for TET3 in non-fibrotic and fibrotic human hearts.

Summarised quantitative findings are shown as mean \pm SEM. Statistical significance was calculated using Welch unpaired two tailed Student's t-test, and P-values correspond to * $p \leq 0.05$. Scale bars represent 10 μm .

4. DISCUSSION

Activation and proliferation of cardiac fibroblasts are the prime mediators of cardiac fibrosis (Khalil et al, 2017). Existing studies indicate that ROS and inflammatory cytokines produced during fibrogenesis not only result in increased proliferative stimuli but also contribute to DNA damage in the form of DSBs (Cheng et al, 2003; Cucoranu et al, 2005; Weyemi et al, 2015). The presence of DSBs normally halts the cell cycle and activates DNA repair machinery to resolve the damage (Delacote & Lopez, 2008). However, in pathological conditions, such as fibrosis, there is a continuous need for activation and proliferation. Therefore, to maintain a sustained proliferation of cardiac fibroblasts, the activation of a distinct DNA repair mechanism is essential. Previous studies from our lab have highlighted the protective role of TET3, a DNA demethylase enzyme in organ fibrosis (Tampe et al, 2014; Xu et al, 2015; Xu et al, 2018). Notably, emerging studies have linked the role of TET3 to DDR response. In line with these observations, the entire work of my dissertation is focused on understanding (a) the expression of TET3 and DNA damage in cardiac fibrosis (b) the role of TET3 in dictating the DNA repair pathway choice, and (c) whether TET3 has a role in facilitating proliferation of the fibroblasts in the fibrotic niche via modulation of DNA damage and repair response.

Thus far, we have demonstrated that TET3 affects DNA damage response mechanisms via orchestrating checkpoint-assisted homologous recombination-mediated DDR and that TGF- β , in combination with the lack of TET3 in cardiac fibrosis, leads to a shift from HR-mediated DNA damage response to a checkpoint-independent non-homologous end-joining DDR (**Figure 33**). Using γ -H2AX and TET3 staining, we demonstrate DNA DSB accumulation and a reduction of TET3 expression in fibrotic fibroblasts in the angiotensin-II mouse model of cardiac fibrosis (**Figure 11 and Figure 14**). The DNA repair kinetics *in vitro* in MCFs revealed that, when challenged with DNA damage, TET3 is recruited to the γ H2AX foci. Recruitment of TET3 to the DSBs was confirmed using high definition laser confocal microscopy and a sensitive PLA assay *in vitro* in MCFs (**Figure 17, Figure 18 and Figure 19**). By using DNA repair reporter constructs for HR and NHEJ, respectively, we further confirmed that TET3 mediates the error-free, but checkpoint-assisted slower HR to repair DNA DSBs in MCFs (**Figure 23**). Additionally, using CRISPR/Cas9-based knockdown in MCFs, we demonstrate that the loss of TET3 results in the compaction of chromatin and the production of endogenous DSBs in the absence of any external damage stimuli (**Figure 22 and Figure 27**). Notably, we also demonstrated that the decreased HR efficacy in TET3 knockdown MCFs is a result of diminished DNA end resection (**Figure 24**). The most interesting aspect of the entire study is that, upon pre-treatment with TGF- β in MCFs, we demonstrate that loss of TET3 is accompanied by a switch to NHEJ-based DDR, faster clearance of DNA damage, re-entry into the cell

cycle, and increased proliferation, which can be rescued by overexpression of TET3 (**Figure 31 and Figure 33**).

A summary of the mechanism is illustrated in **Figure 36**.

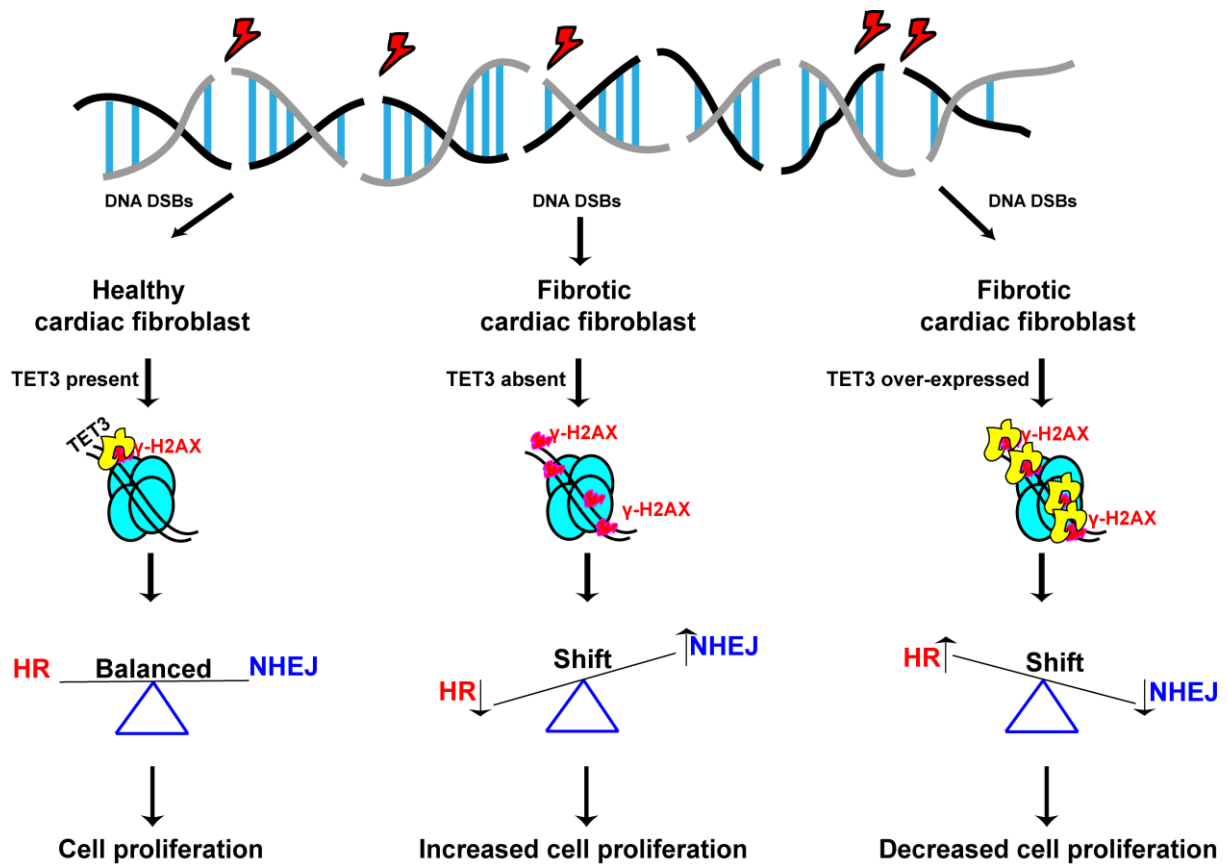


Figure 36. Schematic representation illustrating the role of TET3 in modulating the DDR response in healthy and fibrotic fibroblasts.

4.1 TET3 affects DNA damage and repair in cardiac fibroblasts

Studies are highlighting the role of DNA demethylases as a new independent factor in orchestrating the DNA damage and repair responses (Wu & Zhang, 2017). In line with these observations, a recent study has shown that TET3 plays a key role in efficient repair of DNA lesions, thereby providing protection against genomic instability in mouse embryonic fibroblasts (Jiang et al, 2017). However, it is not quite clear from these studies whether TET3 could be involved in the repair of DNA DSBs or whether TET3 is actually recruited to the DNA DSBs.

If TET3 recruits to DNA DSBs, does it have an influence on the two most common DSB repair pathways, HR and NHEJ? In the present study, using confocal imaging and the PLA assay, we demonstrated that TET3 is recruited to the DNA DSBs. In addition, using readouts from the DNA repair reporter constructs, we showed that TET3 facilitates HR-mediated but not NHEJ-mediated DNA repair (**Figure 23**). To our

knowledge in the context of cardiac fibroblasts, this is the first study to demonstrate that TET3 is recruited at the DNA DSBs and mediates the choice for HR-mediated DNA repair. In the context of cardiac fibroblasts, these findings open interesting research avenues on the role of TET3 in DNA DSB repair responses.

As per the literature, post-translational modifications of the proteins are crucial for their involvement in DSB repair (Polo & Jackson, 2011). This idea is in line with a previously published study in glial and MEFs cells in which ATM and ATR kinase were reported to phosphorylate TET1 and TET3 to stabilize their expression during DNA damage (Jiang et al, 2017; Jiang et al, 2015). Mass-spectrometry studies in HEK293 cells show that the N-terminal domain of TET3 is highly subjected to post-translational modifications (Bauer et al, 2015). In the same study, it was also reported that the phosphorylation serine-362 position competes with oGlcNAcylation, the outcome of which dictates TET3 nuclear retention (Bauer et al, 2015). This report is well supported by a previous study on Hela cells, where oGlcNAcylation of TET3 is shown to promote cytoplasmic export (Zhang et al, 2014). In line with these results, it would be noteworthy to precisely explore the phosphorylation status of TET3 because it could explain whether post-translational phosphorylation is indispensable for the recruitment of TET3 to the γ -H2AX foci.

The TET proteins are best known for their role in DNA hydroxymethylation (Tahiliani et al, 2009). The existing studies in MEFs demonstrate that TET3 mediates increased hydroxymethylation at DSBs (Jiang et al, 2017). Notably, these studies provide no evidence for the recruitment of TET3 to DNA damage sites. In line with these observations, our results demonstrate that TET3 recruits to DNA damage sites. Meanwhile, new studies are emerging which highlight a non-catalytic role of TET3 (Krueger et al, 2017; Montalban-Loro et al, 2019), Therefore, it is possible that this independent catalytic activity of TET3 may play a role in DDR response. More investigations are necessary to evaluate this idea.

As all the TET proteins are shown to be involved in DDR, one of the questions that remain unanswered is whether, in the absence of TET3, TET1 and TET2 can compensate for the DNA repair. Previous studies have shown that TET1 and TET2 facilitate NHEJ-mediated DDR response (Lu et al, 2016; Zhong et al, 2017), surprisingly which is quite opposite to our present findings on the role of TET3 in facilitating HR-mediated DNA repair response. Moreover, as in the present study we propose a non-catalytic role of TET3 in DNA repair, hence, it would be interesting to investigate whether the other isoforms can also participate in DNA repair response independent of their catalytic function. In line with this idea, a recent study in HEK293 and MEFs demonstrate, a hydroxymethylation independent role of TET1 in NHEJ-mediated DNA repair, by forming a chromatin associated complex with sin3a and hMOF transcriptional factors (Zhong et al, 2017). Therefore, further investigations are necessary to understand the in-depth mechanism on how specific TET isoforms and their distinct domains play a decisive role in DNA DSB repair response.

In the present study, we illustrate that TET3 is involved in HR-mediated DDR (**Figure 23**). One of the crucial stages of HR is the resection of DNA around DSBs to expose ssDNA, which is necessary to orchestrate RAD51-mediated strand invasion (Huertas, 2010). We observed that TET3 deficiency results in impairment of BrdU incorporation (**Figure 24**), which is a direct readout for ongoing DNA end resection (Mukherjee et al, 2015). Furthermore, we also observed improper loading of RAD51 at the γ -H2AX foci in TET3-deficient cardiac fibroblasts, strengthening our hypothesis about diminished DNA end resection. However, we do not observe any change in NHEJ repair efficiency or recruitment of NHEJ core proteins 53bp1 between TET3-deficient or control fibroblasts (**Figure 23**). Hence, it is highly likely that such an outcome can also result from a direct interaction of TET3 with RAD51 (mediating HR) but not with 53bp1 (mediating NHEJ).

4.2 TET3 may affect replication stress in cardiac fibroblasts

In the present study, we demonstrate that the loss of TET3 in MCFs results in impaired recruitment of RAD51 to the DSB (**Figure 25**). Interestingly, studies have shown that impaired recruitment of RAD51 is also associated with replication stress (Ait Saada et al, 2018). Persistent replication stress can result in endogenous DNA DSBs. This potentially explains our observed results on the generation of DSBs upon TET3 knockdown. Additionally, a pathway analysis using the string database surprisingly illustrates that most TET3 predicted interaction partners, apart from carbonic anhydrase2 and nanog, are associated with either proper maintenance or processing of the replicating fork (**Figure 37**) (Hervouet et al, 2018; Rehman et al, 2018; Rondinelli et al, 2017; Slenn et al, 2014). It is therefore highly likely, that TET3, apart from its role in DNA damage and repair, can also be involved in the proper maintenance and functioning of replicating forks in cells.

As replicating origins are highly enriched in GC content (Cadoret et al, 2008), we hypothesize that TET3 can catalyze hydroxymethylation in these regions to mediate the maintenance of the replicating origins. This idea is supported by a recent study wherein TET2-mediated hydroxymethylation is reported to play a crucial role in the maintenance of replicating fork origins (Prikrylova et al, 2019). As most TET proteins are highly redundant in function, it is possible that, as per our hypothesis, TET3 can also be involved in replication stress and the maintenance of replicating fork origins. Further investigation could seek to answer whether TET3 is also involved in fine-tuning the replication fork or may be involved in orchestrating the DNA replication origin firing.

In line with these ideas, increased replication stress is a common feature in Doxorubicin-induced cardiac failure (Yang et al, 2014). Similarly, increased replication stress is also observed in cardiac failure due to mutations in laminin A/C genes (Graziano et al, 2018). Notably, so far in pathological cardiac diseases, the role and involvement of replication stress are not well known. In the present study, we report that TET3 expression is downregulated during cardiac fibrosis; therefore, further

research can link the possible role of TET3 in fine-tuning the replication stress during cardiac fibrosis.

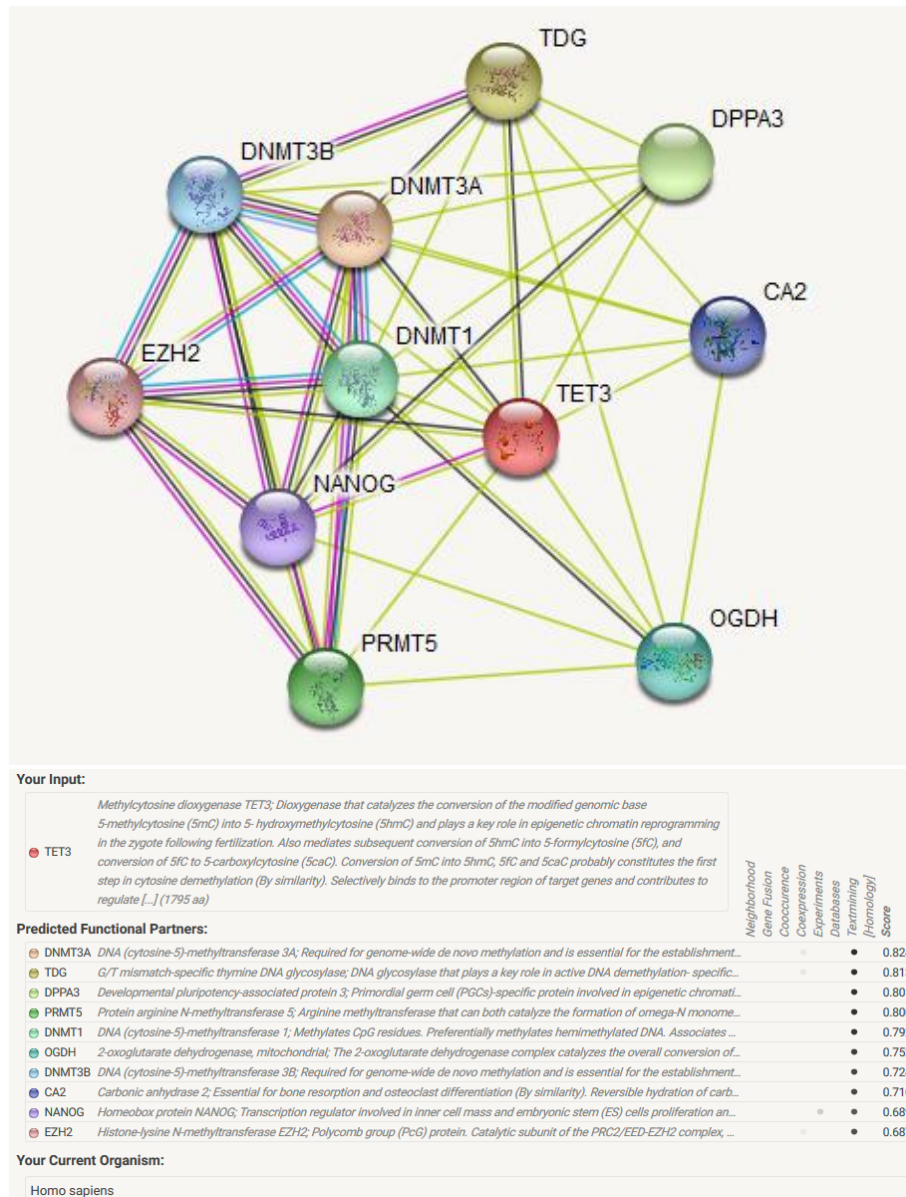


Figure 37. Schematic representation of TET3 interaction partners analysed from the string database (Jensen et al, 2009).

4.3 TET3 affects chromatin relaxation during DNA damage response in cardiac fibroblasts

One of the key findings of the present study is that TET3 also plays a role in relaxing chromatin (**Figure 27**). This finding is in line with a recent report in the literature wherein the loss of TET3 is shown to facilitate heterochromatin formation via an increase in H3k27me3 (Cao et al, 2019). It is well known that unrelaxed chromatin can hinder the proper operation of DNA damage and repair response (Hauer & Gasser, 2017). In line with these observations, our results also show impaired recruitment of

RAD51 to the DNA DSBs in TET3 knockdown MCFs. Thus, we hypothesize that changes in the chromatin landscape might affect the loading of RAD51 to the DNA DSBs in TET3-deficient cells. Studies also indicate that one of the essential prerequisites for proper HR-mediated DDR is the availability of relaxed chromatin architecture (Densham & Morris 2019). In a relaxed chromatin architecture, eviction of nucleosomes around the DSBs would facilitate smooth DNA end resection followed by strand invasion (Garvin et al, 2013). Our results are coherent with previously published findings, as we also observed that TET3 deficient cells with a compacted chromatin architecture show inefficient DNA end resection (**Figure 24**). However, it is unclear whether compacted chromatin in TET3-deficient cells is due to physiological tight nucleosome sliding or due to increased tail bridging of histones. More research is needed in this area.

Existing studies have highlighted both catalytic domain dependent and independent roles of TET3. Thus, it is of interest in the future to investigate which domain of the TET3 aids in relaxing chromatin during DNA damage. Moreover, more investigations are necessary to determine whether chromatin compaction by loss of TET3 is the cause or consequence of the observed endogenous DNA DSBs. Interestingly, a recent study in mouse embryonic stem cells illustrates that exon number 4 of TET3 is present in the N-terminal domain (not in the catalytic domain), is highly conserved and helps in relaxing the chromatin (Krueger et al, 2017). In the same study, using only the exon 4 overexpression studies, the authors displayed extensive relaxed chromatin by ATAC sequencing. Moreover, the authors also claimed that such a conserved region is absent in TET1 and TET2, suggesting that the chromatin relaxation is a unique feature of TET3 among all the other isoforms. More investigations are also required to verify that the exon 4 of TET3 is critical in relaxing the chromatin in response to DNA DSBs. We also propose that generating the truncated versions of TET3 can help us to understand the precise role of each part of the domain in chromatin relaxation and DDR response.

Interestingly, as previously discussed, the N-terminal domain of the protein is highly subject to post-translational modifications; therefore, it is likely that TET3 can play a role in DNA damage and repair response, independent of its catalytic domain due to its involvement in relaxing the chromatin. Apart from DDR, the extent of chromatin relaxation upon TET3 knockdown can also help us to understand the dynamics of chromatin looping and bending, which in turn tightly controls gene expression during fibrosis. Hence, for the future, we propose that a detailed Hi-C chromatin conformation capture analysis overlapped with an ATAC analysis in TET3 knockdown MCFs can aid in exploring the intricacy of chromatin loops and enhancer organization during fibrotic progression.

4.4 TGF- β affects DNA repair and proliferation in cardiac fibroblasts

In a physiological state, cardiac fibroblasts are more or less quiescent, but in pathological conditions, their proliferation is critical for fibrotic scarring. Interestingly, we have observed that fibrotic fibroblasts have an increased proliferation rate despite accumulating DNA damage (**Figure 11**). This led to the question: How do fibrotic

fibroblasts enter proliferation? In order to provide an answer to this question, we contemplated two hypotheses: First, they may be adapting and tolerating DNA damage, or second, they could actually harness the fibrotic niche to accelerate DNA repair. Adaptation to DNA damage leads to genomic instability (GI) (Tubbs & Nussenzweig, 2017), but, to our knowledge, there are no reports of GI during cardiac fibrosis. Moreover, we also looked for abnormal anaphasic bridges (an indicator of GI) in murine fibrotic hearts, and no such abnormality was detected, at least in our sample size.

Therefore, we focused on the second hypothesis that the fibrotic fibroblasts enter proliferation in a fibrotic niche due to a switch in DDR. To test this idea, we treated cardiac fibroblasts *in vitro* with TGF- β (a key molecule driving fibrotic progression). Our data show that MCFs treated with TGF- β tend to accelerate the clearance of DSBs by engaging increased NHEJ-mediated DDR response (**Figure 29 and Figure 30**). This is also coherent with the existing literature, where TGF- β is shown to accelerate clearance of the DSBs induced by ionizing radiation via NHEJ engagement in various cancer models (Kim et al, 2015).

However, in the present study, we have not addressed whether the increase in NHEJ efficacy due to TGF- β treatment is due to increased 53bp1 expression or increased ligase 4 expression. Further experiments are needed to answer these questions. Moreover, TGF- β is primarily cytoplasmic by localization, and as per previous studies, most of its action in the nucleus is due to activated p-Smad2/3. It is of high interest to investigate whether activated p-Smad2/3 also plays a role in NHEJ DDR response in cardiac fibroblasts.

Interestingly, our results also demonstrate that MCFs upon treatment with TGF- β show decreased TET3 expression. This is in line with previously published studies, wherein a similar effect of TGF- β was observed (Gong et al, 2017; Tampe et al, 2014; Xu et al, 2015; Ye et al, 2016; Zhang et al, 2014). So far, the exact mechanism that impairs TET3 expression has not been addressed in cardiac fibroblasts. In light of this observation, as the TET3 promoter consists of both smad binding sites as well as CpG islands, it would be interesting to address, if either of these axes together or independently regulate TET3 expression in MCFs. We propose bisulfite sequencing of TET3 promoter region along with ChIP studies on activated smad-3 binding to help resolve this question.

4.5 TET3 affects DNA repair and proliferation in cardiac fibroblasts

In the present study, we established that TET3 plays a role in HR in MCFs and TGF- β -treatment downregulates TET3 expression (**Figure 28**). Altogether, these results led us to hypothesize that decreased TET3 expression is a strategy employed by the fibrotic fibroblasts to evade activation of checkpoint arrest assisted HR-mediated repair response to promote increased cell proliferation. However, we also demonstrated that further knockdown of TET3 has no additive effect on the change in the cell proliferation

state in TGF- β -treated MCFs (**Figure 31**). But, interestingly, our results demonstrate that TET3 overexpression in TGF- β -treated MCFs also leads to shift in NHEJ repair efficacy (**Figure 33**). We propose, such result could be a consequence of increased DNA end resection in a relaxed chromatin. This idea is consistent with a recent study, wherein knockdown of CCAR2 is reported to decrease in the NHEJ repair efficacy due to an increase in HR-mediated DNA end resection (Lopez-Saavedra et al, 2016). Therefore, altogether from the results in the present study we can conclude that the anti-proliferative effect of TET3 in fibrotic fibroblasts is in part due to a shift in DNA repair. Hence, more investigations are necessary to understand whether the observed decreased cell proliferation upon TET3 overexpression is due to the altered chromatin architecture or DNA end resection or a consequence of both.

5. Conclusion and Therapeutic Outlook

Taking the patient data and *in vitro* and *in vivo* results in mouse hearts together, we demonstrated that fibrotic fibroblasts show a loss of TET3 expression. Moreover, using MCFs as in *in vitro* model, here, we demonstrate that TET3 additionally impacts DNA damage response (DDR) mechanisms via orchestrating checkpoint-assisted homologous recombination (HR)-mediated DDR, and that TGF- β , in combination with lack of TET3 in cardiac fibrosis, leads to an increase of a checkpoint-independent non-homologous end joining (NHEJ) DDR. In addition, from our *in vitro* results, we demonstrated that TET3 relaxes the chromatin which we propose may facilitate HR-mediated DNA repair. Altogether from our results, we suggest a protective role of TET3 in cardiac fibrosis. However, the *in vivo* landscape in heart is highly dynamic and regulated by cross-talks between different cell types. In line with these observations, there are still many unanswered questions concerning the findings of our results precisely in the *in vivo* situation. Hence, more investigations are necessary to address these answers using a TET3 knockout mouse challenged with fibrosis.

From a therapeutic point of view, a previous study from our lab demonstrated a dose-dependent anti-fibrotic effect of the anti-hypertensive drug hydralazine which upregulates TET3 expression (Tampe et al, 2015). Hence, it would be interesting to recapitulate these findings in fibrotic mouse hearts and look upon the protective role of TET3 during fibrosis in context of DNA repair. Hydralazine has a definite effect on other factors, too, but as it upregulates TET3 expression, it appears highly likely that it exerts a positive effect on HR-mediated DDR.

References

- AbdulSalam SF, Thowfeik FS, Merino EJ (2016) Excessive Reactive Oxygen Species and Exotic DNA Lesions as an Exploitable Liability. *Biochemistry* **55**: 5341-5352
- Ahnesorg P, Smith P, Jackson SP (2006) XLF interacts with the XRCC4-DNA ligase IV complex to promote DNA nonhomologous end-joining. *Cell* **124**: 301-313
- Ait Saada A, Lambert SAE, Carr AM (2018) Preserving replication fork integrity and competence via the homologous recombination pathway. *DNA Repair* **71**: 135-147
- Akahori H, Guindon S, Yoshizaki S, Muto Y (2015) Molecular Evolution of the TET Gene Family in Mammals. *Int J Mol Sci* **16**: 28472-28485
- An J, González-Avalos E, Chawla A, Jeong M, López-Moyado IF, Li W, Goodell MA, Chavez L, Ko M, Rao A (2015) Acute loss of TET function results in aggressive myeloid cancer in mice. *Nature Communications* **6**: 10071
- Arnoult N, Correia A, Ma J, Merlo A, Garcia-Gomez S, Maric M, Tognetti M, Benner CW, Boulton SJ, Saghatelian A, Karlseder J (2017) Regulation of DNA repair pathway choice in S and G2 phases by the NHEJ inhibitor CYREN. *Nature* **549**: 548-552
- Bahjat M, Bloedjes TA, van der Veen A, de Wilde G, Maas C, Guikema JEJ (2017) Detection and Visualization of DNA Damage-induced Protein Complexes in Suspension Cell Cultures Using the Proximity Ligation Assay. *J Vis Exp* **9**: 55703
- Barcellos-Hoff MH, Cucinotta FA (2014) New tricks for an old fox: impact of TGFβ on the DNA damage response and genomic stability. *Sci Signal* **7**: 2005474
- Bauer C, Göbel K, Nagaraj N, Colantuoni C, Wang M, Müller U, Kremmer E, Rottach A, Leonhardt H (2015) Phosphorylation of TET proteins is regulated via O-GlcNAcylation by the O-linked N-acetylglucosamine transferase (OGT). *J Biol Chem* **290**: 4801-4812
- Berk BC, Fujiwara K, Lehoux S (2007) ECM remodeling in hypertensive heart disease. *J Clin Invest* **117**: 568-575
- Brilla CG, Weber KT (1992) Reactive and reparative myocardial fibrosis in arterial hypertension in the rat. *Cardiovasc Res* **26**: 671-677
- Burgess RC, Burman B, Kruhlak MJ, Misteli T (2014) Activation of DNA damage response signaling by condensed chromatin. *Cell Rep* **9**: 1703-1717
- Cadoret J-C, Meisch F, Hassan-Zadeh V, Luyten I, Guillet C, Duret L, Quesneville H, Prioleau M-N (2008) Genome-wide studies highlight indirect links between human replication origins and gene regulation. *Proceedings of the National Academy of Sciences* **105**: 15837-15842
- Callén E, Jankovic M, Wong N, Zha S, Chen HT, Difilippantonio S, Di Virgilio M, Heidkamp G, Alt FW, Nussenzweig A, Nussenzweig M (2009) Essential role for DNA-PKcs in DNA double-strand break repair and apoptosis in ATM-deficient lymphocytes. *Mol Cell* **34**: 285-297

- Cao T, Jiang Y, Wang Z, Zhang N, Al-Hendy A, Mamillapalli R, Kallen AN, Kodaman P, Taylor HS, Li D, Huang Y (2019) H19 lncRNA identified as a master regulator of genes that drive uterine leiomyomas. *Oncogene* **38**: 5356-5366
- Chang HH, Watanabe G, Gerodimos CA, Ochi T, Blundell TL, Jackson SP, Lieber MR (2016) Different DNA End Configurations Dictate Which NHEJ Components Are Most Important for Joining Efficiency. *J Biol Chem* **291**: 24377-24389
- Chatzifrangkeskou M, Le Dour C, Wu W, Morrow JP, Joseph LC, Beuvin M, Sera F, Homma S, Vignier N, Mougnot N, Bonne G, Lipson KE, Worman HJ, Muchir A (2016) ERK1/2 directly acts on CTGF/CCN2 expression to mediate myocardial fibrosis in cardiomyopathy caused by mutations in the lamin A/C gene. *Hum Mol Genet* **25**: 2220-2233
- Chen HB, Rud JG, Lin K, Xu L (2005) Nuclear targeting of transforming growth factor-beta-activated Smad complexes. *J Biol Chem* **280**: 21329-21336
- Chen LL, Lin HP, Zhou WJ, He CX, Zhang ZY, Cheng ZL, Song JB, Liu P, Chen XY, Xia YK, Chen XF, Sun RQ, Zhang JY, Sun YP, Song L, Liu BJ, Du RK, Ding C, Lan F, Huang SL, Zhou F, Liu S, Xiong Y, Ye D, Guan KL (2018) SNIP1 Recruits TET2 to Regulate c-MYC Target Genes and Cellular DNA Damage Response. *Cell Rep* **25**: 1485-1500
- Chen SN, Lombardi R, Karmouch J, Tsai JY, Czernuszewicz G, Taylor MRG, Mestroni L, Coarfa C, Gurha P, Marian AJ (2019) DNA Damage Response/TP53 Pathway Is Activated and Contributes to the Pathogenesis of Dilated Cardiomyopathy Associated With LMNA (Lamin A/C) Mutations. *Circ Res* **124**: 856-873
- Chen W, Frangogiannis NG (2013) Fibroblasts in post-infarction inflammation and cardiac repair. *Biochim Biophys Acta* **4**: 945-953
- Cheng TH, Cheng PY, Shih NL, Chen IB, Wang DL, Chen JJ (2003) Involvement of reactive oxygen species in angiotensin II-induced endothelin-1 gene expression in rat cardiac fibroblasts. *J Am Coll Cardiol* **42**: 1845-1854
- Chiong M, Wang ZV, Pedrozo Z, Cao DJ, Troncoso R, Ibacache M, Criollo A, Nemchenko A, Hill JA, Lavandero S (2011) Cardiomyocyte death: mechanisms and translational implications. *Cell Death Dis* **2**: 130
- Coulter JB, Lopez-Bertoni H, Kuhns KJ, Lee RS, Laterra J, Bressler JP (2017) TET1 deficiency attenuates the DNA damage response and promotes resistance to DNA damaging agents. *Epigenetics* **12**: 854-864
- Cucoranu I, Clempus R, Dikalova A, Phelan PJ, Ariyan S, Dikalov S, Sorescu D (2005) NAD(P)H oxidase 4 mediates transforming growth factor-beta1-induced differentiation of cardiac fibroblasts into myofibroblasts. *Circ Res* **97**: 900-907
- Daley JM, Gaines WA, Kwon Y, Sung P (2014) Regulation of DNA pairing in homologous recombination. *Cold Spring Harb Perspect Biol* **6**
- Davis AJ, Chen DJ (2013) DNA double strand break repair via non-homologous end-joining. *Transl Cancer Res* **2**: 130-143

- Delacote F, Lopez BS (2008) Importance of the cell cycle phase for the choice of the appropriate DSB repair pathway, for genome stability maintenance: the trans-S double-strand break repair model. *Cell Cycle* **7**: 33-38
- Densham RM, Morris JR *Moving Mountains—The BRCA1 Promotion of DNA Resection*: Front Mol Biosci. 2019 Sep 3;6:79. doi: 10.3389/fmolb.2019.00079. eCollection 2019.
- Desmoulière A, Redard M, Darby I, Gabbiani G (1995) Apoptosis mediates the decrease in cellularity during the transition between granulation tissue and scar. *Am J Pathol* **146**: 56-66
- Dong Z, Bode AM (2006) The role of histone H3 phosphorylation (Ser10 and Ser28) in cell growth and cell transformation. *Mol Carcinog* **45**: 416-421
- Eastman A, Barry MA (1992) The origins of DNA breaks: a consequence of DNA damage, DNA repair, or apoptosis? *Cancer Invest* **10**: 229-240
- Falquet B, Rass U (2017) A new role for Holliday junction resolvase Yen1 in processing DNA replication intermediates exposes Dna2 as an accessory replicative helicase. *Microb Cell* **4**: 32-34
- Fan D, Takawale A, Lee J, Kassiri Z (2012) Cardiac fibroblasts, fibrosis and extracellular matrix remodeling in heart disease. *Fibrogenesis Tissue Repair* **5**: 1755-1536
- Felisbino MB, McKinsey TA (2018) Epigenetics in Cardiac Fibrosis: Emphasis on Inflammation and Fibroblast Activation. *JACC Basic Transl Sci* **3**: 704-715
- Fell VL, Schild-Poulter C (2015) The Ku heterodimer: function in DNA repair and beyond. *Mutat Res Rev Mutat Res* **763**: 15-29
- Filipczak PT, Leng S, Tellez CS, Do KC, Grimes MJ, Thomas CL, Walton-Filipczak SR, Picchi MA, Belinsky SA (2019) p53-Suppressed Oncogene TET1 Prevents Cellular Aging in Lung Cancer. *Cancer Res* **79**: 1758-1768
- Foster CR, Zha Q, Daniel LL, Singh M, Singh K (2012) Lack of ataxia telangiectasia mutated kinase induces structural and functional changes in the heart: role in β -adrenergic receptor-stimulated apoptosis. *Exp Physiol* **97**: 506-515
- Frank S, Madlener M, Werner S (1996) Transforming growth factors beta1, beta2, and beta3 and their receptors are differentially regulated during normal and impaired wound healing. *J Biol Chem* **271**: 10188-10193
- Fuster JJ, MacLauchlan S, Zuriaga MA, Polackal MN, Ostriker AC, Chakraborty R, Wu CL, Sano S, Muralidharan S, Rius C, Vuong J, Jacob S, Muralidhar V, Robertson AA, Cooper MA, Andres V, Hirschi KK, Martin KA, Walsh K (2017) Clonal hematopoiesis associated with TET2 deficiency accelerates atherosclerosis development in mice. *Science* **355**: 842-847
- Garvin AJ, Densham RM, Blair-Reid SA, Pratt KM, Stone HR, Weekes D, Lawrence KJ, Morris JR (2013) The deSUMOylase SENP7 promotes chromatin relaxation for homologous recombination DNA repair. *EMBO Rep* **14**: 975-983

Gong F, Guo Y, Niu Y, Jin J, Zhang X, Shi X, Zhang L, Li R, Chen L, Ma RZ (2017) Epigenetic silencing of TET2 and TET3 induces an EMT-like process in melanoma. *Oncotarget* **8**: 315-328

Graziano S, Kreienkamp R, Coll-Bonfill N, Gonzalo S (2018) Causes and consequences of genomic instability in laminopathies: Replication stress and interferon response. *Nucleus* **9**: 258-275

Greco CM, Kunderfranco P, Rubino M, Larcher V, Carullo P, Anselmo A, Kurz K, Carell T, Angius A, Latronico MVG, Papait R, Condorelli G (2016) DNA hydroxymethylation controls cardiomyocyte gene expression in development and hypertrophy. *Nature Communications* **7**: 12418

Greenberg EF, Hirsch CM, Pan F, Jha BK, Guan Y, Visconte V, You D, Qu G, Graham A, Przychodzen BP, Laframboise T, Makishima H, Gackowski D, Ólinski R, Cheng Y-W, Sekeres MA, Xu M, Maciejewski JP (2017) TET2 and MSH6: A Novel Role for MMR in the Pathogenesis of Myeloid Malignancies. *Blood* **130**: 1668-1668

Greulich S, Mayr A, Gloekler S, Seitz A, Birkmeier S, Schaufele T, Bekeredjian R, Zuern CS, Seizer P, Geisler T, Muller KAL, Krumm P, Nikolaou K, Klug G, Reinstadler S, Pamminger M, Reindl M, Wahl A, Traupe T, Seiler C, Metzler B, Gawaz M, Windecker S, Mahrholdt H (2019) Time-Dependent Myocardial Necrosis in Patients With ST-Segment-Elevation Myocardial Infarction Without Angiographic Collateral Flow Visualized by Cardiac Magnetic Resonance Imaging: Results From the Multicenter STEMI-SCAR Project. *J Am Heart Assoc* **8**: 11

Guo JL, Yu Y, Jia YY, Ma YZ, Zhang BY, Liu PQ, Chen SR, Jiang JM (2014) Transient receptor potential melastatin 7 (TRPM7) contributes to H₂O₂-induced cardiac fibrosis via mediating Ca²⁺ influx and extracellular signal-regulated kinase 1/2 (ERK1/2) activation in cardiac fibroblasts. *J Pharmacol Sci* **125**: 184-192

Haeger SM, Thompson JJ, Kalra S, Cleaver TG, Merrick D, Wang XJ, Malkoski SP (2016) Smad4 loss promotes lung cancer formation but increases sensitivity to DNA topoisomerase inhibitors. *Oncogene* **35**: 577-586

Hakem R (2008) DNA-damage repair; the good, the bad, and the ugly. *Embo J* **27**: 589-605

Hans F, Dimitrov S (2001) Histone H3 phosphorylation and cell division. *Oncogene* **20**: 3021-3027

Hauer MH, Gasser SM (2017) Chromatin and nucleosome dynamics in DNA damage and repair. *Genes Dev* **31**: 2204-2221

Hayashi H, Sakai T (2012) Biological Significance of Local TGF- β Activation in Liver Diseases. *Frontiers in Physiology* **3**

He Y, Ling S, Sun Y, Sheng Z, Chen Z, Pan X, Ma G (2019) DNA methylation regulates alpha-smooth muscle actin expression during cardiac fibroblast differentiation. *J Cell Physiol* **234**: 7174-7185

- Hervouet E, Peixoto P, Delage-Mourroux R, Boyer-Guittaut M, Cartron PF (2018) Specific or not specific recruitment of DNMTs for DNA methylation, an epigenetic dilemma. *Clin Epigenetics* **10**: 018-0450
- Higo T, Naito AT, Sumida T, Shibamoto M, Okada K, Nomura S, Nakagawa A, Yamaguchi T, Sakai T, Hashimoto A, Kuramoto Y, Ito M, Hikoso S, Akazawa H, Lee JK, Shiojima I, McKinnon PJ, Sakata Y, Komuro I (2017) DNA single-strand break-induced DNA damage response causes heart failure. *Nat Commun* **8**
- Hilmi K, Jangal M, Marques M, Zhao T, Saad A, Zhang C, Luo VM, Syme A, Rejon C, Yu Z, Krum A, Fabian MR, Richard S, Alaoui-Jamali M, Orthwein A, McCaffrey L, Witcher M (2017) CTCF facilitates DNA double-strand break repair by enhancing homologous recombination repair. *Science Advances* **3**: e1601898
- Hinderer S, Schenke-Layland K (2019) Cardiac fibrosis - A short review of causes and therapeutic strategies. *Adv Drug Deliv Rev* **31**: 30061-30064
- Ho CY, López B, Coelho-Filho OR, Lakdawala NK, Cirino AL, Jarolim P, Kwong R, González A, Colan SD, Seidman JG, Díez J, Seidman CE (2010) Myocardial Fibrosis as an Early Manifestation of Hypertrophic Cardiomyopathy. *New England Journal of Medicine* **363**: 552-563
- Huertas P (2010) DNA resection in eukaryotes: deciding how to fix the break. *Nat Struct Mol Biol* **17**: 11-16
- Humeres C, Frangogiannis NG (2019) Fibroblasts in the Infarcted, Remodeling, and Failing Heart. *JACC Basic Transl Sci* **4**: 449-467
- Humeres C, Vivar R, Boza P, Munoz C, Bolivar S, Anfossi R, Osorio JM, Olivares-Silva F, Garcia L, Diaz-Araya G (2016) Cardiac fibroblast cytokine profiles induced by proinflammatory or profibrotic stimuli promote monocyte recruitment and modulate macrophage M1/M2 balance in vitro. *J Mol Cell Cardiol* **27**: 30392-30393
- Iliakis G, Murmann T, Soni A (2015) Alternative end-joining repair pathways are the ultimate backup for abrogated classical non-homologous end-joining and homologous recombination repair: Implications for the formation of chromosome translocations. *Mutat Res Genet Toxicol Environ Mutagen* **793**: 166-175
- Ivanov A, Cragg MS, Erenpreisa J, Emzinsh D, Lukman H, Illidge TM (2003) Endopolyploid cells produced after severe genotoxic damage have the potential to repair DNA double strand breaks. *J Cell Sci* **116**: 4095-4106
- Iyama T, Wilson DM, 3rd (2013) DNA repair mechanisms in dividing and non-dividing cells. *DNA Repair* **12**: 620-636
- Jensen LJ, Kuhn M, Stark M, Chaffron S, Creevey C, Muller J, Doerks T, Julien P, Roth A, Simonovic M, Bork P, von Mering C (2009) STRING 8--a global view on proteins and their functional interactions in 630 organisms. *Nucleic Acids Res* **37**: 21
- Jiang D, Wei S, Chen F, Zhang Y, Li J (2017) TET3-mediated DNA oxidation promotes ATR-dependent DNA damage response. *EMBO Rep* **18**: 781-796

- Jiang D, Zhang Y, Hart RP, Chen J, Herrup K, Li J (2015) Alteration in 5-hydroxymethylcytosine-mediated epigenetic regulation leads to Purkinje cell vulnerability in ATM deficiency. *Brain* **138**: 3520-3536
- Jiang W, Crowe JL, Liu X, Nakajima S, Wang Y, Li C, Lee BJ, Dubois RL, Liu C, Yu X, Lan L, Zha S (2015) Differential phosphorylation of DNA-PKcs regulates the interplay between end-processing and end-ligation during nonhomologous end-joining. *Mol Cell* **58**: 172-185
- Kafer GR, Li X, Horii T, Suetake I, Tajima S, Hatada I, Carlton PM (2016) 5-Hydroxymethylcytosine Marks Sites of DNA Damage and Promotes Genome Stability. *Cell Rep* **14**: 1283-1292
- Kakarougkas A, Jeggo PA (2014) DNA DSB repair pathway choice: an orchestrated handover mechanism. *Br J Radiol* **87**: 20130685
- Kanisicak O, Khalil H, Ivey MJ, Karch J, Maliken BD, Correll RN, Brody MJ, SC JL, Aronow BJ, Tallquist MD, Molkentin JD (2016) Genetic lineage tracing defines myofibroblast origin and function in the injured heart. *Nat Commun* **7**
- Khalil H, Kanisicak O, Prasad V, Correll RN, Fu X, Schips T, Vagnozzi RJ, Liu R, Huynh T, Lee SJ, Karch J, Molkentin JD (2017) Fibroblast-specific TGF-beta-Smad2/3 signaling underlies cardiac fibrosis. *J Clin Invest* **127**: 3770-3783
- Kim HE, Dalal SS, Young E, Legato MJ, Weisfeldt ML, D'Armiento J (2000) Disruption of the myocardial extracellular matrix leads to cardiac dysfunction. *J Clin Invest* **106**: 857-866
- Kim MR, Lee J, An YS, Jin YB, Park IC, Chung E, Shin I, Barcellos-Hoff MH, Yi JY (2015) TGFbeta1 protects cells from gamma-IR by enhancing the activity of the NHEJ repair pathway. *Mol Cancer Res* **13**: 319-329
- Kmietczyk V, Riechert E, Kalinski L, Boileau E, Malovrh E, Malone B, Gorska A, Hofmann C, Varma E, Jürgensen L, Kamuf-Schenk V, Altmüller J, Tappu R, Busch M, Most P, Katus HA, Dieterich C, Völkers M (2019) m(6)A-mRNA methylation regulates cardiac gene expression and cellular growth. *Life Sci Alliance* **2**
- Ko M, An J, Bandukwala HS, Chavez L, Aijo T, Pastor WA, Segal MF, Li H, Koh KP, Lahdesmaki H, Hogan PG, Aravind L, Rao A (2013) Modulation of TET2 expression and 5-methylcytosine oxidation by the CXXC domain protein IDAX. *Nature* **497**: 122-126
- Kong P, Christia P, Frangogiannis NG (2014) The pathogenesis of cardiac fibrosis. *Cell Mol Life Sci* **71**: 549-574
- Krasner DS, Daley JM, Sung P, Niu H (2015) Interplay between Ku and Replication Protein A in the Restriction of Exo1-mediated DNA Break End Resection. *J Biol Chem* **290**: 18806-18816
- Krenning G, Zeisberg EM, Kalluri R (2010) The origin of fibroblasts and mechanism of cardiac fibrosis. *J Cell Physiol* **225**: 631-637

Krueger C, Peat JR, Eckersley-Maslin MA, Hore TA, Mohammed H, Andrews SR, Dean W, Reik W (2017) A non-catalytic role of TET3 promotes open chromatin and enhances global transcription. *bioRxiv*: 177626

Kuhns KJ, Lopez-Bertoni H, Coulter JB, Bressler JP (2019) TET1 regulates DNA repair in human glial cells. *Toxicol Appl Pharmacol* **380**: 3

Kuo WL, Meyn RE, Haidle CW (1984) Neocarzinostatin-mediated DNA damage and repair in wild-type and repair-deficient Chinese hamster ovary cells. *Cancer Res* **44**: 1748-1751

Langenkamp E, Molema G (2009) Microvascular endothelial cell heterogeneity: general concepts and pharmacological consequences for anti-angiogenic therapy of cancer. *Cell and Tissue Research* **335**: 205-222

Lee J, Kim MR, Kim HJ, An YS, Yi JY (2016) TGF-beta1 accelerates the DNA damage response in epithelial cells via Smad signaling. *Biochem Biophys Res Commun* **476**: 420-425

Lee KJ, Saha J, Sun J, Fattah KR, Wang SC, Jakob B, Chi L, Wang SY, Taucher-Scholz G, Davis AJ, Chen DJ (2016) Phosphorylation of Ku dictates DNA double-strand break (DSB) repair pathway choice in S phase. *Nucleic Acids Res* **44**: 1732-1745

Lemaitre C, Grabarz A, Tsouroula K, Andronov L, Furst A, Pankotai T, Heyer V, Rogier M, Attwood KM, Kessler P, Dellaire G, Klaholz B, Reina-San-Martin B, Soutoglou E (2014) Nuclear position dictates DNA repair pathway choice. *Genes Dev* **28**: 2450-2463

Lenart P, Zlamal F, Machal J, Hlinomaz O, Groch L, Bienertova-Vasku J (2017) Increased age-adjusted hazard of death associated with a common single nucleotide polymorphism of the human RAD52 gene in a cardiovascular cohort. *Mech Ageing Dev* **167**: 56-63

Li L, Zhao Q, Kong W (2018) Extracellular matrix remodeling and cardiac fibrosis. *Matrix Biol* **69**: 490-506

Lin S, Yang J, Elkahlon AG, Bandyopadhyay A, Wang L, Cornell JE, Yeh IT, Agyin J, Tomlinson G, Sun LZ (2012) Attenuation of TGF- β signaling suppresses premature senescence in a p21-dependent manner and promotes oncogenic Ras-mediated metastatic transformation in human mammary epithelial cells. *Mol Biol Cell* **23**: 1569-1581

Liu G, Ma C, Yang H, Zhang PY (2017) Transforming growth factor β and its role in heart disease. *Exp Ther Med* **13**: 2123-2128

Liu Q, Ma L, Jones T, Palomero L, Pujana MA, Martinez-Ruiz H, Ha PK, Murnane J, Cuartas I, Seoane J, Baumann M, Linge A, Barcellos-Hoff MH (2018) Subjugation of TGFbeta Signaling by Human Papilloma Virus in Head and Neck Squamous Cell Carcinoma Shifts DNA Repair from Homologous Recombination to Alternative End Joining. *Clin Cancer Res* **24**: 6001-6014

Liu R, Jin Y, Tang WH, Qin L, Zhang X, Tellides G, Hwa J, Yu J, Martin KA (2013) Ten-eleven translocation-2 (TET2) is a master regulator of smooth muscle cell plasticity. *Circulation* **128**: 2047-2057

Lopez-Saavedra A, Gomez-Cabello D, Dominguez-Sanchez MS, Mejias-Navarro F, Fernandez-Avila MJ, Dinant C, Martinez-Macias MI, Bartek J, Huertas P (2016) A genome-wide screening uncovers the role of CCAR2 as an antagonist of DNA end resection. *Nat Commun* **7**

Lopez B, Gonzalez A, Varo N, Laviades C, Querejeta R, Diez J (2001) Biochemical assessment of myocardial fibrosis in hypertensive heart disease. *Hypertension* **38**: 1222-1226

Lu G, Duan J, Shu S, Wang X, Gao L, Guo J, Zhang Y (2016) Ligase I and ligase III mediate the DNA double-strand break ligation in alternative end-joining. *Proceedings of the National Academy of Sciences* **113**: 1256-1260

Ma CJ, Gibb B, Kwon Y, Sung P, Greene EC (2017) Protein dynamics of human RPA and RAD51 on ssDNA during assembly and disassembly of the RAD51 filament. *Nucleic Acids Res* **45**: 749-761

Maréchal A, Zou L (2013) DNA damage sensing by the ATM and ATR kinases. *Cold Spring Harb Perspect Biol* **5**

Mathiyalagan P, Keating ST, Du X-J, El-Osta A (2014) Chromatin modifications remodel cardiac gene expression. *Cardiovascular Research* **103**: 7-16

Mehta A, Haber JE (2014) Sources of DNA double-strand breaks and models of recombinational DNA repair. *Cold Spring Harb Perspect Biol* **6**

Melamed P, Yosefzon Y, David C, Tsukerman A, Pnueli L Tet Enzymes, Variants, and Differential Effects on Function. *Front Cell Dev Biol* **2018 Mar 5;6:22**. doi: 10.3389/fcell.2018.00022

Mendis S, Puska P, Norrving B, World Health O, World Heart F, World Stroke O. (2011) Global atlas on cardiovascular disease prevention and control / edited by: Shanthi Mendis ... [et al.]. World Health Organization, Geneva.

Mewton N, Liu CY, Croisille P, Bluemke D, Lima JA (2011) Assessment of myocardial fibrosis with cardiovascular magnetic resonance. *J Am Coll Cardiol* **57**: 891-903

Mondal NK, Sorensen E, Hiiivala N, Feller E, Griffith B, Wu ZJ (2013) Oxidative stress, DNA damage and repair in heart failure patients after implantation of continuous flow left ventricular assist devices. *Int J Med Sci* **10**: 883-893

Monier K, Mouradian S, Sullivan KF (2007) DNA methylation promotes Aurora-B-driven phosphorylation of histone H3 in chromosomal subdomains. *Journal of Cell Science* **120**: 101-114

Montalban-Loro R, Lozano-Urena A, Ito M, Krueger C, Reik W, Ferguson-Smith AC, Ferron SR (2019) TET3 prevents terminal differentiation of adult NSCs by a non-catalytic action at Snrpn. *Nat Commun* **10**: 019-09665

- Moore-Morris T, Guimarães-Camboa N, Banerjee I, Zambon AC, Kisseleva T, Velayoudon A, Stallcup WB, Gu Y, Dalton ND, Cedenilla M, Gomez-Amaro R, Zhou B, Brenner DA, Peterson KL, Chen J, Evans SM (2014) Resident fibroblast lineages mediate pressure overload-induced cardiac fibrosis. *J Clin Invest* **124**: 2921-2934
- Moynahan ME, Jasin M (2010) Mitotic homologous recombination maintains genomic stability and suppresses tumorigenesis. *Nat Rev Mol Cell Biol* **11**: 196-207
- Mukherjee B, Tomimatsu N, Burma S (2015) Immunofluorescence-based methods to monitor DNA end resection. *Methods Mol Biol*: 2522-2523_2525
- Nicoglou A, Merlin F (2017) Epigenetics: A way to bridge the gap between biological fields. *Stud Hist Philos Biol Biomed Sci* **66**: 73-82
- Noon AT, Shibata A, Rief N, Loblrich M, Stewart GS, Jeggo PA, Goodarzi AA (2010) 53BP1-dependent robust localized KAP-1 phosphorylation is essential for heterochromatic DNA double-strand break repair. *Nat Cell Biol* **12**: 177-184
- Norbury CJ, Hickson ID (2001) Cellular responses to DNA damage. *Annu Rev Pharmacol Toxicol* **41**: 367-401
- Oliveira DV, Kato A, Nakamura K, Ikura T, Okada M, Kobayashi J, Yanagihara H, Saito Y, Tauchi H, Komatsu K (2014) Histone chaperone FACT regulates homologous recombination by chromatin remodeling through interaction with RNF20. *J Cell Sci* **127**: 763-772
- Olsen MB, Hildrestrand GA, Scheffler K, Vinge LE, Alfsnes K, Palibrk V, Wang J, Neurauter CG, Luna L, Johansen J, Ogaard JDS, Ohm IK, Slupphaug G, Kusnierczyk A, Fiane AE, Brorson SH, Zhang L, Gullestad L, Louch WE, Iversen PO, Ostlie I, Klungland A, Christensen G, Sjaastad I, Saetrom P, Yndestad A, Aukrust P, Bjoras M, Finsen AV (2017) NEIL3-Dependent Regulation of Cardiac Fibroblast Proliferation Prevents Myocardial Rupture. *Cell Rep* **18**: 82-92
- Ozaki K, Sato H, Inoue K, Tsunoda T, Sakata Y, Mizuno H, Lin TH, Miyamoto Y, Aoki A, Onouchi Y, Sheu SH, Ikegawa S, Odashiro K, Nobuyoshi M, Juo SH, Hori M, Nakamura Y, Tanaka T (2009) SNPs in BRAP associated with risk of myocardial infarction in Asian populations. *Nat Genet* **41**: 329-333
- Pal D, Pertot A, Shirole NH, Yao Z, Anaparthi N, Garvin T, Cox H, Chang K, Rollins F, Kendall J, Edwards L, Singh VA, Stone GC, Schatz MC, Hicks J, Hannon GJ, Sordella R (2017) TGF- β reduces DNA ds-break repair mechanisms to heighten genetic diversity and adaptability of CD44⁺/CD24⁻ cancer cells. *Elife* **16**: 21615
- Panth N, Paudel KR, Parajuli K (2016) Reactive Oxygen Species: A Key Hallmark of Cardiovascular Disease. *Adv Med* **9152732**: 28
- Pastor WA, Aravind L, Rao A (2013) TETonic shift: biological roles of TET proteins in DNA demethylation and transcription. *Nat Rev Mol Cell Biol* **14**: 341-356
- Piek A, de Boer RA, Silljé HH (2016) The fibrosis-cell death axis in heart failure. *Heart Fail Rev* **21**: 199-211

- Pierce AJ, Johnson RD, Thompson LH, Jasin M (1999) XRCC3 promotes homology-directed repair of DNA damage in mammalian cells. *Genes Dev* **13**: 2633-2638
- Polo SE, Jackson SP (2011) Dynamics of DNA damage response proteins at DNA breaks: a focus on protein modifications. *Genes Dev* **25**: 409-433
- Prikrylova T, Robertson J, Ferrucci F, Konorska D, Aanes H, Manaf A, Zhang B, Vågbo CB, Kuśnierczyk A, Gilljam KM, Løvkvam-Køster C, Otterlei M, Dahl JA, Enserink J, Klungland A, Robertson AB (2019) 5-hydroxymethylcytosine Marks Mammalian Origins Acting as a Barrier to Replication. *Scientific Reports* **9**: 11065
- Qin F, Lennon-Edwards S, Lancel S, Biolo A, Siwik DA, Pimentel DR, Dorn GW, Kang YJ, Colucci WS (2010) Cardiac-specific overexpression of catalase identifies hydrogen peroxide-dependent and -independent phases of myocardial remodeling and prevents the progression to overt heart failure in G(alpha)q-overexpressing transgenic mice. *Circ Heart Fail* **3**: 306-313
- Ramsden DA (2011) Polymerases in nonhomologous end joining: building a bridge over broken chromosomes. *Antioxid Redox Signal* **14**: 2509-2519
- Rasmussen KD, Helin K (2016) Role of TET enzymes in DNA methylation, development, and cancer. *Genes Dev* **30**: 733-750
- Rassoolzadeh H, Coucoravas C, Farnebo M (2015) The proximity ligation assay reveals that at DNA double-strand breaks WRAP53 β associates with γ H2AX and controls interactions between RNF8 and MDC1. *Nucleus* **6**: 417-424
- Rawluszko-Wieczorek AA, Siera A, Jagodzinski PP (2015) TET proteins in cancer: Current 'state of the art'. *Crit Rev Oncol Hematol* **96**: 425-436
- Rehman I, Basu SM, Das SK, Bhattacharjee S, Ghosh A, Pommier Y, Das BB (2018) PRMT5-mediated arginine methylation of TDP1 for the repair of topoisomerase I covalent complexes. *Nucleic Acids Res* **46**: 5601-5617
- Rockey DC, Bell PD, Hill JA (2015) Fibrosis--a common pathway to organ injury and failure. *N Engl J Med* **372**: 1138-1149
- Rondinelli B, Gogola E, Yucel H, Duarte AA, van de Ven M, van der Sluijs R, Konstantinopoulos PA, Jonkers J, Ceccaldi R, Rottenberg S, D'Andrea AD (2017) EZH2 promotes degradation of stalled replication forks by recruiting MUS81 through histone H3 trimethylation. *Nat Cell Biol* **19**: 1371-1378
- Sag CM, Santos CX, Shah AM (2014) Redox regulation of cardiac hypertrophy. *J Mol Cell Cardiol* **73**: 103-111
- Saraste A, Pulkki K, Kallajoki M, Henriksen K, Parvinen M, Voipio-Pulkki LM (1997) Apoptosis in human acute myocardial infarction. *Circulation* **95**: 320-323
- Scourzic L, Mouly E, Bernard OA (2015) TET proteins and the control of cytosine demethylation in cancer. *Genome Med* **7**: 015-0134
- Shi M, Zhu J, Wang R, Chen X, Mi L, Walz T, Springer TA (2011) Latent TGF- β structure and activation. *Nature* **474**: 343-349

- Shinde AV, Frangogiannis NG (2014) Fibroblasts in myocardial infarction: a role in inflammation and repair. *J Mol Cell Cardiol* **70**: 74-82
- Singh KK, Shukla PC, Quan A, Desjardins JF, Lovren F, Pan Y, Garg V, Gosal S, Garg A, Szmítko PE, Schneider MD, Parker TG, Stanford WL, Leong-Poi H, Teoh H, Al-Omran M, Verma S (2012) BRCA2 protein deficiency exaggerates doxorubicin-induced cardiomyocyte apoptosis and cardiac failure. *J Biol Chem* **287**: 6604-6614
- Slenn TJ, Morris B, Havens CG, Freeman RM, Jr., Takahashi TS, Walter JC (2014) Thymine DNA glycosylase is a CRL4Cdt2 substrate. *J Biol Chem* **289**: 23043-23055
- Sonoda E, Hochegger H, Saberi A, Taniguchi Y, Takeda S (2006) Differential usage of non-homologous end-joining and homologous recombination in double strand break repair. *DNA Repair* **5**: 1021-1029
- Spearman AD, Ke X, Fu Q, Lane RH, Majnik A (2018) Adverse maternal environment leads to cardiac fibrosis in adult male mice. *Birth Defects Res* **110**: 1551-1555
- Špírek M, Mlcoúšková J, Belán O, Gyimesi M, Harami GM, Molnár E, Novacek J, Kovács M, Krejci L (2018) Human RAD51 rapidly forms intrinsically dynamic nucleoprotein filaments modulated by nucleotide binding state. *Nucleic Acids Res* **46**: 3967-3980
- Srinivas US, Tan BWQ, Vellayappan BA, Jeyasekharan AD (2019) ROS and the DNA damage response in cancer. *Redox Biol* **25**: 21
- Stadler J, Richly H (2017) Regulation of DNA Repair Mechanisms: How the Chromatin Environment Regulates the DNA Damage Response. *Int J Mol Sci* **18**
- Steinhorn B, Sorrentino A, Badole S, Bogdanova Y, Belousov V, Michel T (2018) Chemogenetic generation of hydrogen peroxide in the heart induces severe cardiac dysfunction. *Nature Communications* **9**: 4044
- Sullivan MR, Bernstein KA (2018) RAD-ical New Insights into RAD51 Regulation. *Genes* **9**
- Swain L, Kesemeyer A, Meyer-Roxlau S, Vettel C, Zieseniss A, Guntsch A, Jatho A, Becker A, Nanadikar MS, Morgan B, Dennerlein S, Shah AM, El-Armouche A, Nikolaev VO, Katschinski DM (2016) Redox Imaging Using Cardiac Myocyte-Specific Transgenic Biosensor Mice. *Circ Res* **119**: 1004-1016
- Tahiliani M, Koh KP, Shen Y, Pastor WA, Bandukwala H, Brudno Y, Agarwal S, Iyer LM, Liu DR, Aravind L, Rao A (2009) Conversion of 5-methylcytosine to 5-hydroxymethylcytosine in mammalian DNA by MLL partner TET1. *Science* **324**: 930-935
- Takahashi T, Shishido T, Kinoshita D, Watanabe K, Toshima T, Sugai T, Narumi T, Otaki Y, Tamura H, Nishiyama S, Arimoto T, Takahashi H, Miyamoto T, Watanabe T, Woo CH, Abe JI, Takeishi Y, Kubota I, Watanabe M (2019) Cardiac Nuclear High-Mobility Group Box 1 Ameliorates Pathological Cardiac Hypertrophy by Inhibiting DNA Damage Response. *JACC Basic Transl Sci* **4**: 234-247

- Takimoto E, Kass DA (2007) Role of oxidative stress in cardiac hypertrophy and remodeling. *Hypertension* **49**: 241-248
- Talman V, Ruskoaho H (2016) Cardiac fibrosis in myocardial infarction—from repair and remodeling to regeneration. *Cell Tissue Res* **365**: 563-581
- Tampe B, Tampe D, Müller CA, Sugimoto H, LeBleu V, Xu X, Müller GA, Zeisberg EM, Kalluri R, Zeisberg M (2014) Tet3-mediated hydroxymethylation of epigenetically silenced genes contributes to bone morphogenic protein 7-induced reversal of kidney fibrosis. *J Am Soc Nephrol* **25**: 905-912
- Tampe B, Tampe D, Zeisberg EM, Müller GA, Bechtel-Walz W, Koziol M, Kalluri R, Zeisberg M (2015) Induction of Tet3-dependent Epigenetic Remodeling by Low-dose Hydralazine Attenuates Progression of Chronic Kidney Disease. *EBioMedicine* **2**: 19-36
- Tan L, Shi YG (2012) Tet family proteins and 5-hydroxymethylcytosine in development and disease. *Development* **139**: 1895-1902
- Tao H, Yang JJ, Chen ZW, Xu SS, Zhou X, Zhan HY, Shi KH (2014) DNMT3A silencing RASSF1A promotes cardiac fibrosis through upregulation of ERK1/2. *Toxicology* **323**: 42-50
- Tao H, Yang JJ, Shi KH, Deng ZY, Li J (2014) DNA methylation in cardiac fibrosis: new advances and perspectives. *Toxicology* **323**: 125-129
- Travers JG, Kamal FA, Robbins J, Yutzey KE, Blaxall BC (2016) Cardiac Fibrosis: The Fibroblast Awakens. *Circ Res* **118**: 1021-1040
- Tubbs A, Nussenzweig A (2017) Endogenous DNA Damage as a Source of Genomic Instability in Cancer. *Cell* **168**: 644-656
- Vaidya A, Mao Z, Tian X, Spencer B, Seluanov A, Gorbunova V (2014) Knock-in reporter mice demonstrate that DNA repair by non-homologous end joining declines with age. *PLoS Genet* **10**
- van den Berg J, Joosten SEP, Kim Y, Manjón AG, Krenning L, Koob L, Feringa FM, Klomp maker R, van den Broek B, Jalink K, Zwart W, Medema RH (2019) DNA end-resection in highly accessible chromatin produces a toxic break. *bioRxiv*: 691857
- Weyemi U, Redon CE, Aziz T, Choudhuri R, Maeda D, Parekh PR, Bonner MY, Arbiser JL, Bonner WM (2015) Inactivation of NADPH oxidases NOX4 and NOX5 protects human primary fibroblasts from ionizing radiation-induced DNA damage. *Radiat Res* **183**: 262-270
- WHO. (2018) The top 10 causes of death. Internet.
- Williams SM, Golden-Mason L, Ferguson BS, Schuetze KB, Cavasin MA, Demos-Davies K, Yeager ME, Stenmark KR, McKinsey TA (2014) Class I HDACs regulate angiotensin II-dependent cardiac fibrosis via fibroblasts and circulating fibrocytes. *J Mol Cell Cardiol* **67**: 112-125

- Wu J, Jackson-Weaver O, Xu J (2018) The TGF- β superfamily in cardiac dysfunction. *Acta Biochimica et Biophysica Sinica* **50**: 323-335
- Wu X, Zhang Y (2017) TET-mediated active DNA demethylation: mechanism, function and beyond. *Nat Rev Genet* **18**: 517-534
- Xu X, Tan X, Tampe B, Nyamsuren G, Liu X, Maier LS, Sossalla S, Kalluri R, Zeisberg M, Hasenfuss G, Zeisberg EM (2015) Epigenetic balance of aberrant Rasal1 promoter methylation and hydroxymethylation regulates cardiac fibrosis. *Cardiovascular Research* **105**: 279-291
- Xu X, Tan X, Tampe B, Wilhelmi T, Hulshoff MS, Saito S, Moser T, Kalluri R, Hasenfuss G, Zeisberg EM, Zeisberg M (2018) High-fidelity CRISPR/Cas9- based gene-specific hydroxymethylation rescues gene expression and attenuates renal fibrosis. *Nat Commun* **9**: 018-05766
- Yang F, Teves SS, Kemp CJ, Henikoff S (2014) Doxorubicin, DNA torsion, and chromatin dynamics. *Biochim Biophys Acta* **1**: 84-89
- Yang X, Li L, Liang J, Shi L, Yang J, Yi X, Zhang D, Han X, Yu N, Shang Y (2013) Histone acetyltransferase 1 promotes homologous recombination in DNA repair by facilitating histone turnover. *J Biol Chem* **288**: 18271-18282
- Ye B, Hou N, Xiao L, Xu Y, Xu H, Li F (2016) Dynamic monitoring of oxidative DNA double-strand break and repair in cardiomyocytes. *Cardiovasc Pathol* **25**: 93-100
- Ye Z, Li J, Han X, Hou H, Chen H, Zheng X, Lu J, Wang L, Chen W, Li X, Zhao L (2016) TET3 inhibits TGF- β 1-induced epithelial-mesenchymal transition by demethylating miR-30d precursor gene in ovarian cancer cells. *J Exp Clin Cancer Res* **35**: 016-0350
- Yin X, Xu Y (2016) Structure and Function of TET Enzymes. *Adv Exp Med Biol* **945**: 275-302
- Yoon SW, Kim DK, Kim KP, Park KS (2014) Rad51 regulates cell cycle progression by preserving G2/M transition in mouse embryonic stem cells. *Stem Cells Dev* **23**: 2700-2711
- Zeisberg EM, Kalluri R (2010) Origins of cardiac fibroblasts. *Circ Res* **107**: 1304-1312
- Zeisberg EM, Tarnavski O, Zeisberg M, Dorfman AL, McMullen JR, Gustafsson E, Chandraker A, Yuan X, Pu WT, Roberts AB, Neilson EG, Sayegh MH, Izumo S, Kalluri R (2007) Endothelial-to-mesenchymal transition contributes to cardiac fibrosis. *Nat Med* **13**: 952-961
- Zhang P, Su J, Mende U (2012) Cross talk between cardiac myocytes and fibroblasts: from multiscale investigative approaches to mechanisms and functional consequences. *Am J Physiol Heart Circ Physiol* **303**: 12
- Zhang Q, Liu X, Gao W, Li P, Hou J, Li J, Wong J (2014) Differential regulation of the ten-eleven translocation (TET) family of dioxygenases by O-linked β -N-acetylglucosamine transferase (OGT). *J Biol Chem* **289**: 5986-5996

- Zhang QQ, Xu MY, Qu Y, Hu JJ, Li ZH, Zhang QD, Lu LG (2014) TET3 mediates the activation of human hepatic stellate cells via modulating the expression of long non-coding RNA HIF1A-AS1. *Int J Clin Exp Pathol* **7**: 7744-7751
- Zhang YE (2009) Non-Smad pathways in TGF-beta signaling. *Cell Res* **19**: 128-139
- Zhang YW, Wang Z, Xie W, Cai Y, Xia L, Easwaran H, Luo J, Yen RC, Li Y, Baylin SB (2017) Acetylation Enhances TET2 Function in Protecting against Abnormal DNA Methylation during Oxidative Stress. *Mol Cell* **65**: 323-335
- Zheng H, Jarvis IWH, Bottai M, Dreij K, Stenius U (2019) TGF beta promotes repair of bulky DNA damage through increased ERCC1/XPF and ERCC1/XPA interaction. *Carcinogenesis* **40**: 580-591
- Zhong J, Li X, Cai W, Wang Y, Dong S, Yang J, Zhang J, Wu N, Li Y, Mao F, Zeng C, Wu J, Xu X, Sun ZS (2017) TET1 modulates H4K16 acetylation by controlling auto-acetylation of hMOF to affect gene regulation and DNA repair function. *Nucleic Acids Res* **45**: 672-684
- Zhou BB, Elledge SJ (2000) The DNA damage response: putting checkpoints in perspective. *Nature* **408**: 433-439
- Zhou P, Pu WT (2016) Recounting Cardiac Cellular Composition. *Circulation Research* **118**: 368-370

